Stony Brook University

1,4 Poly(diiododiacetylene): Production and Characterization

A Dissertation Presented

by

Christopher Wilhelm

to

The Graduate School

in Partial fulfillment of the

Requirements

for the Degree of

Doctor of Philosophy

in

Chemistry

Stony Brook University

May 2009

Stony Brook University

The Graduate School

Christopher Wilhelm

We, the dissertation committee for the above candidate for the
Doctor of Philosophy degree, hereby recommend
acceptance of this dissertation.

Nancy S. Goroff, Dissertation Advisor
Professor, Department of Chemistry

Clare P. Grey, Chairperson of Defense
Professor, Department of Chemistry

Philip Johnson, Third Member
Professor, Department of Chemistry

Gary Kolks, Outside Member
Professor, Department of Chemistry, Manhattan College

This dissertation is accepted by the Graduate School

Dean of the Graduate School
Lawrence Martin

Abstract of the Dissertation

1,4-Poly(diiododiacetylene): Production and Characterization

by

Christopher Wilhelm

Doctor of Philosophy

in

Chemistry

Stony Brook University

2009

This dissertation describes the production of 1,4-poly(diiododiacetylene) via topochemical polymerization within a variety of co-crystals, and its subsequent characterization, within the co-crystal lattice, and after isolation. The host molecules of the co-crystal systems are designed to arrange the diiodobutadiyne monomer in a position conducive to a 1,4-polymerization. The polymerization reaction may then occur spontaneously, under ambient conditions, or it can be induced by radiation or mechanical stress. Following the successful production of 1,4-poly(diiododiacetylene), the polymer has been characterized by methods ranging from XRD, for single-crystal-to-single-crystal transitions and MAS-NMR, for partially polymerized materials, to ESR, for the characterization of reactive intermediates. These methods

give insight into the physical properties of 1,4-poly(diiododiacetylene) and lead to improved design of host molecules. Finally, a new series of bis-pyridyl oxalamides hosts is described, one of which provides the appropriate alignment for the topochemical polymerization of diiodobutadiyne.

Table of Contents

List of Figures

Figure **Page**

List of Schemes

Scheme **Page**

List of Tables

Scheme **Page**

Acknowledgments

The author of this dissertation would like to thank the many professors and students who aided in this collaborative research project. Thank you:
Drs. Jeffery Webb and Sean Curtis, who started this project as graduate students. Dr. Frank Fowler who helped developed the host molecules used in this host guest system, and preceded this study with his own work on di-acetylenes. Dr. Joseph Lauher for both his work with Dr. Fowler as well as his knowledge of crystallography. Dr. John Parise for his knowledge and advice in high-pressure chemistry as well as for his collaborative efforts and enthusiasm. Dr. C. Dave Martin and Cathy Tarabrella for their work on the pressure study. Drs. Clare Grey and Philip Johnson for guidance, knowledge, and patience. The entire Grey research group, but especially Dr. Clare Grey, Stephen Boyd, and Paul Sideris for their collective knowledge and patience in teaching me MAS-NMR as well as their willingness to give up their time to help with this research project. Dr. Gary Halada and Samrat Chawda for their knowledge of Raman Spectroscopy. Dr. Paul Lahti for his expertise in ESR and for his time. Jim Marececk and Francis Picart for their help in solutions state NMR. Dr. Richard Gambino for his guidance in impedance studies. Katherine Hughes for her administrative help. I'd also like to thank The NSF and GAANN for funding my research at SUNY Stony Brook.

The author of this dissertation would like to give special thanks to the entire Goroff group, both past and present members, but specifically Dave Connors, Lei Li, and Liang Luo for their synthetic knowledge and help. Above all others I would like to thank Dr. Nancy Goroff for advising me, helping me, trusting me, and being patient with my development during my time here at SUNY Stony Brook. This project, and my academic career, would never have been successful with out her. Thank you Nancy.

Finally, I would like to thank my wife, Anna-Laura Wilhelm. Without her support and love I wouldn't be the person that I am today. I love you!

Chapter 1. Introduction and Background

1.1 Introduction: Polydiacetylenes

Certain crystalline diynes are known to undergo single-crystal-to-single-crystal transformations to produce polydiacetylenes (PDAs). Gerhard Wegner first reached the conclusion that these systems undergo a topochemical polymerization reaction in the late 1960's.[1] Since then, polydiacetylenes have become one of the most widely studied classes of materials. They are not only studied in the pursuit of novel materials, but also as a model for understanding topochemical polymerization reactions in general.

Crystalline polydiacetylenes are particularly useful for the study of the topochemical reaction because they posses certain unique physical characteristics. The monomer is typically soluble in organic solvents and forms transparent crystals, if pure, while the polymer crystal is typically deeply colored and insoluble in all common solvents. The color of the polymer arises from the lowest π-electron transition of the conjugated backbone, which has its maximum near 600 nm.[2]

A second, and probably the most useful, characteristic of these materials is that diacetylene monomers can polymerize within the perfect lattice of a crystal structure, and because the packing of the monomer controls the polymerization reaction, perfect crystals of the polymer can be produced in a single-crystal-to-

single-crystal transformation. Since the polymer produced is nearly defect free, they can be studied magnetically and by using high-resolution optical techniques.[2] This ability makes crystalline diacetylenes particularly useful towards the study of polymerization reactions in general.

Although these characteristics alone are enough to interest polymer and materials scientists, polydiacetylenes have also peaked the interest of biochemists and biophysicists because they can be used to construct micelles and vesicles that can be permanently stabilized by photopolymerization. They can be incorporated into phospholipids for reconstitution experiments, and can even be inserted into the cell membranes of microorganisms with subsequent polymerization. Furthermore, because polydiacetylenes are known to undergo chromatic phase transitions, often reversible from blue to red, they are also being developed as biosensors.[3-5]

Charch et. al. were able to exploit this behavior of PDAs for the detection of the influenza virus. In 1993 they demonstrated that the binding properties of influenza to sialic acid could be used to bind influenza to the polydiacetylene functionality. A Langmuir-Blodgett film of a polydiacetylene was synthesized containing 2-5% of a carbon linked sialic acid group. Initially a blue film, the color changed to red when the film was incubated with the influenza virus.[3] A later study by this group demonstrated that this same effect can be seen in

liposomes, specifically designed to resemble the organization and functionality of cell membranes.[6]

A second example of this is the work done by Jelinek et. al. In 2005 Jelinek incorporated nanopatches of polydiacetylene vesicles into leukemic cells. This was done by incubating the cells with vesicles composed of dimyristoylphosphatidylethanolamine (DMPE), dimyristoylphosphatidylglycerol (DMPG), and the diacetylene monomer 10,12-tricosadyinoic acid in a 1:1:3 ratio.[7,8] The monomer was subsequently polymerized using UV irradiation. Two separate assays showed that most of the cells lived for at least three hours after the polymerization reaction. SEM experiments that followed revealed an abundance of bright, 50-100 nm sized patches localized at the cell surface.[7,8]

The cells were first tested using lidocaine, believed to increase bilayer fluidity. They were initially tested for fluorescence, and demonstrated none. However, after treatment with lidocaine the cells demonstrated the appearance of fluorescent spots concentrated exclusively on the cell surface. This was attributed to the lidocaine having induced a structural change of the PDA to the fluorescent, red phase.[7,8]

In a follow up study, Jelinek et. al. report the testing of mammalian cells for pesticide cytotoxicity using the same method.[7,8] 14 pesticides were tested, four of which were demonstrated to have significant membrane activities. These tests were further confirmed using fluorescence anisotropy experiments of membrane

embedded 1-(4-trimethylammoniumphenyl)-6-phenyl-1,3,5-hexatriene, a widely used probe of the lipid bilayer environment. Both experiments provided comparable results. However, the PDA method has two distinct advantages. First, the PDA method does not rely on measuring small changes in anisotropy; it is a simple "on-off" testing method. Second, the PDA fluorescence is a direct result of membrane perturbation, and therefore provides an effective probe for localized disruption of the membrane bilayer.[7,8]

1.2 Introduction: Crystal Design Towards the Topochemical Polymerization of Monomeric Diacetylenes

Wegner's early work on crystalline diynes was based on the principles of topochemical polymerization developed by Gerhard Schmidt and his co-workers, dating back to 1964. Schmidt et. al. developed these principles as a result of their work on α- and β-unsaturated acids.[1] Using Schmidt's principles, Wegner concluded that the color change observed in certain crystalline diacetylene materials must be the result of a topochemical polymerization reaction in which C1 and C4 of adjacent diacetylene moieties become attached.[1]

Wegner described two types of polymerization methods that may occur in a single-crystal-to-single-crystal transition of a diacetylene monomer to 1,4-polydiacetylene. The first, depicted in Figure 1.1a, is the heterogeneous method. The first step in this method is the formation of nuclei of the polymer phase. The polymer growth is connected to the formation of a second morphological crystal

phase, in which one obtains domains of polymer growth and then small polymer crystallites.[1]

In the second method, the homogeneous method, polymerization may proceed without, or with almost no change in the lattice parameters; because the center of gravity of each monomer remains in the same position as the individual molecule becomes a unit in the polymer.[1] This method of polymerization is depicted in Figure 1.1b.

Lastly, Wegner states that attaching a monomer unit to a running polymer chain during the topochemical polymerization reaction is an exothermic process, but it must surpass an initial energy barrier. The energy barrier results from the reacting carbons (C1 and C4) need to rotate towards each other, acting against their repulsive forces.[2]

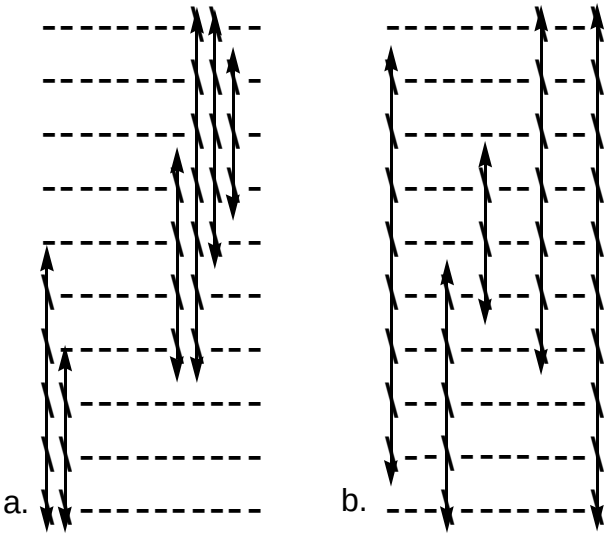

Figure 1.1 Heterogeneous and homogeneous polymer growth, respectively.[1]

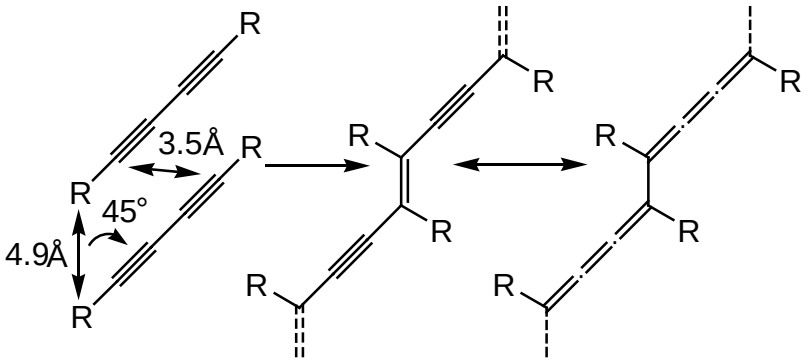

Scheme 1.1 Polymerization of monomer leading to the two different electronic structures, the ene-yne and cumulenic respectively.

Expanding on Wegner's early work, Baughman first reported the necessary parameters for the 1,4-polymerization of crystalline diacetylenes in 1974.[9,10] Baughman concluded that a translational distance of 4.9Å is optimal for the 1,4-polymerization of diacetylene moieties to occur. This distance corresponds to the repeat distance within the resulting polymer. Baughman also found that the polymerization reaction occurs most effectively when two reacting diyne molecules have an orientation angle of 45° along the axis of translation.[9,10] In this orientation the two reacting carbon atoms, C1 and C4, have a distance of 3.5Å. This distance is close to the van der Waals radius of carbon. When these parameters are met there is a minimal amount of motion by the carbon atoms in the diyne molecule during the polymerization reaction.[9,10] See Scheme 1.1. The final polymer that is produced is then expected to take on one of the two electrical confirmations depicted in Scheme 1.1, the ene-yne structure or the cumulenic structure.[2] The ene-yne structure is expected to be the dominant confirmation,

and will be the assumed confirmation throughout this body of work unless the cumulenic structure is specifically mentioned.

Finally, the more recent work of Fowler and Lauher has adapted Baughman's parameters into co-crystal systems designed to induce the single-crystal-to-single-crystal transformation of monomeric diacetylenes to 1,4-polydiacetylenes.[11-18] Before their work the alignment of the diacetylene moieties was typically carried out as a function of the side-groups of the monomeric diacetylene molecules. However, the work of Fowler and Lauher has made it possible to polymerize simpler diacetylenes by using the supramolecular scaffold provided by a co-crystal system. The co-crystal system uses a "host" molecule to align a diacetylene "guest" molecule appropriately for the topochemical polymerization reaction to occur, resulting in the production of the 1,4-polydiacetylene. Fowler and Lauher have developed a series of functionalities that can be incorporated into the design of a host molecule resulting in an α-network with specific repeat distances within the crystal lattice.[11-14] These repeat distances can then be transferred to the monomeric acetylene guest, aligning them for a variety of topochemical polymerization reactions.[15-17]

Although Fowler and Lauher have developed many functionalities for use with dienes and trienes, among other monomeric molecules, the two that will be focused on in the body of work presented here are the oxalamide- and urea-functionalities shown in Figure 1.2.[11-18]

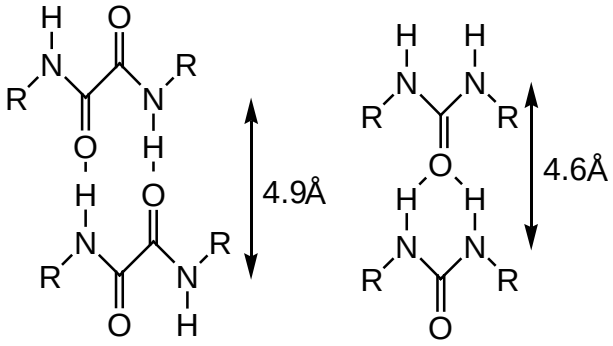

Figure 1.2 Oxalamide and urea functionalities, respectively, along with their expected repeat distance within an α-network.[11-17]

The majority of the co-crystal systems developed by Fowler and Lauher use hydrogen bonding to transfer the alignment of the host molecule to the guest diene.[11-17] However, this is not possible in the systems discussed in this body of work, as will be demonstrated later, but the theory of the Fowler/Lauher co-crystal systems and the systems discussed here are almost identical.

1.3 Reactive Species Involved in the Topochemical Polymerization Reaction

In the mid-1970's Stevens and Bloor published a series of electron spin resonance (ESR) studies on the polymerization reaction that occurs in crystalline samples of the *bis* (p-toluene sulphonate) of 2,4-hexadiyne-1,6-diol (TSHD) (side chain = $CH_2OSO_2C_6H_4CH_3$).[19-22] Stevens and Bloor first identified the evolution of a singlet absorption with no resolvable hyperfine structure.[19] They reported that the spin concentration of this of this absorption decreases smoothly with the increase of the polymer fraction of the sample, and that this original signal persists, with a spin concentration of ~8.6 X 10^{15} spins per gram, at 100%

polymerization.[19] Since it had already been demonstrated that this crystalline diacetylene, TSHD, undergoes a homogeneous polymerization, indicating the presence of long polymer chains at all stages of polymerization, they assigned this signal as being produced by the polymer itself, probably a bonding defect, and not the result of a reactive species.[19]

Stevens and Bloor then investigated a triplet signal that they assigned to the reactive species, a carbene, which they depict using the mesomeric structures depicted in Figure 1.3.[20-22] They made this assignment because this signal was observed in a partially polymerized crystal, at room temperature (in which the polymerization reaction rate is negligible), but it disappeared at the end of the polymerization period.[20-22]

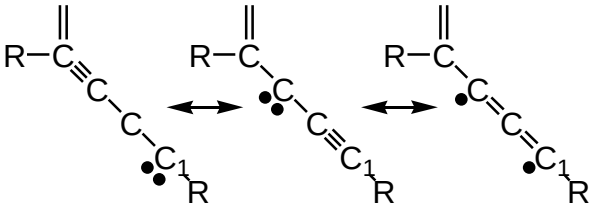

Figure 1.3 Mesomeric forms of carbene reactive species assigned by Stevens and Bloor.

Ronald Chance, however, did not believe this reactive species to the be the polymerization initiating species, and in the late 1970s Chance performed a series of optical and energy studies that supported his hypothesis.[23-25] According to Chance's Diffuse Reflectance Spectroscopy (DRS) the spectral evolution produced during a topochemical polymerization of TSHD demonstrated the

growth of a band system with a 572 nm maximum.[23] Bloor had also identified this maximum, and stated that it shifts to 615 nm as the percent polymerization increases. Bloor attributed this phenomenon to strain within the crystal lattice. TSHD undergoes a ~5% reduction in the lattice distance along the backbone of the polymer during the topochemical polymerization reaction, leading to a lattice strain of the short oligomers.[21] Chance, however, hypothesized that this 572 nm maximum does not shift, but in fact may become buried by the 615 nm peak.[23] Chance et. al. assigned the 572 nm peak to the diradical butatriene structure **M*** depicted in Figure 1.4, and supported this assignment with a Differential Scanning Calorimetry (DSC) study performed on the polymerization of a TSHD crystal.[23,25]

Chance et. al. report the observed energy of activation (E_a) of the thermal polymerization of TSHD to be 22.5 kcal/mol, or ~1.0 eV.[24] They associate the E_a primarily with the initiation event, and evaluate the heat of polymerization (ΔH_p) to be ~-36.6 kcal/mol, or –1.6 eV.[24] According to Chance, the lowest energy excited state of the monomer is best represented as the diradical butatriene **M***, see Figure 1.4. The addition of a monomer to the "living" or reactive polymer chain end **RC**, also depicted in Figure 1.4, will be 1.6 eV. The addition of **M*** to **RC**, shown in Scheme 1.2, should be exothermic by ~4.1 eV, the sp^2-sp^2 σ bond energy. This leads to an **M** to **M*** energy of ~2.5 eV, a reasonable value.[24] Chance concluded by stating that a dimerization of two diacetylene molecules, depicted in Scheme 1.3, would therefore require an energy input of ~0.9 eV. (2.5

eV + 2.5 eV – 4.1eV), which is in good agreement with his experimentally observed results. The use of a carbene initiator would give a unacceptably high value for E_a, ~2.5 eV.[24]

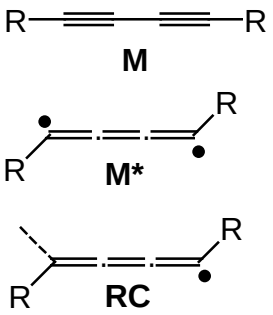

Figure 1.4 Reactive species involved in 1,4 polymerization of a diacetylene moiety according to Chance.

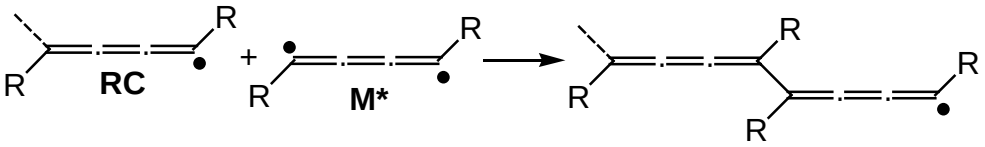

Scheme 1.2 Addition of diradical butatriene to the reactive end on a polydiacetylene.

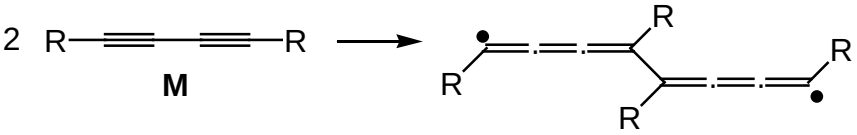

Scheme 1.3 Dimerization of two diacetylene moieties.

In 1978, Hori and Kispert performed an ESR study of x-irradiated single-crystal samples of TSHD at 77 K which demonstrated the production of a radical S=1/2 initiation species when a TSHD crystal is irradiated to a dose of ~0.2 Mrad, supporting Chance's assignment of a radical intiator.[26] The spectrum produced consists of a triplet of triplets centered near g = 2.0023. The hyperfine coupling

this radical demonstrated is consistent with a coupling of β protons, ~18 MHz, and the signal was attributed to the radical species **RC** shown in Figure 1.4.[26] All other possible radical structures were eliminated by the presence of α protons.

Hori and Kispert supported these experiments by Intermediate Neglect of Differential Overlap (INDO) molecular orbital calculations performed on the similar radical depicted in Figure 1.5.[26] The results of these calculations demonstrate isotropic proton hyperfine couplings of $H_{\beta 1}$ = 16.46 and $H_{\beta 2}$ = 16.63.[26] Not only were these results in excellent agreement with the experimental results, a_{iso} = 16.1, but there is evidence of two different angular dependant anisotropic components as the sample orientation is rotated within the magnetic field.[26] It should be noted however, that a small amount of carbene species was observed by Hori and Kispert while performing these experiments.

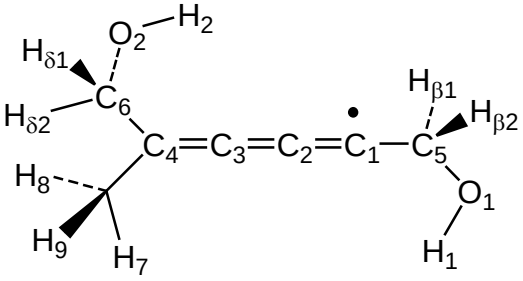

Figure 1.5 Model compound for INDO calculations performed by Hori and Kispert.[26]

Then, Hori and Kispert made another important discovery while working on the 1,4-polymerization reaction of 5,7-dodecadiyne-1,12-diol bis phenyl urethane (TCDU). The experiments performed on TCDU demonstrated that while a small

amount of a radical S = 1/2 species was generated upon x-irradiation of a single-crystal sample, a much larger amount of a radical pair species was produced.[27] This species is designated to be a radical pair, or diradical, because plots of the angular dependence of the peaks, as the sample is rotated in the magnetic field about the (0,0,1) and (0,1,0) axes, cross through zero, a feature which does not arise from S=1/2 radicals.[27]

As the sample was warmed from 160 K to 180 K the diradical lines disappeared, during which the color of the crystal sample permanently changed from colorless to red, indicating polymerization. The hyperfine structure of the diradical signal indicates couplings with either 4 nearly equivalent protons or two equivalent protons and one nitrogen with $A_N = A_H$.[27] Hori also determined that the spin is delocalized over several atoms and that the spin-spin direction of the radical pair is close to the direction of the polymer backbone. After having eliminated all of the other possible diradicals, Hori and Kispert assigned this signal to the structure shown in Figure 1.6, one similar to the structure of **M*** as designated by Chance.[24,27]

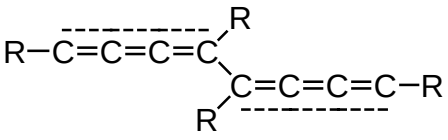

Figure 1.6 Radical pair observed and assigned by Hori and Kispert during polymerization of TCDU.[27]

In the late 70s and early 80s Hans Sixl published a series of works that completed the description of all of the reactive species involved in the polymerization of diacetylenes, and confirmed all of the work done previously.[28-33] Using a series of Optical Transmission Spectroscopy (OTS) and ESR studies performed on the low temperature, UV induced polymerization of TSHD crystal samples, Sixl demonstrated that a carbene-type reactive species is generated during the topochemical polymerization reaction, supporting Bloor's description of the reactive species.[28-30] The carbene structure was described as having a fine structure parameter $D > 0$, meaning that the electron distribution of the two unpaired electrons is disc-shaped relative to the z-axis.[28] However, the low D/hc value ($D/hc = \pm 0.2731$) indicates that these electrons are delocalized and that the structure is possibly bent at the C1 atom, akin to Bloor's mesomeric structures shown in Figure 1.3.[28] A later paper describes the spin density at C1 to be 0.4 ± 0.2.[30]

Then, in 1980 Sixl and Neumann reported their observation of diradical ESR signals during the UV initiated polymerization of TSHD crystal samples at ~4 K.[31-33] They attributed these signals to a diradical structure because of the observed hyperfine structure, determined to be produce by four protons of two CH_2 groups, and stated that the unpaired electrons are preferentially located at both ends of extremely short oligomer chains. They reported this diradical

structure for short chain oligomer molecules up to four or five monomer units in length, a tetramer or pentamer.[31]

In a follow up kinetics study Sixl and Neumann described the steps involved in the photo-induced polymerization of TSHD as follows:[32]

1. Initiation: Dimer radical states are produced by optical excitation of the monomer, S0 → S1. ($\lambda \leq 310$ nm)
2. Addition: Monomer unites are added to the dimer, trimer … units by direct or indirect optical excitation of the monomer molecules adjacent to the oligomer molecules. Indirect optical excitation is performed by excitation transfer via singlet or triplet excitations after optical excitation of the monomer crystal.
3. Transformation: The diradicals are transformed to the asymmetric carbene radicals either by direct or indirect optical excitation of the diradical oligomer molecules.
4. Termination: The metastable oligomer states react irreversibly to stable oligomer states.

Finally, in 1981 Sixl and Neumann reported a complete analysis of the polymerization of a TSHD crystal at low temperarure.[33] They studied this reaction using ESR spectroscopy on TSHD crystal samples, in which the polymerization reaction is initiated by UV radiation and then allowed to proceed

during thermal annealing. As the ESR signal of the dimer diradical decreased there was a corresponding transient increase in the trimer diradical signal.[33] There was also a transient increase in the tetramer and pentamer diradical signals as the trimer and tetramer signals decrease respectively. However, these changes are not quantitative, as the total intensity of all diradical signals is decreasing, indicating that longer chain diradical species are not stable to transformation reactions. [33]

During the decay of the diradical signals only dicarbene signals were generated.[33] Quintet ($S \approx 2$) dicarbene species were only generated from tetramer and pentamer diradical species. Therefore, Sixl and Neumann described the shortest chain dicarbene as a pentamer. The same evolution of ESR signals was observed throughout the dicarbene series.[33] The signal of the hexamer dicarbene increased as the signal of the pentamer dicarbene signal decreased, etc. All the while, the total intensity of all dicarbene species signals decreased as they were transformed to extended chains or chain termination products. The same phenomenon was also true for the series of asymmetric carbene intermediates. Since these oligomer molecules cannot be transformed to diradical or dicarbenes by thermal or optical reactions, only addition polymerization of the asymmetric carbene intermediates was observed.[33] Scheme 1.4 illustrates these transitions.

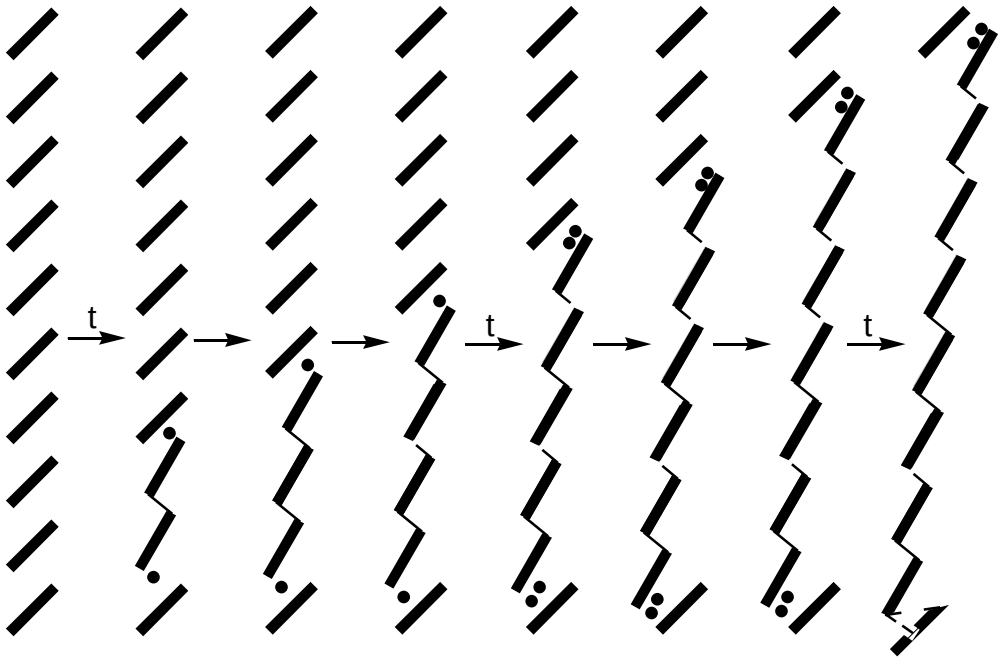

Scheme 1.4 The transitions discussed by Sixl and Neumann during the topochemical polymerization of a TSHD crystal at low temperature.

Finally, Sixl defines three reactive species that are produced during the course of a topochemical polymerization of a diacetylene; a diradical, a dicarbene, and an asymmetric carbene, depicted in Figure 1.7.[34] According to Sixl et. al. the diradical form is dominant for an oligomer chain-length of $2 \leq n \leq 5$, the dicarbene is dominant for a chain-length $n \approx 8$, and the asymmetric carbene is

dominant for chain-lengths of n ≥ 20.[34]

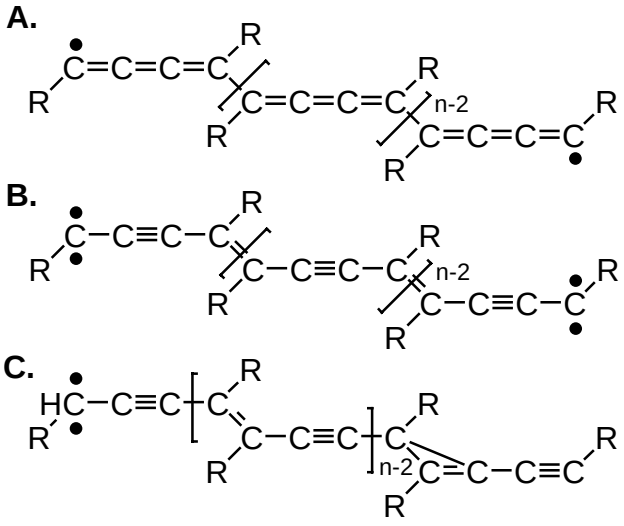

Figure 1.7 Sixl and Neumann's assignment of the reactive species produced during the topochemical polymerization of a diene; diradical (A), dicarbene (B), and asymmetric carbene (C).[34]

He explains that at a chain length of n = 5 there is a 10% admixture of the dicarbene structure, which gradually increases at n = 6.[34] The dicarbene structure is then dominant until a chain-length of n ≈ 17 is reached, approximately where the asymmetric carbene structure becomes dominant. This leads Sixl to the conclusion that the acetylene form of the oligomer chains is more stable than the butatriene form.[34] However, Sixl also reports the conversion of the diradical species directly to the asymmetric carbene species at a chain length of n ≈ 2.[33]

1.4 Realizing 1,4-poly(diiododiacetylene) within a Co-Crystal System and Previous Work

The goal of this research has focused on the successful topochemical, head-to-tail polymerization of diiodobutadiyne to yield 1,4-poly(diiododiacetylene), depicted as compound **1** and polymer **2** respectively in Figure 1.8. While many PDAs have been produced over the last 40 years, 1,4-poly(diiododiacetylene) would be unique because it posses such simple side-chains, a single iodine atom. The iodine side-chains should provide an amount of versatility at the C1 and C4 sites not seen in most other PDAs. This should allow for reactions to occur at these sites, and may enhance the physical properties of the polymer.

The simplicity of the side chains may allow for exchange or elimination of the iodine atom enabling 1,4-poly(diiododiacetylene) to be used as a precursor to PDAs that cannot be prepared through the traditional topochemical reaction. It may also lead to polymers with different carbon to iodine ratios, and possibly even the linear, all carbon polymer carbyne. Carbyne is particularly attractive to chemists because, in theory, it consists of a linear chain of sp hybridized carbon nuclei.[35] Carbyne would likely demonstrate conductive and possibly optical properties that would prove useful in the field of material science.

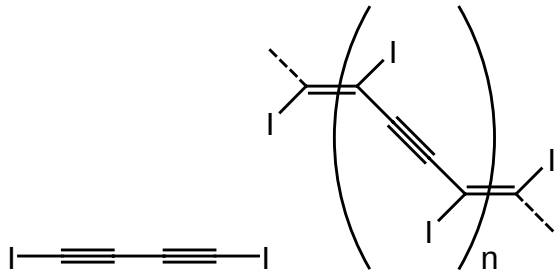

1 **2**

Figure 1.8 Diiodobutadiyne (**1**) and 1,4-poly(diiododiacetylene) (**2**).

Previous routes for achieving a 1,4-polymerization of other diacetylenes have also used the co-crystal system.[15-17] These systems have utilized a variety of host molecules. Figure 1.9 shows the bis-pyridyl and bis-nitrile oxalamides and ureas reported here for use as host molecules in supra-molecular co-crystal systems with the goal of producing 1,4-poly(diiododiacetylene) via a topochemical polymerization reaction. The bis-pyridyl oxalamides contain varying length alkyl-chain tethers and are substituted at the meta and para positions of the pyridyl rings (compounds **M1-4** and **P1-4** respectively, where the integer denotes the length of the alkyl-chain tether), and the bis-nitrile oxalamides contain varying length alkyl-chain tethers from 4 to 6 methylene groups (compounds **N4-6** respectively). The bis-nitrile-ureas (compound **7**) are still under development. The bis-pyridyl oxalamide host molecules were developed by Lauher and Fowler, and have been used with great success in the topochemical polymerization of diynes and triynes.[12-18]

The oxalamide and urea moieties use self-complementary hydrogen bonding to form reliable α-networks containing a specific repeat distance. This interaction leaves the Lewis base functionality, the pyridyl ring or the nitrile group, free for further hydrogen bonding or, in the case of these co-crystal systems, halogen bonding with the guest molecule. The molecules shown in Figure 1.9 were designed to give a translational distance of 4.6-5.1 Å.[12-17]

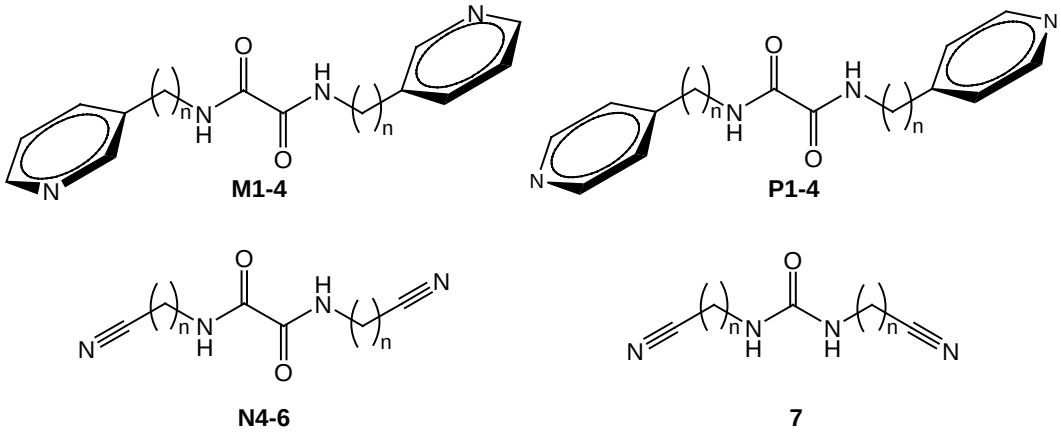

Figure 1.9 Bis-pyridyl and bis-nitrile functionalized oxalamide and urea host molecules.

In the case of diiodobutadiyne there are no terminal hydrogen atoms for hydrogen bonding to the Lewis base. However the "halogen bonding" interaction that occurs between the Lewis acidic, terminal iodine atoms and the nitrogen atoms of the pyridyl rings or nitrile groups serves the same purpose. A halogen bond is similar to a hydrogen bond in the fact that a Lewis acid is associated with a Lewis base by the donation of electron density into a σ* anti-bonding orbital.[36] However, in the case of a hydrogen bond, the Lewis acid promotes an electron

into the H-X σ* orbital (i.e. the N-H bond in the case of these hosts) and in the case of a halogen bond the Lewis base donates an electron in to the X-C σ* orbital (the I-C σ* orbital in the case of diiodobutadiyne).[36]

The bis-pyridyl co-crystal systems used early in this study were first reported in 2005 by Goroff et. al.[37,38] Both the 3-pyridyl oxalamide/diiodobutadiyne, **M1/1,** and 4-pyridal oxalamide/diiodobutadiyne, **P1/1,** co-crystals were synthesized. Figures 1.10 and 1.11 show these structures as determined by single-crystal x-ray defractometry (XRD). They have repeat distances of 5.1 Å and 5.0 Å respectively, and C1-C4 distances of 4.0 Å and 4.9 Å respectively.[37,38]

The parameters of both co-crystal systems are close to the ideal parameters for a head-to-tail polymerization of diiodobutadiyne. However, single-crystal XRD demonstrates that upon synthesis neither of the co-crystal systems leads to the spontaneous production of 1,4-poly(diiododiacetylene), even when exposed to ambient light.[37,38] It was observed that the **M1**/**1** co-crystals undergo a color change, from colorless to shiny gray, over a few days' time when kept at room temperature under ambient light. However, single-crystal XRD experiments performed on a sample of these colored co-crystals indicates that only the starting materials are present, with no polymerization.[37,38] Furthermore, in the case of the **P1**/**1** co-crystals, stability at room temperature for weeks was reported. This has been attributed to the large tilt angles resulting from steric repulsion within the

co-crystal system.[37,38] Therefore, other means of inducing polymerization within these systems will be explored.

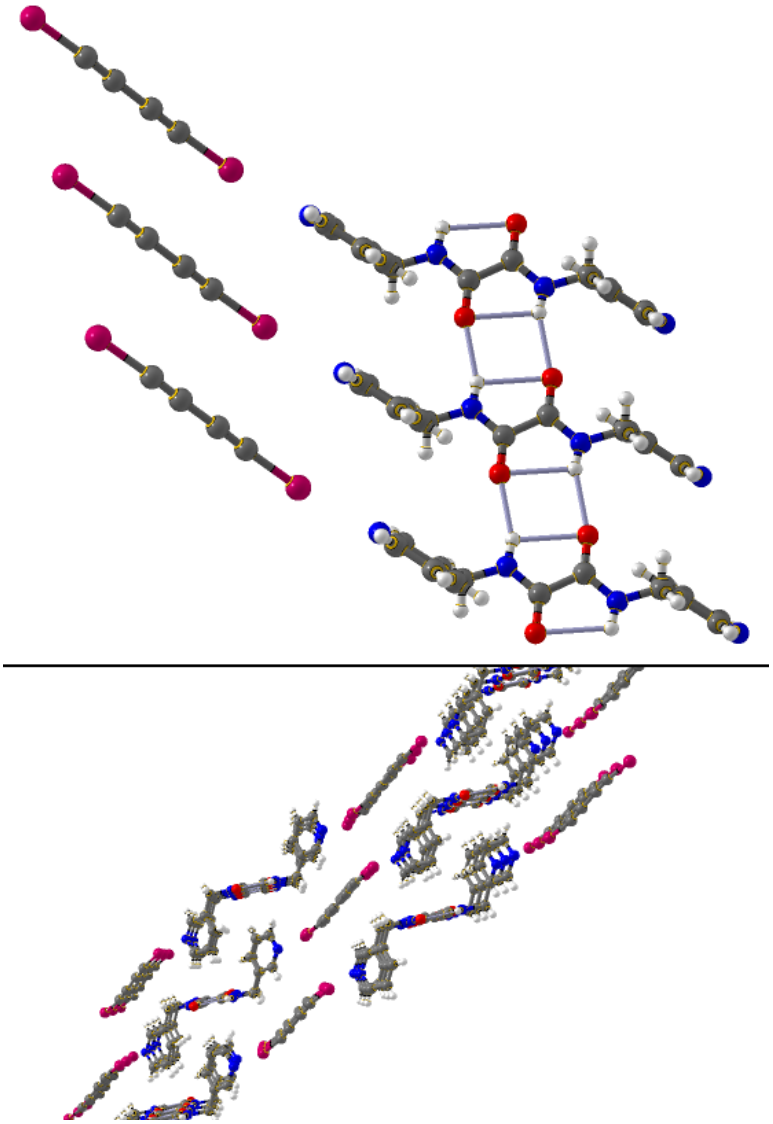

Figure 1.10 Crystal structure of **M1/1** co-crystal, α-network depicted by solid gray lines, packing is shown (bottom).[37,38]

Due to the good fit that the **M1**/**1** co-crystals showed to the ideal parameters for a 1,4 polymerization, polymerization was attempted in these co-crystals by

exposing them to heat, ultraviolet light, and γ-radiation.[37,38] However, these attempts only resulted in crystal destruction, color change with no evidence of polymerization, or no change at all.[37,38]

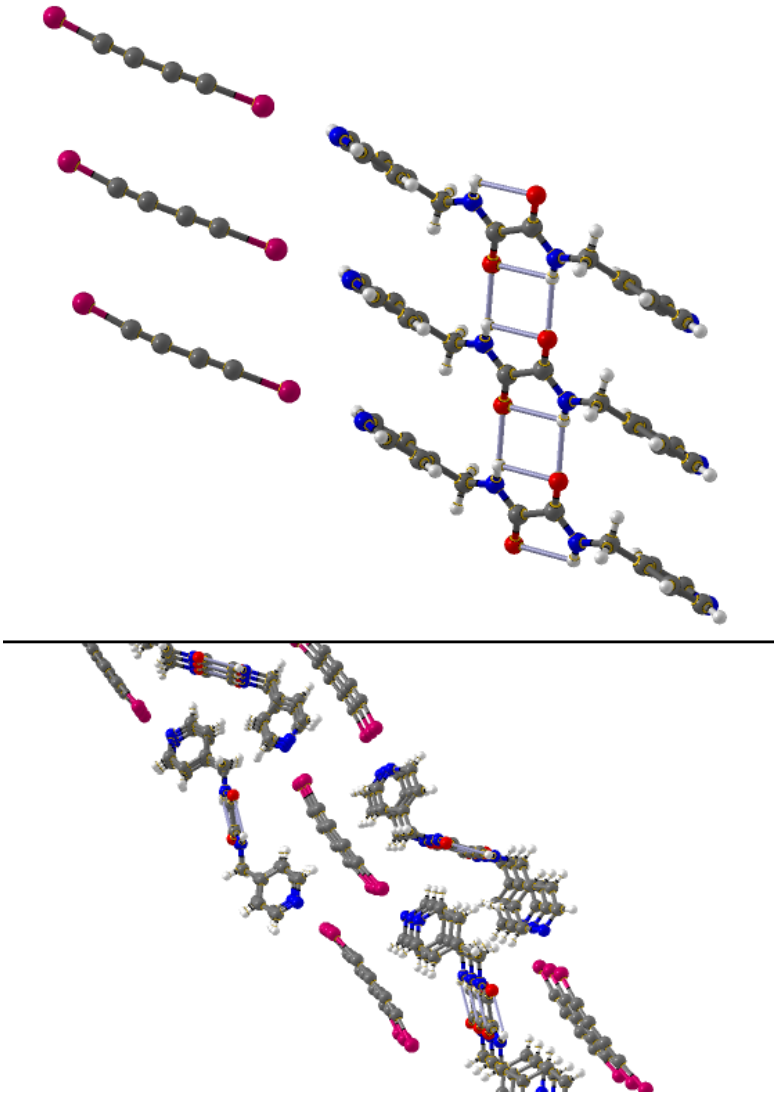

Figure 1.11 Crystal structure of **P1/1** co-crystal, α-network depicted by solid gray lines, packing is shown (bottom).[37,38]

The bis-nitrile co-crystal systems used in this project were first reported in 2006 by Goroff et. al.[39] The bis-nitrile oxalamide/diiodobutadiyne, **N4**/**1,** co-crystals were first synthesized by Aiwu Sun, and were shown to spontaneously polymerize at STP. Figure 1.12 shows this structure as determined by single-crystal XRD. The co-crystal contains 1,4-poly(diiododiacetylene) and the polymer has a repeat distance of 4.9 Å.[39] The single-crystal structure of co-crystal samples containing bis-nitrile oxalamide/diiodobutadiyne, **N6/2,** remains to be resolved, but all other means of analysis indicate that this system also spontaneously polymerizes to produce 1,4-poly(diiododiacetylene).

Through the course of this research project diiodobutadiyne has been co-crystallized with a variety of host molecules. Mixtures of both **M1/1** and **P1/1** readily form colorless co-crystals while mixtures of both **N4**/**1** and **N6**/**1** readily form coppery colored co-crystals. However, x-ray crystallography has failed to demonstrate the presence of polymer **2** in all samples but the **N4**/**2** co-crystal structure shown in Figure 1.12. In the case of the **M1**/**1** and **P1/1** co-crystals no evidence exists that the topochemical polymerization reaction has occurred after traditional induction methods have been used, except for the observation of a color change.[37,38]

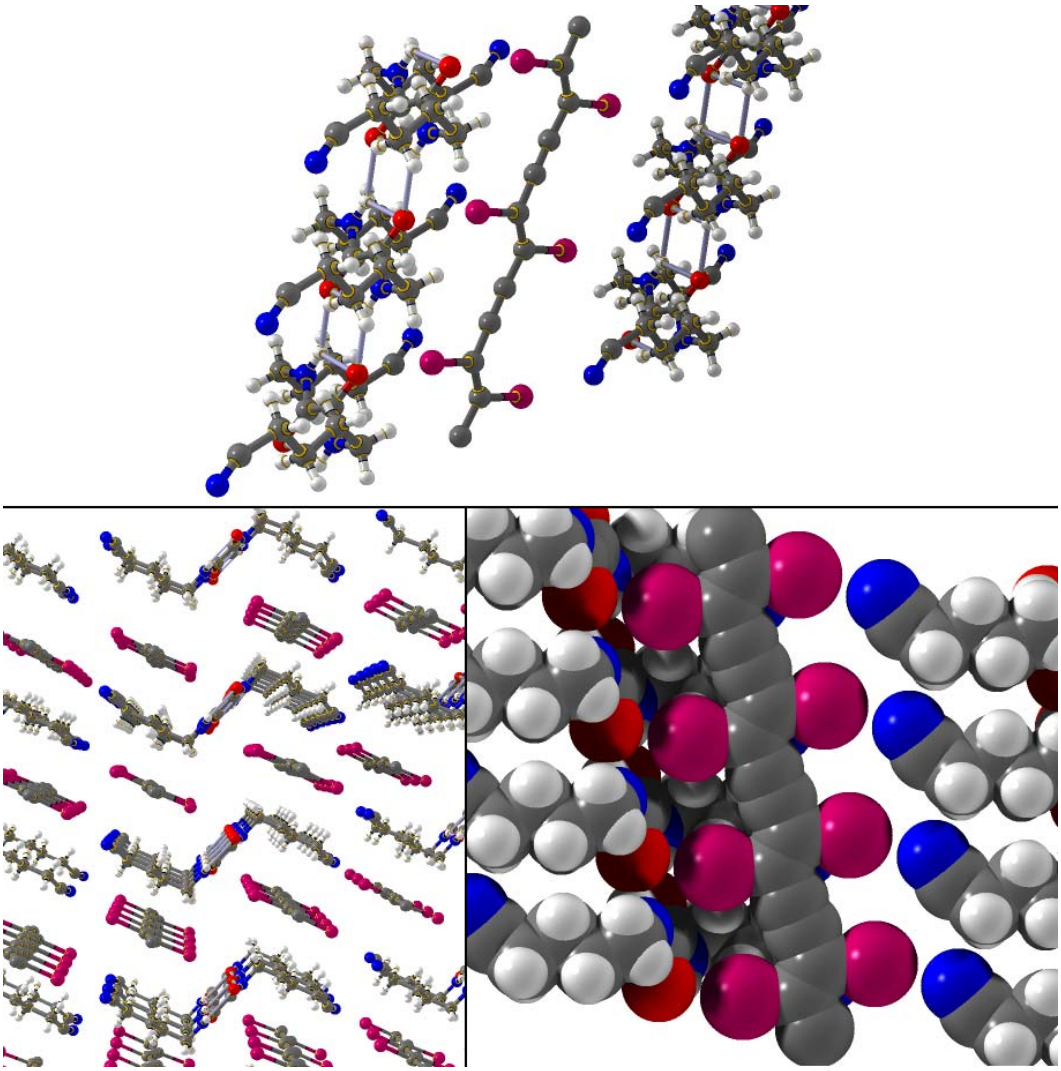

Figure 1.12 Crystal structure of **N4/2**, α-network depicted by solid gray lines, packing shown (bottom).[39]

1.5 References

1. Kaiser, J.; Wegner, G.; and Fischer, E.W. Topochemical Reactions of Monomers with Conjugated Triple Bonds. VII. Mechanism of Transition from Monomer to Polymer Phase During Solid-State Polymerization. *Isr. J. Chem.*, **1972**, *10*, 157-171.

2. Bassler, H.; Sixl, H.; and Enkelmann, V. *Adv. Polymer Sci. 63: Polydiacetylenes*.; 63; H.-J. Cantow: Springer-Verlag, 1984.

3. Charych, D.H.; Nagy, J.O.; Spevak, W.; and Bednarski, M.D. Direct Colorimetric Detection of a Receptor-Ligand Interaction by a Polymerized Bilayer Assembly. *Science* **1993**, *261*, 585-588.

4. Charych, D.H.; Cheng, Q.; Reichert, A.; Kuziemko, G.; Stroh, M.; Nagy, J.O.; Spevak, W.; and Stevens, R.C. A 'Litmus Test' for Molecular Recognition Using Artificial Membranes. *Chem. Biol.* **1996**, *3*, 113-120.

5. Geiger, E.; Hug, P.; and Keller, B.A. Chromatic Transitions in Polydiacetylene Langmuir-Blodgett Films due to Molecular Recognition at the Film Surface Studied by Spectroscopic Methods and Surface Analysis. *Macromol. Chem. Phys.* **2002**, *203*, 2422-2431.

6. Reichert, A.; Nagy, J.O.; Spevak, W.; and Charych, D. Polydiacetylene Liposomes Functionalized with Sialic Acid Bind and Colorimetrically Detect Influenza Virus. *J. Am. Chem. Soc.*, **1995**, *117*, 829-830.

7. Orynbayeva, Z.; Kolusheva, S.; Livneh, E.; Lichtenshtein, A.; Nathan, I.; Jelinek, R. Visualization of Membrane Processes in Living Cells by Surface-Attached Chromatic Polymer Patches. *Angew. Chem. Int. Ed.*, **2005**, *44*, 1092-1096.

8. Mech, A.; Orynbayeva, Z.; Irgebayev, K.; Kolusheva, S.; and Jelinek R. Screening Membrane Interactions of Pesticides by Cells Decorated with Chromatic Polymer Nanopatches. *Chem. Res. Toxicol.*, **2009**, *22*, 90-96.

9. Baughman, R.H. Solid State Polymerization of Diacetylenes. *J. Appl. Phys.* **1972**, *43*, 4362-4370.

10. Baughman, R.H. Solid-State Synthesis of Large Polymer Single Crystals. *J. Polym. Sci., Polym. Phys. Ed.* **1974**, *12*, 1511-1535.

11. Toledo, L.M.; Lauher, J.W.; and Fowler, F.W. Design of Molecular Solids. Application of 2-Amino-4(1H)-pyridones to the Preparation of Hydrogen Bonded α- and β- Networks. *Chem. Mater.* **1994**, *6*, 1222-1226.

12. Toledo, L.M.; Musa, K.; Lauher, J.W.; and Fowler, F.W. Development of Strategies for the Preparation of Designed Solids. An Investigation of the 2-Amino-4(1H)-pyrimidone Ring System for the Molecular Self-Assembly of Hydrogen Bonded α- and β- Networks. *Chem. Mater.* **1995**, *7*, 1639-1647.

13. Coe, S.; Kane, J.J.; Nguyen, T.L.; Toledo, L.M.; Wininger, E.; Fowler, F.W.; and Lauher, J.W. Molecular Symmetry and the Design of Molecular Solids: The Oxalamide Functionality as a Persistent Hydrogen Bonding Unit. *J. Am. Chem. Soc.* **1997**, *119*, 86-93.

14. Nguyen, T.L.; Scott, A.; Dinkelmeyer, B.; Fowler, F.W.; and Lauher, J.W. Design of Molecular Solids: Utility of the Hydroxyl Functionality as a Predictable Design Element. *New J. Chem.* **1998**, *22*, 129-135.

15. Kane, J.J.; Liao, R.-F.; Lauher, J.W.; and Fowler, F.W. Preparation of Layered Diacetylenes as a Demonstration of Strategies for Supramolecular Synthesis. *J. Am. Chem. Soc.* **1995**, *117*, 12003-12004.

16. Schauer, C.L.; Matwey, E.; Fowler, F.W.; and Lauher, J.W. Controlled Spacing of Metal Atoms via Ligand Hydrogen Bonds. *J. Am. Chem. Soc.* **1997**, *119*, 10245-10246.

17. Curtis, S.M.; Le, N.; Fowler, F.W.; and Lauher, J.W. A Rational Approach to the Preparation of Polydipyridyldiacetylenes: An Exercise in Crystal Design. *Crystal Growth and Design* **2005**, *5*, 2313-2321.

18. Hoang, T.; Lauher, J.W.; and Fowler, F.W. The Topochemical 1,6-polymerization of a Triene. *J. Am. Chem. Soc.*, **2002**, *124*, 10656-10657.

19. Stevens, G.C.; and Bloor, D. Solid-State Thermal Polymerization of bis(p-toluene sulfonate) of 2,4-hexadiyne-1,6-diol. III. ESR Study. *J. Poly. Sci. Poly. Phys. Ed.* **1975**, *13*, 2411-2427.

20. Stevens, G.C.; and Bloor, D. Observation of Paramagnetic Triplet Species During the Thermal Polymerization of bis(p-toluene sulfonate) of 2,4-hexadiyne-1,6-diol. *Chem. Phys. Lett.* **1975**, *40*, 37-40.

21. Bloor, D.; Koski, L.; Stevens, G.C.; Preston, F.H.; and Ando, D.J. Solid State Polymerization of bis(p-toluenesulfonate) of 2,4-hexadiyne-1,6-diol. 1. X-ray Diffraction and Spectroscopic Observations. *J. Mat. Sci.* **1975**, *10*, 1678-1688.

22. Eichele, H.; Schwoerer, M.; Huber, R.; and Bloor, D. ESR of a Diacetylene Polymer Single Crystal. *Chem. Phys. Lett.* **1976**, *42*, 342-346.

23. Chance, R.R.; and Sowa, J.M. An Examination of the Thermal Polymerization of a Crystalline Diacetylene Using Diffuse Reflectance Spectroscopy. *J. Am. Chem. Soc.* **1977**, *99*, 6703-6708.

24. Chance, R.R.; Patel, G.N.; Turi, E.A.; and Khanna, Y.P. Energetics of the Thermal Polymerization of a Diacetylene Crystal. *J. Am. Chem. Soc.* **1978**, *100*, 1307-1309.

25. Chance, R.R.; and Patel, G.N. Solid-State Polymerization of a Diacetylene Crystal. Thermal, Ultraviolet and Ray Polymerization of 2,4-hexadiyne-1,6-diol bis-(p-toluene sulfonate). *J. Poly Sci. Poly. Phys. Ed.* **1978**, *16*, 859-881.

26. Hori, Y.; and Kispert, L.D. An ESR Study of X-irradiated Diacetylene Single Crystals at 77 K. *J. Phys. Chem.* **1978**, *69*, 3826-3829.

27. Hori, Y.; and Kispert, L.D. ESR Evidence for a Biradical Dimer Initiator in Diacetylene Polymerization. *J. Am. Chem. Soc.* **1979**, *101*, 3173-3177.

28. Huber, R.; Schwoerer, M.; Bubeck, C.; and Sixl, H. The Sign of D in the Triplet Carbene of a Polydiacetylene Single Crystal (PTS). *Chem. Phys. Lett.* **1978**, *53*, 35-38.

29. Sixl, H.; Hersel, W.; and Wolf, H.C. Photopolymerization of Diacetylene Single Crystals. Optical Transmission Spectroscopy. *Chem. Phys. Lett.* **1978**, *53*, 39-44.

30. Bubeck, C.; Sixl, H.; and Wolf, H.C. ESR of the Low Temperature Photoproducts in a Diacetylene Single Crystal. *Chem. Phys.* **1978**, *32*, 231-237.

31. Bubeck, C.; Sixl, H.; and Neumann, W. ESR Analysis of the Initial Reaction Products in the Solid State Photopolymerization of Diacetylenes. *Chem. Phys.* **1980**, *48*, 269-275.

32. Neumann W.; and Sixl, H. The Kinetics of the Low-Temperature Photochemical Polymerization in a Diacetylene Single Crystal. *Chem. Phys.* **1980**, *50*, 273-280.

33. Neumann, W.; and Sixl, H. The Mechanism of the Low-Temperature Polymerization Reaction in Diacetylene Crystals. *Chem. Phys.* **1981**, *58*, 303-312.

34. Sixl, H.; and Neumann, W. The Mechanism of the Polymerization Reactions in Diacetylene Crystals: ESR Analysis of the Paramagnetic Reaction Intermediates. *Mol. Cryst. Liq. Cryst.* **1984**, *105*, 41-54.

35. Kudryavtsev, Y.P.; Sladkov, A.M.; Aseev, Y.G.; Nedoshivin, Y.N.; Kasatochkin, V.I.; and Korshak, V.V. Properties and Structure of Carbyne. *Dokl. Akad. Nauk SSSR* **1964,** *158*, 389-392.

36. Moss, W. N.; and Goroff, N.S. Theoretical Analysis of the 13C NMR of Iodoalkynes Upon Complexation with Lewis Bases. *J. Org. Chem.* **2005**, *70*, 802-808.

37. Goroff, N.S.; Curtis, S.M.; Webb, J.A.; Fowler, F.W.; and Lauher, J.W. Designed Cocrystals Based on the Pyridine-Iodoalkyne Halogen Bond. *Org. Lett.* **2005,** *7*, 1891-1893.

38. Webb, J.A. Small Molecule Carbon-Rich Compounds: from Polymerization to NMR Studies. PhD. Dissertation. SUNY Stony Brook, 2004.

39. Sun, A.; Lauher, J.W.; and Goroff, N.S. Preparation of Poly(diiododiacetylene), an Ordered Conjugated Polymer of Carbon and Iodine. *Science* **2006**, *312*, 1030-1034.

Chapter 2. Characterization of 1,4-poly(diiododiacetylene)

2.1 Introduction

The host molecules developed herein are designed crystals functionalized with Lewis basic tethers. Under ideal circumstances these compounds will co-crystallize with diiodobutadiyne and then undergo a single-crystal-to-single-crystal transformation to produce 1,4-poly(diiododiacetylene). For this reason, single-crystal XRD is expected to be the ideal method for characterizing both the monomer and polymer co-crystals. However, some of the samples reported here have demonstrated a loss of crystallinity during the topochemical polymerization reaction, making single-crystal XRD a less useful technique for analyzing the product materials. In cases where a heterogeneous polymerization has occurred, and only small crystallites containing the polymer are produced, or in cases where only a small percent of the sample has polymerized, single-crystal XRD may give falsely negative results or no structural information at all may be obtained.

For these reasons it has been necessary to develop other characterization methods for identifying the presence of 1,4-poly(diiododiacetylene) in the produced materials. This Chapter discusses the development of alternative methods for identifying the presence of polymer **2** within the co-crystal lattice. These methods include Raman spectroscopy, Magic Angle Spinning Nuclear

Magnetic Resonance (MAS-NMR), UV-visible spectroscopy, powder XRD, and Electron Spinning Resonance (ESR).

2.2 Single-Crystal XRD

As demonstrated in Chapter 1 of this dissertation, single-crystal XRD is the ideal technique for analyzing the high-quality co-crystals produced by these topochemical polymerizations. Not only can 1,4-poly(diiododiacetylene) be clearly seen in the crystal structures produced, but often the positions of all of the atoms present can be compared with those seen in the starting materials. This is because most of the starting materials are also high-quality crystal samples, even when the polymer containing co-crystals produced from them are not. Single-crystal XRD can demonstrate bond lengths in the polymer, allowing for comparisons between different polymer containing samples, and packing information that can be used to develop more efficient host molecules. Figure 2.1 contains the crystal structure of **M2/2**, a polymer containing co-crystal developed and discussed in Chapter 4.3 of this dissertation. The presence of 1,4-poly(diiododiacetylene) can be seen clearly. Figure 2.2 depicts the host molecule **M2**.

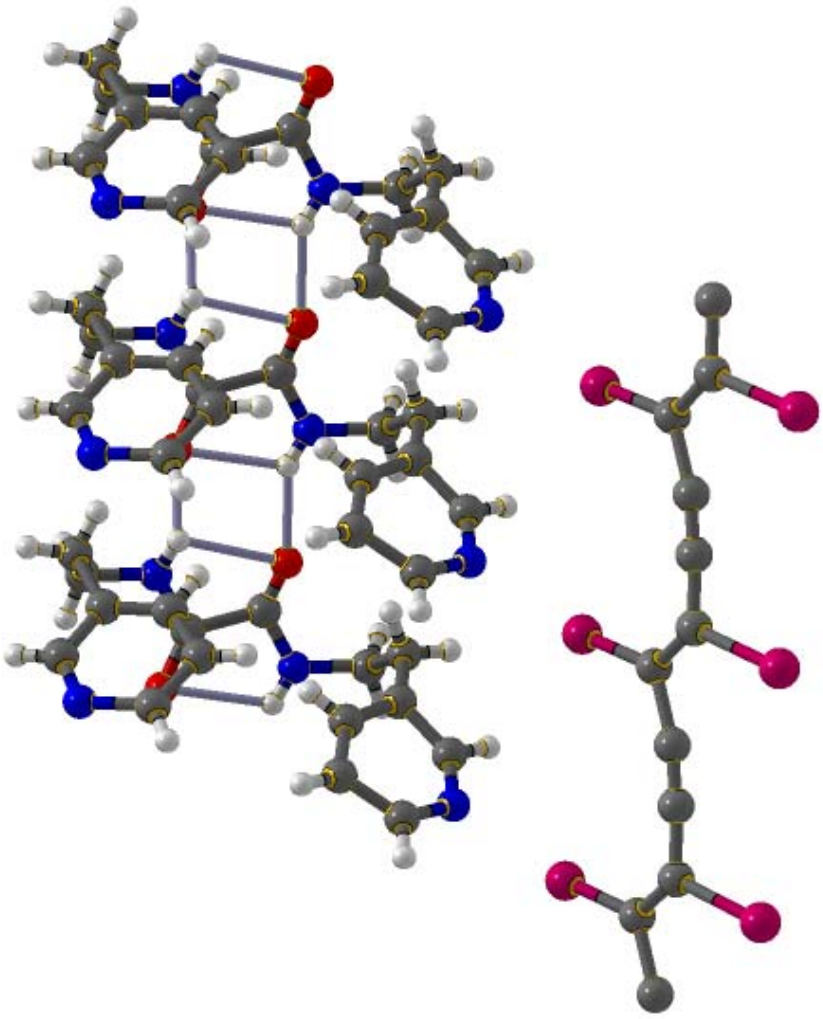

Figure 2.1 Crystal structure of **M2** host/diiodobutadiyne co-crystals indicating the presence of 1,4-poly(diiododiacetylene).

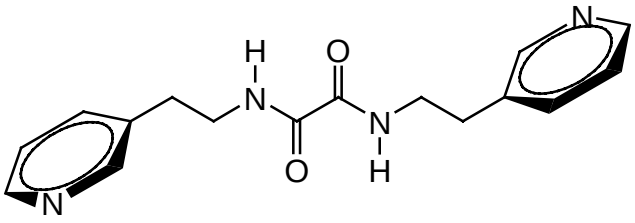

Figure 2.2 Host molecule **M2**.

2.3 Raman Scattering

The use of Raman spectroscopy as an analytical method for identifying the backbone of PDAs dates back to the 1970s and the work of Baughman.[40] However, like single-crystal XRD, this method also has inherent drawbacks. DFT calculations have demonstrated that a successful topochemical polymerization reaction will result in an exponential increase in the signals produced by the carbon-carbon double and triple bonds within the polymer back-bone.[38] This dramatic increase may result in a non-quatitative spectra.

This high degree of conjugation along the backbone of polydiacetylenes will create very intense peaks in Raman scattering experiments, and will lead to a distinct spectrum. Because Raman will detect the strongest scatterer in the sample by mass, a small amount 1,4-poly(diiododiacetylene) will drown out most other Raman active species present in these samples. This gives us the ability to identify the presence of very small amounts of polymer.

Co-crystals of **M2**/**2** produce three peaks in Raman, occurring at ~900, 1400, and 2100 cm^{-1}, see Figure 2.3. The peaks result from the presence of the single, double, and triple bonds (respectively) present in the polydiacetylene backbone. The Raman shifts of these peaks are consistent with DFT calculations performed on 1,4-poly(diiododiacetylene) by Jeffery Webb, and previously reported Raman spectra of other polydiacetylenes.[38,40-42]

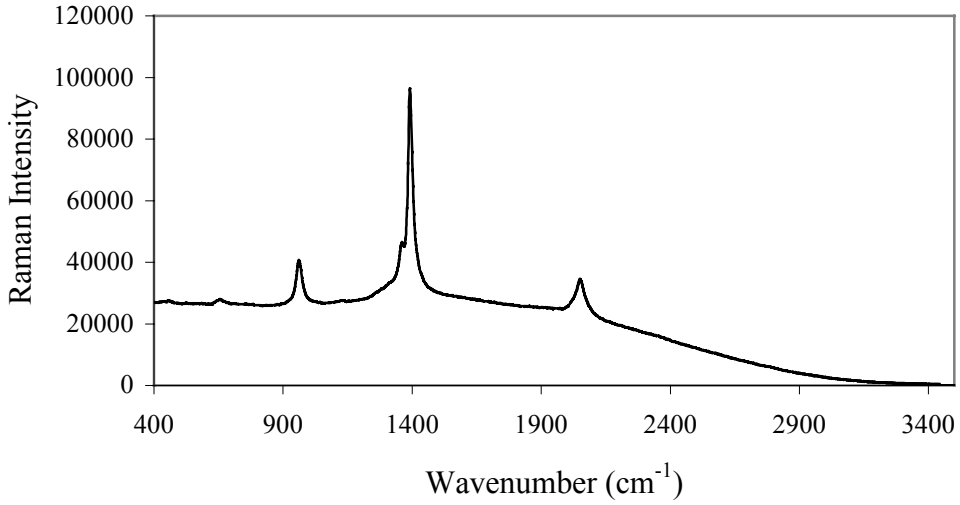

Figure 2.3 Raman spectrum produced by a co-crystal sample of **M2**/**2**, indicating the presence of three peaks occurring at ~900, 1400, and 2100 cm^{-1}.

2.4 MAS-NMR

The use of magic angle spinning nuclear magnetic resonance (MAS-NMR) for analyzing and identifying PDAs dates back to the 1980s.[43] Many PDAs are insoluble in common solvents, including 1,4-poly(diiododiacetylene), preventing the use of solution state NMR.[2,44] However, ^{13}C MAS-NMR is appropriate because our samples are designed to be solids and the polymerization reaction occurs at carbon atoms, the changes being identifiable in an NMR spectrum (^{13}C nuclei are NMR active). The isotropic chemical shifts of the C1 and C4 nuclei in the monomer and polymer should demonstrate a shift as their hybridization changes from sp to sp^2 during the topochemical polymerization reaction, see

Figure 2.4. This should make MAS-NMR a useful technique for analyzing samples that do not undergo a single-crystal-to-single-crystal transformation.

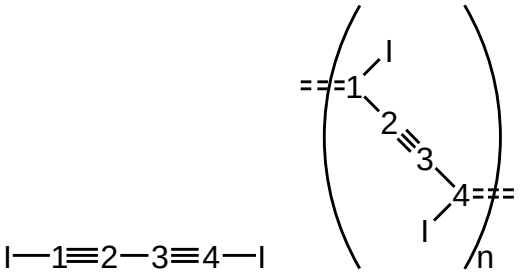

Figure 2.4 Carbon positions in monomer and polymer.

MAS-NMR also has advantages over both single-crystal XRD and Raman scattering as an analytical method. MAS-NMR can be more sensitive to local structural changes (such as bonding changes) than single-crystal XRD, particularly in amorphous or disordered materials. X-ray diffraction probes an average of the entire structure of a sample present in the cross-section of the x-ray beam, MAS-NMR, on the other hand, probes the individual environments of the nuclei present. This will give us the ability to see both the polymer and monomer if they co-exist in a sample, unlike single-crystal XRD and Raman spectroscopy.

A hydrogen-carbon cross-polarization (CP) experiment has been chosen because of both the slow relaxation time of the ^{13}C nucleus and its low natural abundance.[45] In a CP experiment, a dilute nucleus (in our case ^{13}C) derives its magnetization from a more abundant nucleus (in our case ^{1}H).[45] More importantly, the slow T_1 relaxation of the ^{13}C nuclei, which can be on the order of

minutes in the solid-state, can be over come because the CP experiment relies on the T_1 relaxation of the ^1H nuclei, which is much shorter. This allows for a shorter pulse delay, which means more scans can be collected in a given time, increasing the signal noise.

A RAMP CP improves the signal intensities observed in simple CP experiments by varying the cross-polarization field strength in a ramp of monotonically increasing amplitudes, which broadens the Hartman-Hahn match conditions. This allows efficient CP experiments to be performed, even when weak ^1H-^1H dipole coupling exists, while using fast magic angle spinning frequencies.[46] Fast MAS is required to produce simpler spectra with less overlapping peaks, requiring the use of a pulse sequence that works at high spinning speeds. The RAMP CP pulse sequence used in these experiments is depicted in Figure 2.5, where the X channel is tuned to carbon.

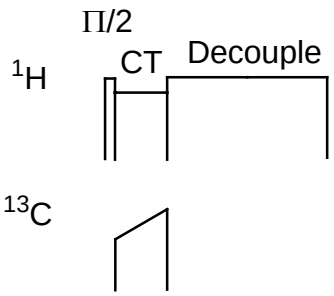

Figure 2.5 Cross-Polarization Pulse Sequence.[46]

When a ^{13}C MAS-NMR spectrum is taken at a spinning speed that is less than 3 or 4 times greater than the chemical shift anisotropy of carbon, "spinning

sidebands" are created in the spectrum.[45] Spinning sidebands are peaks that radiate out from the isotropic resonance at a distance equal to the spinning frequency. The isotropic chemical shift is not necessarily the most intense peak at slow spinning speeds, but one characteristic of the isotropic peak is that its frequency will not change with a change in spinning speed.[45] The ^{13}C CP MAS-NMR spectra of many of the samples reported here were taken at 3 spinning speeds; 6 kHz, 8 kHz, and 15 kHz. Only the 15 kHz spectra will be depicted in this dissertation because 15 kHz is a fast enough spinning speed to remove most of the spinning side-bands, however the peaks were compared at all 3 spinning speeds and the chemical shifts reported here were determined to be the isotropic chemical shifts.[47]

In order to follow the topochemical polymerization reaction, it is necessary to know, or assign, the isotropic chemical shifts of the C1,C4 and C2,C3 nuclei in both the monomer and polymer. The carbon labeling is depicted in Figure 2.6. To determine the chemical shifts of the monomer carbons ^{13}C CP MAS-NMR experiments were performed on various samples known to contain compound **1**, solution-state NMR experiments were also performed on diiodobutadiyne in solvents possessing different degrees of Lewis-Base strength, and DFT calculations were performed on both the monomer and polymer as depicted in Figure 2.6 at the LanL2DZ/B3LYP level of theory.[47]

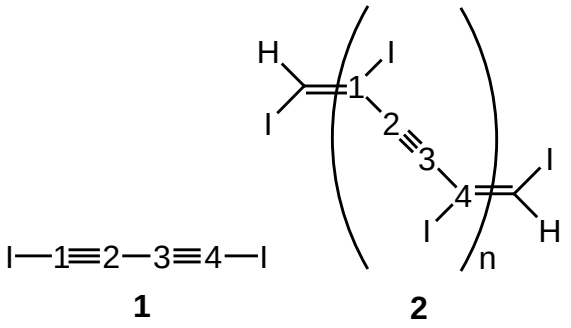

Figure 2.6 Nomenclature of carbon atoms in both the monomer and polymer for DFT calculations.

All of these experiments demonstrate the effect of a Lewis base on a terminal iodo-alkyne. Gao et. al. have demonstrated that when an iodoalkyne is associated with a Lewis base there are significant effects on the ^{13}C NMR chemical shifts.[48] Furthermore, Webb and coworkers have shown that an association with a pyridine molecule can change the chemical shift of the α-carbon by roughly 15 ppm.[49] Goroff and Moss showed that this results from the transfer of electron density from a nitrogen lone pair to the carbon-iodine anti-bonding orbital, and can shift the isotropic peak to a higher frequency when the iodine atom is associated with a Lewis base.[50] Figure 2.7, the spectrum resulting from a solution-state NMR experiment performed on diiodobutadiyne dissolved in pyridine$_{d5}$, shows that this results in isotropic chemical shifts of ~11 and 80 ppm for the C1,C4 and C2,C3 nuclei of compound **1** respectively. The result is a C1,C4 isotropic shift of more

than 17 ppm higher than that of diiodobutadiyne dissolved in hexanes$_{d14}$, see Figure 2.8.

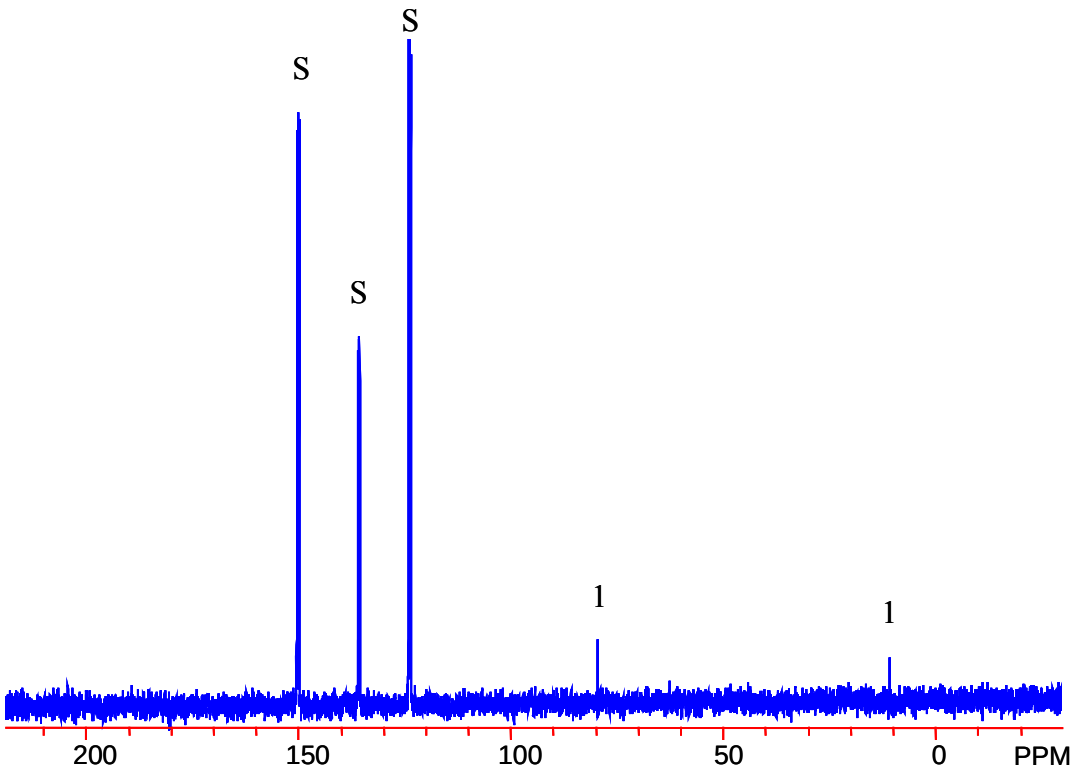

Figure 2.7 ^{13}C Solution State NMR of diiodobutadiyne in pyridine$_{d5}$ showing peaks at ~80 and 11 ppm, solvent peaks (S) centered at ~150, 136, and 124 ppm; the experiment was performed at 400 MHz.

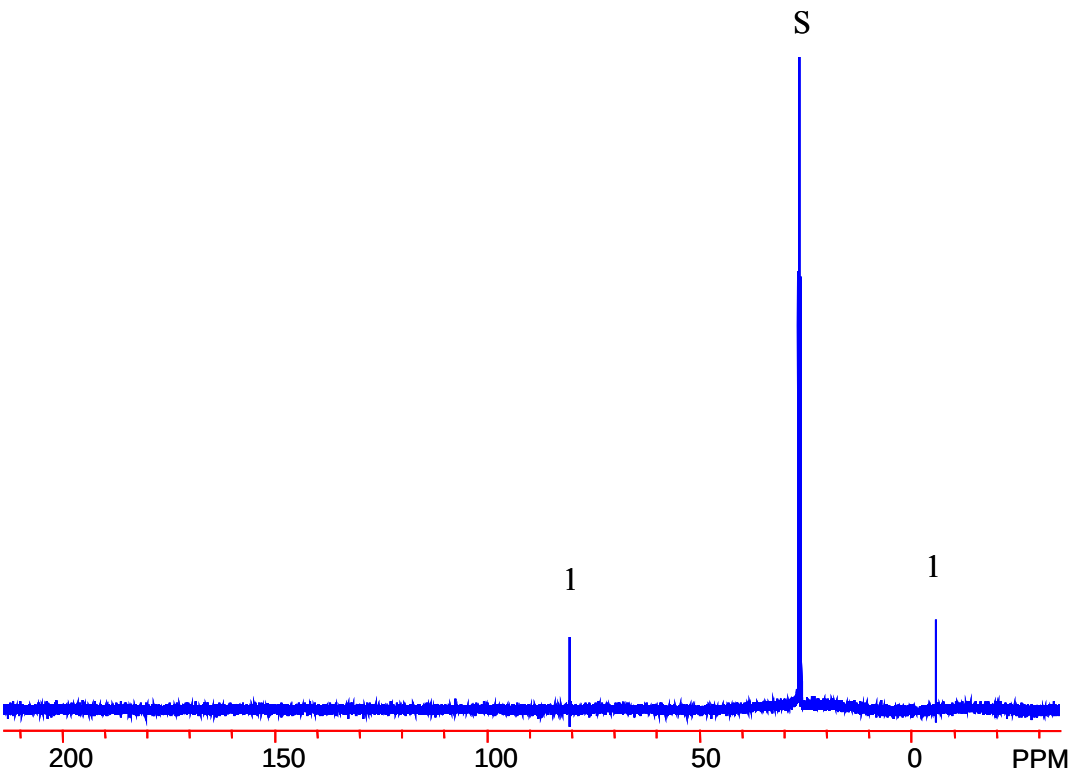

Figure 2.8 ^{13}C Solution State NMR of diiodobutadiyne in $hexane_{d14}$ showing peaks at ~81 and –6 ppm, solvent peak (S) centered at ~26 ppm; the experiment was performed at 400 MHz.

The effect of the Lewis-Base interaction in the solid-state can be clearly seen in Figure 2.9. In this Figure we see the ^{13}C CP MAS-NMR spectrum produced by a co-crystal sample of compound **1** and phenazine (in the inset of Figure 2.9). Phenazine contains only aromatic carbons, so there is no overlap with the isotropic chemical shifts produced by compound **1**, indicated by the blue arrows. This spectrum demonstrates that C1,C4 produce a peak at ~12 ppm, which is higher that the expected chemical shift of ~-5 ppm.

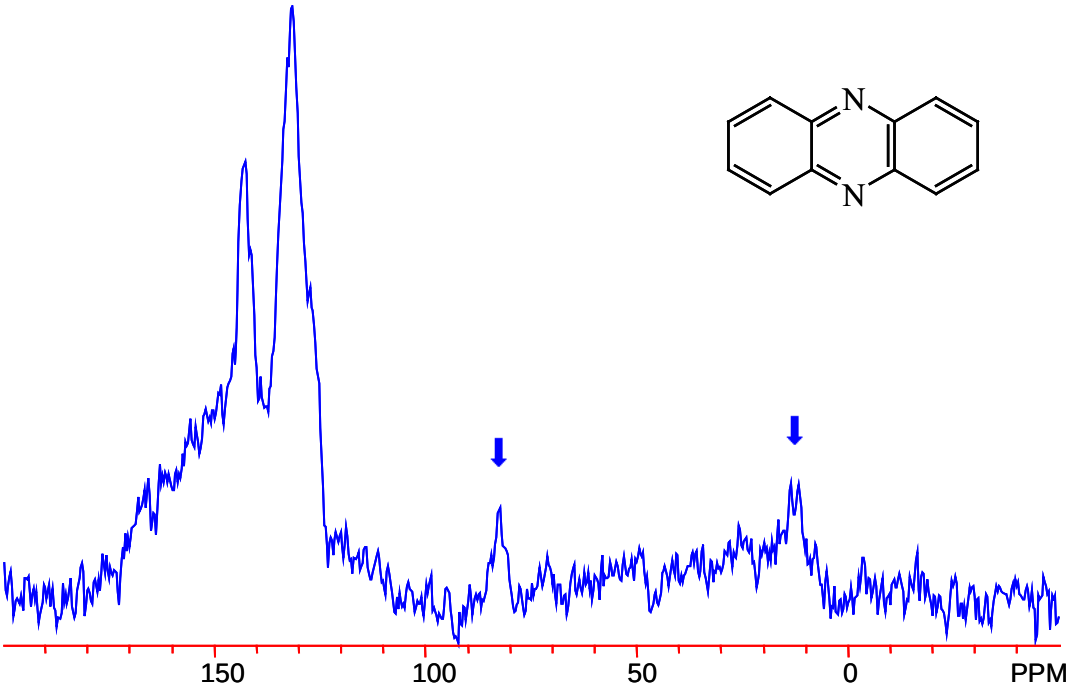

Figure 2.9 RAMP ^{13}C CP MAS-NMR spectrum of compound **1** and phenazine, diiodobutadiyne isotropic peaks are indicated with arrows; Experiment was performed at 500 MHz with a 15 kHz spinning speed.

Characterizing the isotropic peaks produced by the polymer was more difficult because a solution-state NMR of 1,4-poly(diiododiacetylene) could not be acquired. However, this task became more plausible when Aiwu Sun and Liang Luo developed a method for synthesizing polymer-bearing co-crystals in large enough quantities for ^{13}C CP MAS-NMR experiments.[39,44] Previously reported DFT calculations predicted that the C1,C4 and C2,C3 peaks in the polymer would resonate at ~90 and 110 ppm respectively.[47] ^{13}C CP MAS-NMR experiments performed on **N4**/**2**, a sample demonstrated by single-crystal XRD to contain PIDA, confirmed that these assignments are true. Host molecule **N4** is depicted

in Figure 2.10. Figure 2.11 depicts the ^{13}C CP MAS-NMR spectrum of **M2/2**, a second co-crystal demonstrated by single-crystal XRD to contain PIDA, further confirming these assignments.

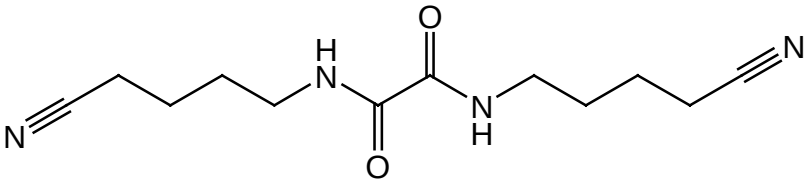

Figure 2.10 Host molecule **N4**.

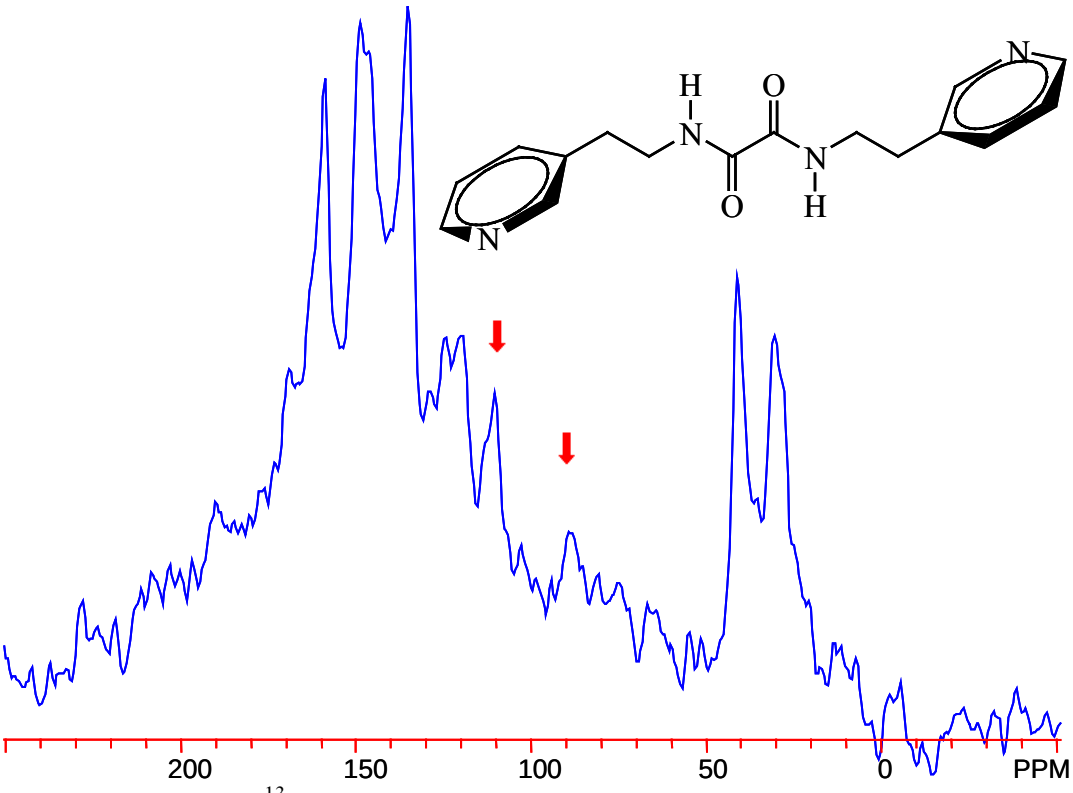

Figure 2.11 RAMP ^{13}C CP MAS-NMR spectrum of **M2/2**, polymer isotropic peaks are indicated by red arrows; Experiment was performed at 360 MHz with a 15 kHz spinning speed.

In the spectrum produced by the co-crystal sample of **M2**/**2** the carbon peaks demonstrate isotropic resonances at ~90 and 110 ppm respectively. The isotropic shifts produced by the C1,C4 nuclei in the **M2**/**2** co-crystal are ~10 ppm higher than those produced by the same carbon nuclei in the **N4**/**2** sample.[44] However, this can easily be accounted for by the lower Lewis base effect inherent in the **N4**/**2** sample. According to Webb et. al. the difference in the Lewis base effect of a nitrile group compared to a pyridyl group can be up to –8 ppm.[49]

2.5 UV-visible Spectroscopy

UV-visible spectroscopy of polydiacetylenes also dates back to the 1970s. The polymer itself, and its conjugated backbone produce a strong and unique UV-vis spectrum.[2] This technique may also useful for observing the topochemical polymerization reaction as it occurs.[51] The UV-Visible spectrum produced by a sample of **M2**/**2** co-crystals suspended in de-ionized water is shown in Figure 2.12 and is consistent with the typical spectrum produced by PDAs.[2]

One of the extremely useful benefits of UV-Vis as an analytical technique is that it allows for observation of the production of PIDA as it occurs. Host and guest molecules can be prepared at low temperatures to prevent spontaneous polymerization, and then placed into the spectrometer so the polymerization reaction can be observed.[44]

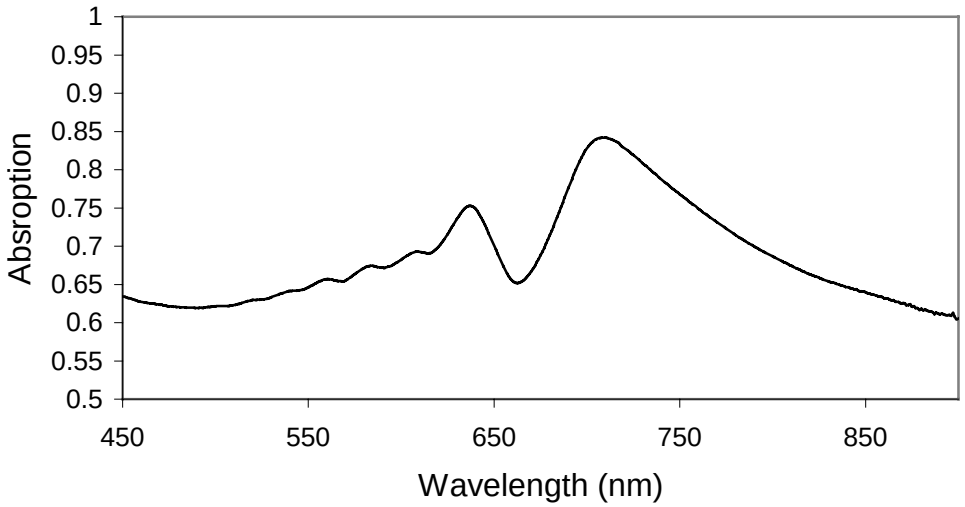

Figure 2.12 UV-visible spectrum of **M2**/**2** co-crystal sample sonicated in DI water.

2.6 Powder XRD

Powder XRD has also been used for analyzing polydiacetylene samples dating back to the 1980s.[52] While it is true that many of the samples reported here are not of sufficiently high quality to analyze using single-crystal XRD, they do appear to diffract x-rays. They may diffract strongly enough to produce powder patterns, which could give insight into changes in the crystal lattice as a result of polymerization. Since these topochemical polymerization reactions are expected to result in a decreased volume of the unit cell, this technique may prove useful.

However, thus far our samples have not demonstrated large changes in unit cell dimension upon topochemical polymerization. In one sample, co-crystals of **P1**/**1**, we see a significant change in the morphology of the crystal structure. This

is the one case where Powder XRD might be an adequate method for following the polymerization reaction. However, thus far the changes in the a-dimension of the unit cell are too small, compared to the error, to be an indication that polymerization has occurred. However, some Powder XRD studies have been carried out, and some high-resolution Powder XRD studies will be performed in the near future.

2.7 Characterization of PIDA and Reaction Intermediates

The characterization of isolated PIDA and the reaction intermediates produced during the topochemical polymerization reaction is more difficult task than characterizing the co-crystals samples. Once the supra-molecular scaffold is removed PIDA may no longer remain crystalline, likely eliminating single-crystal XRD as a viable analytical tool. Furthermore, with the removal of the host molecules it is no longer possible to use the RAMP CP pulse sequence, since PIDA contains no hydrogen nuclei for cross polarization. This likely limits the useful analytical tools to Raman spectroscopy, MAS-NMR single pulse programs, and UV-visible spectroscopy. The Raman and UV-visible spectra of isolated PIDA are reported in Chapter 5 of this dissertation, along with the MAS-NMR experiments performed on isolated PIDA. However, it is prudent to discuss the changes in the MAS NMR experiments necessary to study isolated PIDA here.

The lack of hydrogen in the PIDA polymer limits the number of useable MAS-NMR pulse sequences. The spectrum produced by a carbon 1-pulse experiment

performed on PIDA is shown in Figure 2.13. This spectrum further confirms the assignment of the isotropic peaks produced by the polymer. However, this technique is limited because PIDA is known to be a contact explosive and can react while the NMR rotor is being packed or while the sample is spinning at high speeds. A diagram of the pulse sequence that was used is depicted in Figure 2.14.

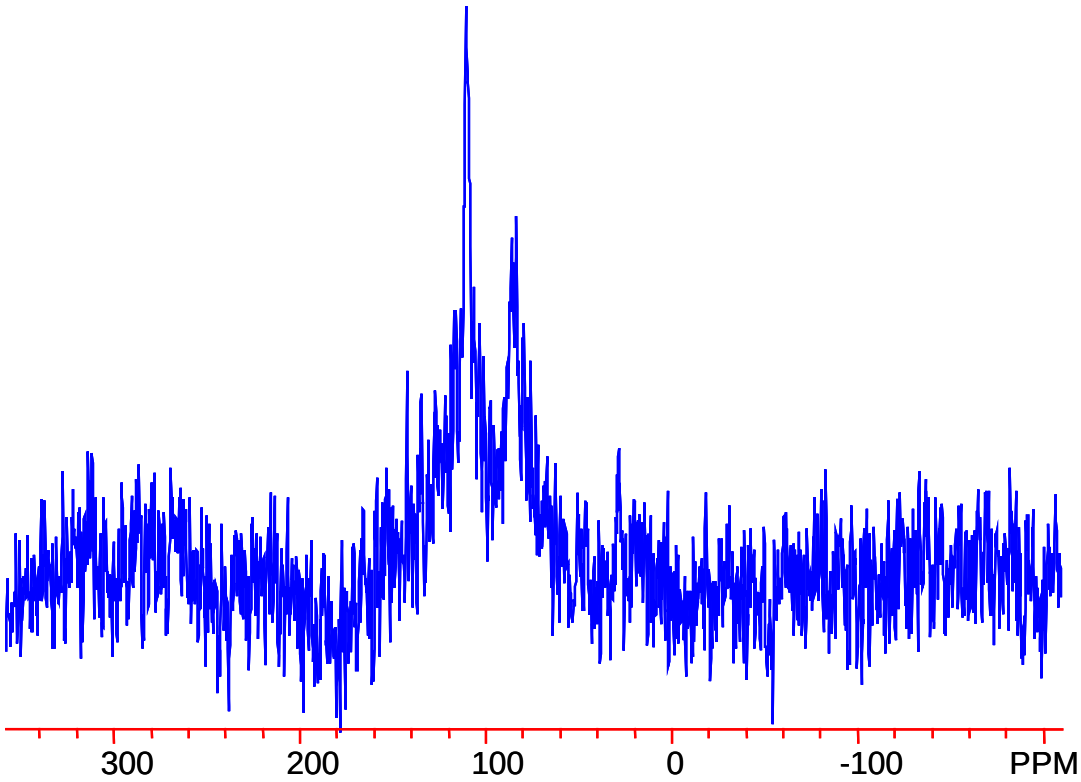

Figure 2.13 ^{13}C 1-Pulse MAS-NMR spectrum of **2** demonstrating isotropic shifts at ~110 and 85 ppm; Experiment was performed at 700 MHz with a 31 kHz spinning speed.

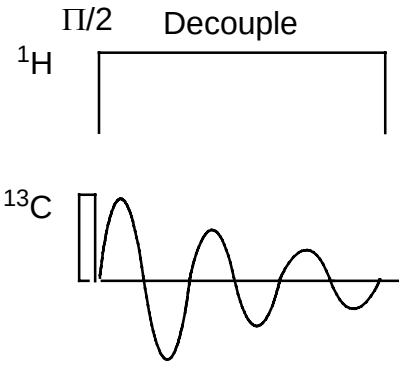

Figure 2.14 ^{13}C 1-Pulse Pulse Sequence with decoupling.[45]

In Chapters 3 and 5 of this dissertation partially polymerized co-crystal samples will be discussed. It may be possible to use these partially polymerized samples to study the intermediate species that are produced during the topochemical reaction. However, these species are expected to contain unpaired electrons, and therefore may be NMR invisible.[2] Therefore, Electron Spin Resonance (ESR) is being developed as a method for analyzing these samples.

2.8 Conclusions

Several useful methods for demonstrating that the desired topochemical polymerization reaction has occurred have been developed. These methods; Single-Crystal XRD, Raman Scattering, MAS-NMR and UV-vis; should prove more than adequate for analyzing any samples produced, and for indicating the presence of 1,4-poly(diiododiacetylene). These methods have also proven useful for incomplete polymerizations and in-situ polymerizations, and in cases where the polymer-containing product is no longer crystalline in nature. These

analytical methods have also been adapted for isolated PIDA. The development of these analytical methods have allowed this project to move forward such that a variety of host molecules can be developed, co-crystallized with diiodobutadiyne, and the samples produced can be analyzed for the effectiveness of the host material towards producing 1,4-poly(diiododiacetylene).

2.9 Experimental

Compounds and Co-Crystals

Compound 1
Diiodobutadiyne was synthesized according to the previously published procedure.[38]

Compound M2
Bis-pyridyl-oxalamide **M2** was synthesized according to procedure reported in Chapter 4 of this dissertation.

Co-crystals
Co-crystals of **M2**/**1** were prepared by dissolving compounds **M2** and **1** in warm methanol in a 1:1.5 ratio. The solution was subjected to centrifugation and decanted into a crystallization dish. The dish was covered with perforated aluminum foil and the solvent was allowed to evaporate.

Single-Crystal X-Ray Diffraction
Crystals were obtained as described, and then selected with an optical microscope and epoxied on thin glass fibers. The crystal was centered and the x-ray intensity data were measured on a Bruker AXS diffractometer. The data were collected using graphite-monochromated Mo radiation and then structures were solved by direct methods and refined using full matrix least squares methods (SHELX97). SHELX97 – Programs for Crystal Structure Analysis (Release 97-2): G.M. Sheldick, SHELX-98, Program for the Solution of Crystal Structures, University of Göttingen, Göttingen (Germany), 1998.

Raman Spectroscopy

Raman spectroscopy was performed using a Thermo Nicolet Almega dispersive Raman spectrometer coupled with an infinity corrected, confocal design microscope. The spectrometer uses a 785 nm class I laser, and the data were collected in the reflection mode of the microscope at a slit width of 25 μm. The data were collected and analyzed using the Omnic software suite (Nicolet, USA).

RAMP ^{13}C CP MAS-NMR

All RAMP ^{13}C CP MAS-NMR spectra were taken at room temperature using either a Varian Infinity Plus 500 NMR spectrometer or a Varian Infinity Plus 360 NMR spectrometer (as noted in the Results section), with either the 5 mm double resonance probe or 4 mm double resonance probe, (as noted in the Results section), with the 5 mm or 4 mm zirconia rotor respectively. The probe was tuned to 125.7 MHz for ^{13}C and 499.8 MHz for ^{1}H on the Varian Infinity Plus 500 NMR spectrometer and 90.5 MHz for ^{13}C and 360.0 MHz for ^{1}H on the Varian Infinity Plus 360 NMR spectrometer (as noted in the Results section). The ^{13}C MAS-NMR spectra were collected using a CP RAMP pulse program with a contact time of 2ms, a pulse delay of 2s.[46] The number of steps in the CP RAMP ranged from 8-12 and the amplitude step size ranged from .001 to .01. These parameters lead to an X channel amplitude range of .2050-.6500 for the Varian Infinity Plus 500 NMR spectrometer and .3100-.4000 for the Varian Infinity Plus 360 NMR spectrometer. Over 1000 scans were acquired. Hexamethylbenzene (HMB) was used to set the Hartman-Hahn match condition, the 131 ppm resonance acting as a secondary reference.

Solution State NMR

Solvents were used as purchased without further purification. Diiodobutadiyne was dissolved in $pyridine_{d5}$ and $hexanes_{d14}$. NMR spectra were collected at 25° C using a Varian 400 operating at 100.5 MHz for ^{13}C.

UV-visible Spectroscopy

All UV-visible spectroscopy were taken at room temperature using a Cary 100 UV/Visible Scan Spectrophotometer scanning from 450 to 900 nm with a resolution of 1 nm.

^{13}C 1-Pulse MAS-NMR

^{13}C 1-Pulse MAS-NMR spectra were taken at room temperature using a Bruker Advance 700 NMR spectrometer, with the 2.5 mm double resonance probe, with the 2.5 mm zirconia rotor spinning at 31 kHz. The probe was tuned to 176.1 MHz. The ^{13}C MAS-NMR spectra were collected using a ^{13}C 1-Pulse pulse program with decoupling, and a pulse delay of 10s. Over 1000 scans were acquired.

2.10 References.

2. Bassler, H.; Sixl, H.; and Enkelmann, V. *Adv. Polymer Sci. 63: Polydiacetylenes*.; 63; H.-J. Cantow: Springer-Verlag, 1984.

38. Webb, J.A. Small Molecule Carbon-Rich Compounds: from Polymerization to NMR Studies. PhD. Dissertation. SUNY Stony Brook, 2004.

39. Sun, A.; Lauher, J.W.; and Goroff, N.S. Preparation of Poly(diiododiacetylene), an Ordered Conjugated Polymer of Carbon and Iodine. *Science* **2006**, *312*, 1030-1034.

40. Baughman, R.H.; Witt, J.D.; Yee, K.C. Raman spectral shifts relevant to electron delocalization in polydiacetylenes. *J. Chem. Phys.*, **1974**, *60*, 4755-4759.

41. Exarhos, G.J.; Risen, W.M.; and Baughman, R.H. Resonance Raman Study of the Thermochromic Phase Transition of a Polydiacetylene. *J. Am. Chem. Soc.*, **1976**, *98*, 481-487.

42. Iqbal, Z.; Chance, R.R.; and Baughman, R.H. Electronic Structure Change at a Phase Transition in a Polydiacetylene Crystal. *J. Chem. Phys.*, **1977**, *66*, 5520-5525.

43. Galambos, A.F.; Stockton, W.B.; Koberstein, J.T.; Sen, A.; Weiss, R.A.; and Russell, T.P. Study of the Thermochromic Phase Transition of Polydiacetylene by Solid State ^{13}C NMR. *Macromol.*, **1987**, *20*, 3094-3097.

44. Luo, L.; Wilhelm, C.; Sun, A.; Grey, C.P.; Lauher, J.W.; and Goroff, N.S. Poly(diiododiacetylene): Preparation, Isolation, and full Characterization of a Very Simple Poly(diacetylene). *J. Am. Chem. Soc.*, **2008**, *130*, 7702-7709.

45. Duer, M. J. *Introduction to Solid State NMR Spectroscopy*, Blackwell Publishing Limited: Malden, 2004.

46. Metz, G.; Wu, X.; and Smith, S. Ramped-Amplitude Cross Polarization in Magic-Angle-Spinning NMR. *J. Mag. Res. A*, **1994,** (110), 219-227.

47. Wilhelm, C.; Boyd, S.A.; Chawda, S.; Fowler, F.W.; Goroff, N.S.; Halada, G.P.; Grey, C.P.; Lauher, J.W.; Luo, L.; Martin, C.D.; Parise, J.B.; Tarabrella, C.; Webb, J.A. Pressure-Induced Polymerization of Diiodobutadiyne in Assembled Co-crystals. *J. Am. Chem. Soc.*, **2008**, *130*, 4415-4420.

48. Gao, K.; and Goroff, N.S. Two New Iodine Capped Rods. *J. Am. Chem. Soc.* **2000**, (122), 9320-9321.

49. Webb, J.A.; Klijn, J.E.; Hill, P.A.; Bennett, J.L.; Goroff, N.S. Experimental Studies of the 13C NMR of Iodoalkynes in Lewis-Basic Solvents. *J. Org. Chem.* **2004**, *69*, 660-664.

50. Moss, W. N.; and Goroff, N.S. Theoretical Analysis of the 13C NMR of Iodoalkynes Upon Complexation with Lewis Bases. *J. Org. Chem.* **2005**, *70*, 802-808.

51. Wenz, G.; Müller, M.A.; Schmidt, M.; and Wegner, G. Structure of Poly(diacetylenes) in Solution. *Macromol.*, **1984**, *17*, 837-850.

52. Iqbal, Z.; Murthy, N.S.; Khanna, Y.P.; Szobota, J.S.; Dalterio, R.A.; and Owens, F.J. The Mechanism of the Solid State Phase Transitions in the Polydiacetylene, Poly-4BCMU: Thermal, X-ray Diffraction and Raman Scattering Studies. *J. Phys. C.: Solid State Phys.*, **1987**, *20*, 4283-4295.

Chapter 3. Pressure Induced Polymerization of Diiodobutadiyne

3.1 Introduction and Background

The single-crystal XRD work of Curtis and Webb in 2005 demonstrated that no spontaneous polymerization reaction occurs in either the **M1**/**1** or **P1**/**1** co-crystal systems, even when they are exposed to ambient light. Their work also indicated that heat, UV- and γ-radiation failed to induce polymerization in the **M1**/**1** co-crystal system.[37] Finally, in a collaborative effort with the research group of Dr. John Parise, Webb and C. David Martin tested mechanical strain as a method for inducing the topochemical polymerization within the **P1**/**1** co-crystal system. Webb and Martin exposed a single-crystal sample of the **P1**/**1** co-crystals to pressures up to 7 GPa in a diamond anvil cell (DAC), shown in Figure 3.1.[53] During these experiments, two distinct color changes were observed in the crystal sample, depicted in Figure 3.1.

The color transitions, both from colorless to blue and from blue to black, are irreversible, with the color change remaining after the pressure is removed. This indicates that a non-reversible change is occurring within the crystal. The first color change that Webb and Martin observed occurred at 2-3 GPa. It started with a pocket of blue color that then spread throughout the crystal. This phase will be referred to as the "blue phase" of the co-crystal system throughout this

dissertation. The second color change, from blue to black, was observed at 4-7 GPa and resulted in what will be referred to as the "black phase".[38]

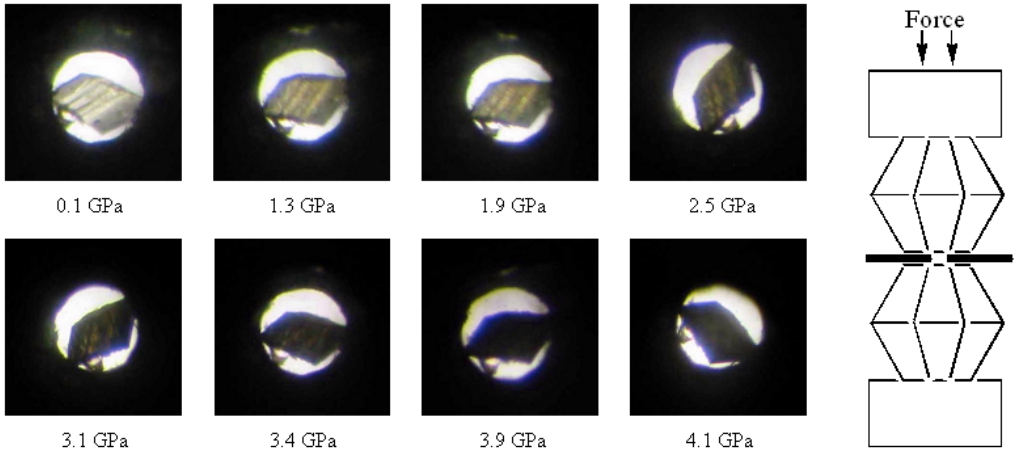

Figure 3.1 Demonstration of the color change observed throughout the pressure study of the **P1**/**1** co-crystals, single-crystal sample; and a reproduced schematic of the diamond anvil press (DAC).[38]

These color changes are a possible indication that diiodobutadiyne, within this co-crystal lattice, undergoes a topochemical, 1,4 polymerization when exposed to mechanical strain. However, Webb's single-crystal XRD experiments indicated that the blue phase of the **P1/1** co-crystal system contained only the diiodobutadiyne monomer with no evidence of polymerization, although a change in the morphology of the unit cell was observed.[38] Webb further showed that the black phase of this co-crystal system is not a high-quality crystal, and no structural information can be obtained from single-crystal XRD studies.[38]

Webb then measured the Raman vibrational spectra of samples of the **P1/1** co-crystals. Un-pressed co-crystal samples containing the monomer, blue phase co-crystal samples, and black phase co-crystal samples were all studied by Webb using Raman vibrational spectroscopy.[38] The Raman spectrum of the starting phase **P1**/**1** co-crystal sample contained multiple peaks of low intensity, however the blue phase **P1/1** co-crystal contained only three peaks, ~900, ~1300, and ~2000 cm^{-1}, of far greater intensity than the starting material.[38] The black phase **P1**/**1** co-crystal demonstrated a large amount of fluorescence when exposed to Raman scattering, and no structural information could be obtained.

Webb then compared these results with the results of Density Functional Theory (B3LYP/LanL2DZ) calculations that were designed to predict the Raman spectra intensities and shifts produced by a growing oligomer-chain of 1,4-poly(diiododiacetylene).[38] The calculations demonstrate that the Raman signals produced by the double and triple bond in a growing oligomer increase exponentially in intensity and shift to lower frequencies as monomer units are added. According to the calculations, this increase in intensity leads the double and triple bond signals to dominate the spectrum, with peaks at ~1500 and ~2180 cm^{-1} respectively.[38] These calculations correlate nicely with the actual Raman spectrum of the **P1/1** co-crystal sample that Webb measured. Webb was left with two contradictory results. Single-crystal XRD indicted that no polymerization had occurred. However, Raman spectroscopy correlated closely to DFT

calculations and literature precedence to indicate that diiodobutadiyne had in-fact successfully polymerized.

The contradictory results that Webb obtained are not unusual. As Chapter 2 of this dissertation discusses, both single-crystal and Raman scattering can lead to false results. For this reason, a more in-depth study of the 1,4-polymerization of diiodobutadiyne within both the **M1**/**1** and **P1**/**1** co-crystal systems was initiated. A series of ^{13}C CP MAS-NMR experiments, in conjunction with single-crystal XRD and Raman Spectroscopy experiments, were performed on samples of both the **M1**/**1** and **P1**/**1** co-crystal systems after varying amounts of external pressure were applied.

^{13}C CP MAS-NMR and Raman spectroscopy were used because both of these samples had already demonstrated a lack of crystallinity in the black phase. However, because of the decision to use ^{13}C CP MAS-NMR as an analytical method, we could no longer rely on the diamond anvil cell (DAC) as the source of mechanical stress. The DAC is used to press single crystal samples, but ^{13}C CP MAS-NMR requires a large amount of powder sample, so a Multi-Anvil Press (MAP) was used in conjunction with the DAC as a pressure source.[54] Figure 3.2 depicts a schematic of a Multi-Anvil Press. The pressure readings on the MAP are less accurate, since they are based on the pressure of the hydraulic fluid in the lines of the press and there can be a large amount of sheer in the powder sample,

so visual inspection of the sample's color change was used to determine that the powder samples had entered the proper crystal-phase.

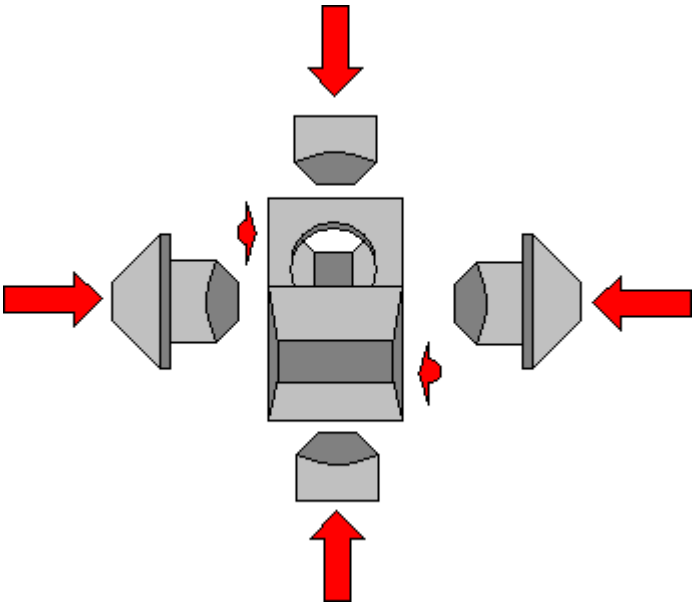

Figure 3.2 Reproduced schematic of a multi-anvil press.[54]

3.2 The Pressure Study

First, a polarized light microscopy (PLM) study of freshly pressed single-crystal samples was performed. The two samples analyzed in this manner were the **M1/1** black phase co-crystals and the **P1/1** blue phase co-crystals. Both co-crystal samples were visually inspected and determined to have entered the proper crystal-phase. Both the **M1**/**1** and **P1**/**1** co-crystal samples exhibit anisotropic coloring when rotated through a field of polarized light. This is strong evidence that the color of these samples is being produced by an ordered structure within the co-crystal.

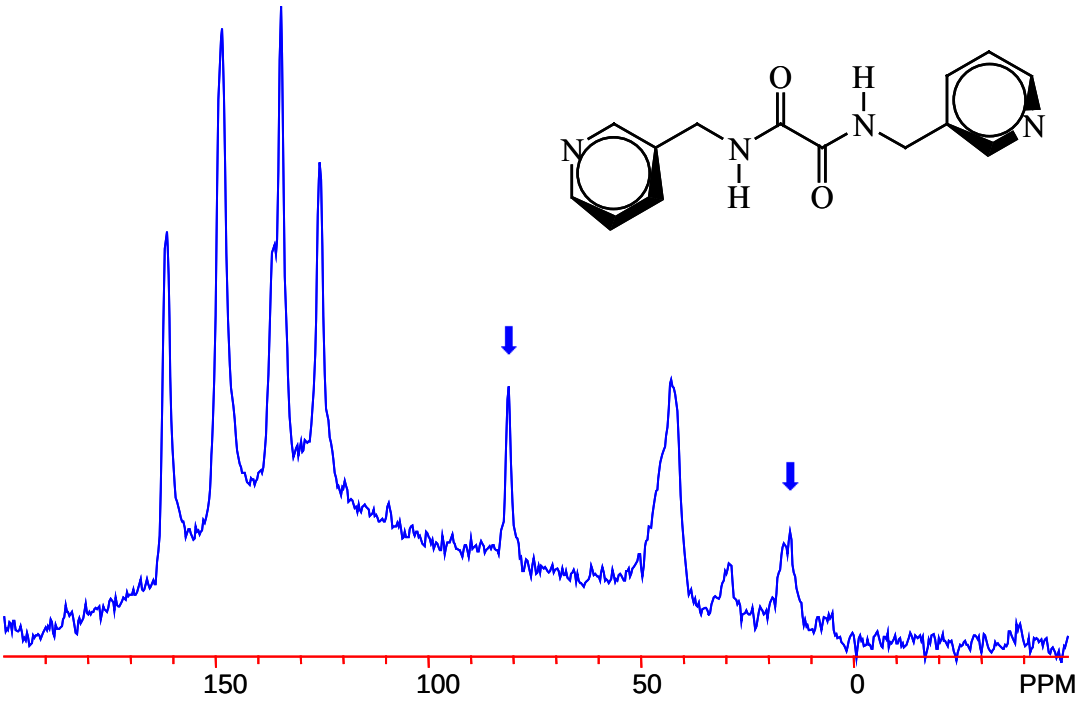

Figure 3.3 RAMP ^{13}C CP MAS-NMR spectrum of **M1/1**, host and guest isotropic peaks are indicated with arrows, all other peaks are due to spinning sidebands; Experiment was performed at 500 MHz with a 15 kHz spinning speed.

Fresh powder samples of **M1**/**1** and **P1**/**1** co-crystals were produced and ^{13}C CP MAS-NMR experiments were performed on both samples, the spectra are shown in Figures 3.3 and 3.4 respectively. Both samples demonstrate characteristic isotropic chemical shifts at ~20 ppm and ~81 ppm corresponding to the C1/C4 and C2/C3 nuclei respectively, indicated by blue arrows in the figures. The MAS-NMR peaks produced by the host molecules can also be seen in these figures, but are unmarked. The assignment of the peaks produced by the host molecule and monomer are further confirmed in the ^{13}C CP MAS-NMR spectrum of compound **M1**. This spectrum is shown in Figure 3.5.

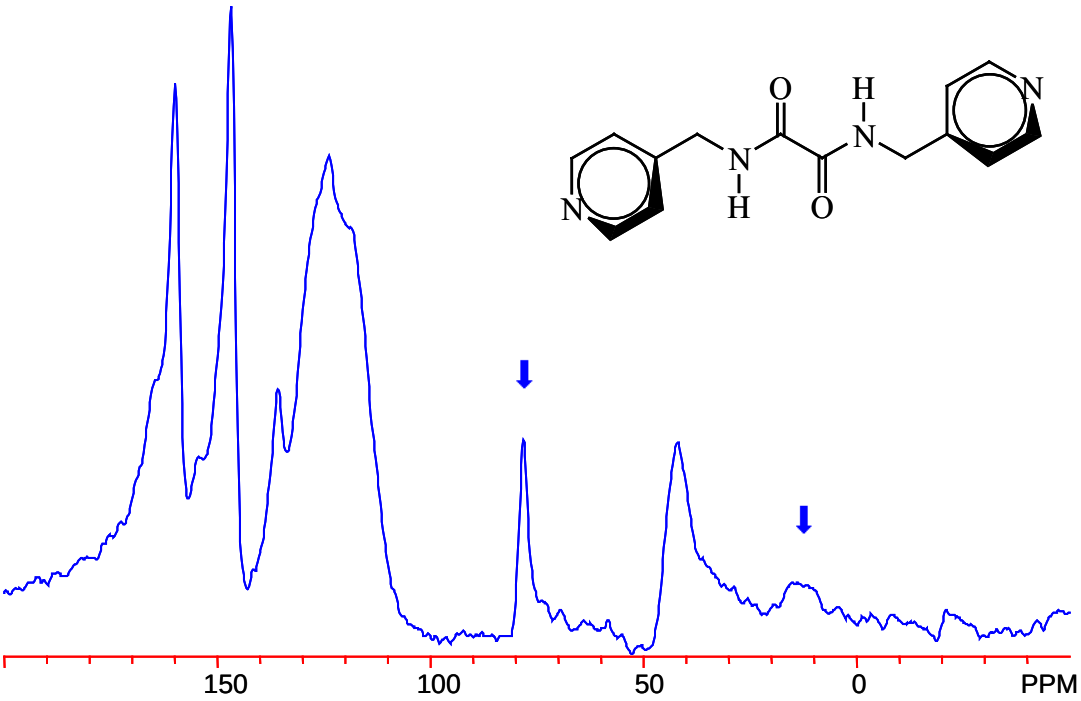

Figure 3.4 RAMP ^{13}C CP MAS-NMR spectrum of **P1/1**, host and guest molecules are indicated with arrows, all other peaks are due to spinning sidebands; Experiment was performed at 360 MHz with a 15 kHz spinning speed.

Raman spectra of the **M1**/**1** and **P1**/**1** co-crystal samples were also collected. These spectra demonstrate the presence of the monomer only. Again, this is indicated by the presence of multiple, low-intensity peaks. See Figures 3.6 and 3.7. The analysis of these results are consistent with both the single-crystal XRD results reported in Chapter 1 and DFT calculations performed on both the monomer and polymer structures.[38,47]

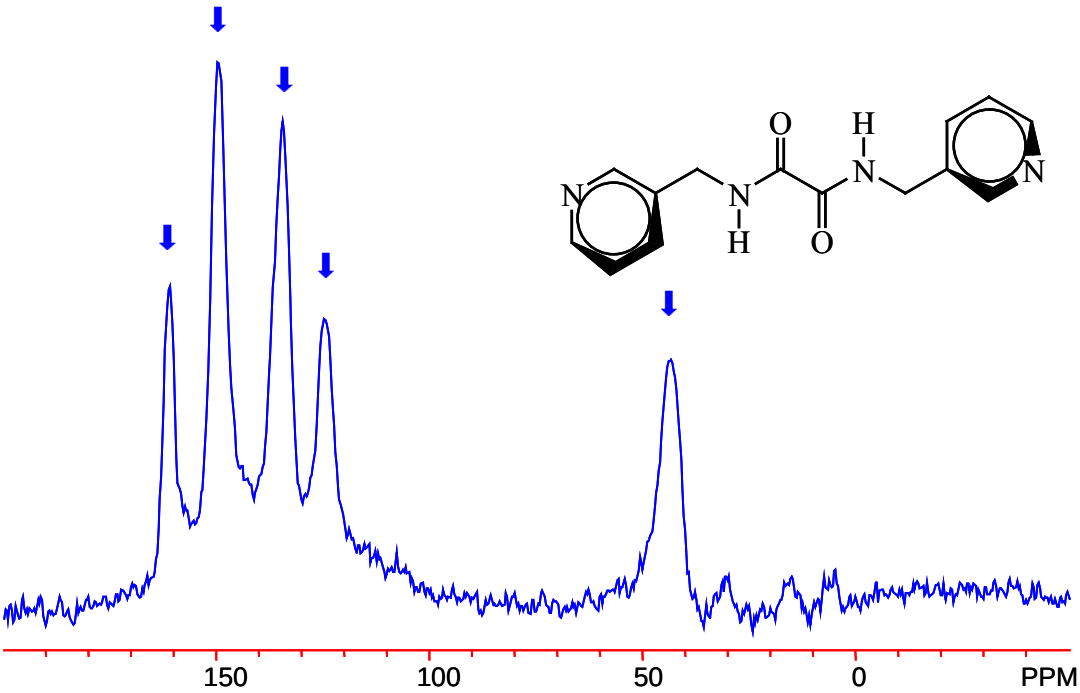

Figure 3.5 RAMP ^{13}C CP MAS-NMR spectrum of **M1**, host isotropic peaks are indicated with arrows, all other peaks are due to spinning sidebands; Experiment was performed at 500 MHz with a 15 kHz spinning speed.

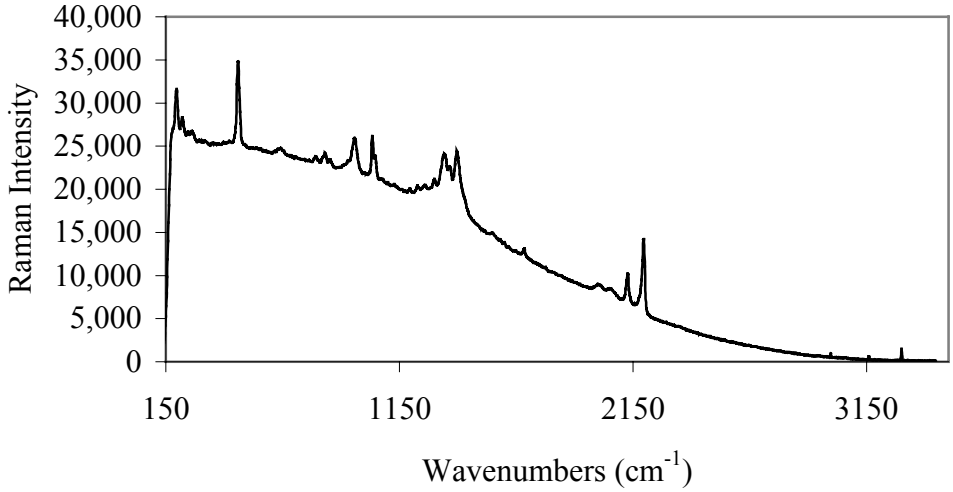

Figure 3.6 Raman spectrum of starting phase **M1**/**1** co-crystal sample, indicating the absence of polymer **2**.

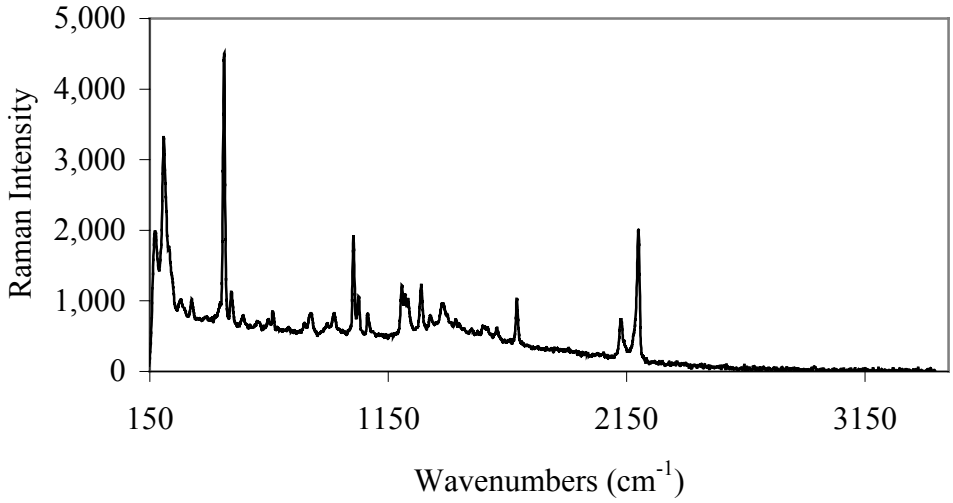

Figure 3.7 Raman spectrum of starting phase **P1**/**1** co-crystal sample, indicating the absence of polymer **2**.

Single-crystal samples were then selected from both batches of co-crystals, and using the DAC, both samples were pressed to ~2.5 GPa. Both the **M1**/**1** and **P1**/**1** co-crystal samples were visually inspected and observed to have entered to blue crystal-phase of the co-crystal lattice. These samples were then analyzed using Raman spectroscopy and single-crystal XRD.

The Raman spectra of both the **M1**/**1** and **P1**/**1** co-crystal samples in the blue-crystal phase demonstrate a significant and similar change. Figures 3.8 and 3.9 show a dramatic increase in three of the Raman scattering peaks, occurring at ~900, ~1300, and ~2000 cm^{-1}. These results are consistent with the presence of polymer **2**, and indicate a successful 1,4 topochemical polymerization reaction.

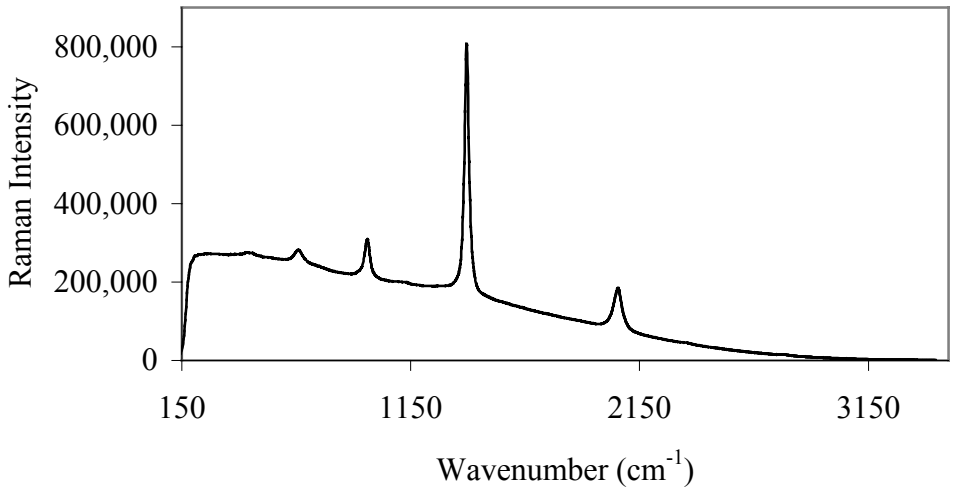

Figure 3.8 Raman spectrum of blue phase **M1**/**1** co-crystal sample, indicating the presence of polymer **2**.

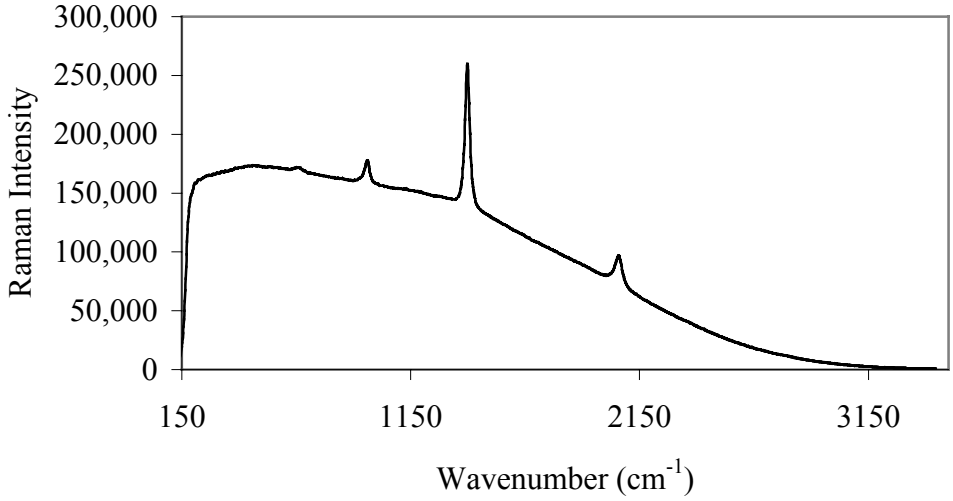

Figure 3.9 Raman spectrum of blue phase **P1**/**1** co-crystal sample, indicating the presence of polymer **2**.

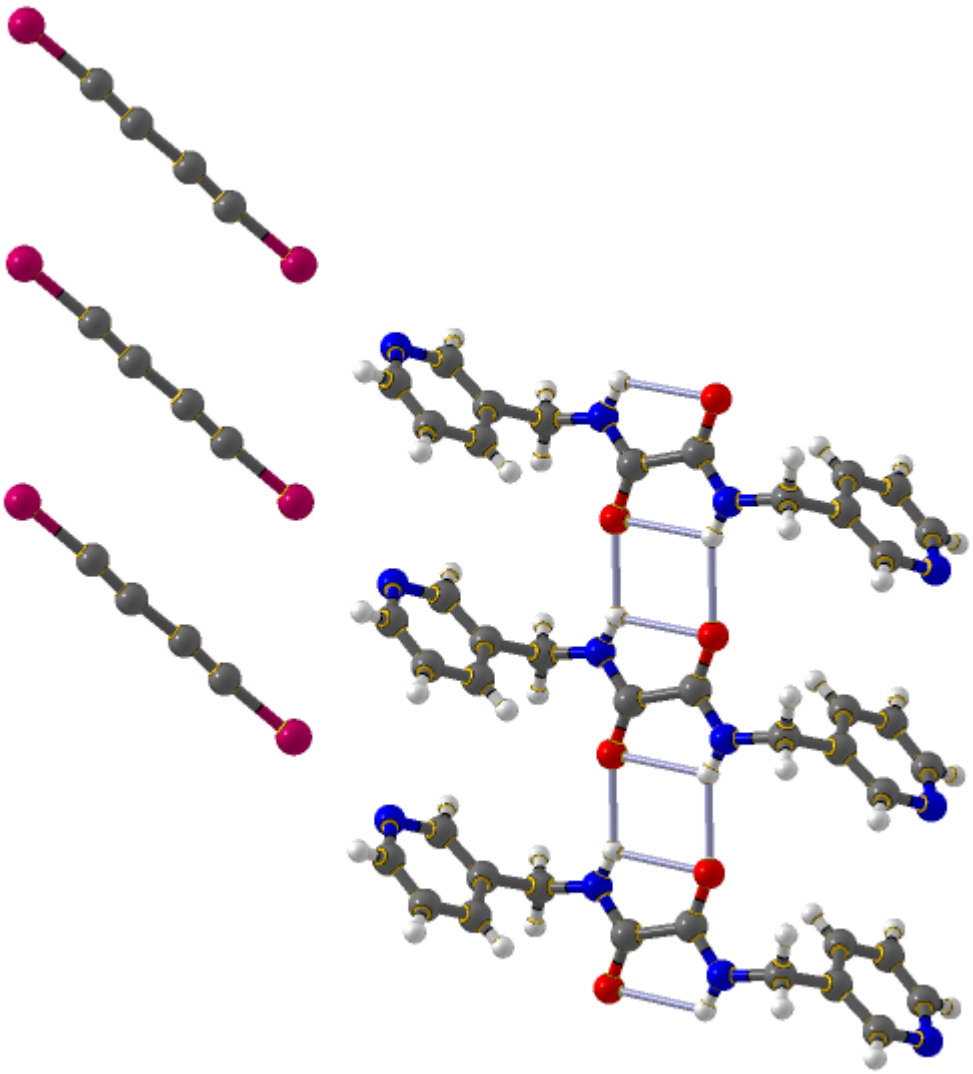

Figure 3.10 Single-crystal structure of blue phase **M1**/**1** co-crystal sample in blue phase, indicating absence of polymer **2**.

However, consistent with Webb's results, single-crystal XRD indicates the absence of polymer **2** in both single-crystal samples. Figures 3.10 and 3.11 clearly depict that only the monomer is present within the co-crystal lattice. The crystal structure of the blue **M1**/**1** co-crystal sample demonstrates a shorter C1-C4

distance, but since the error in this sample has increased this is inconclusive evidence of polymerization. The crystal structure of the **P1**/**1** co-crystal demonstrates the introduction of a new point of symmetry within the unit cell as a result of the twisting of one of the pyridyl rings in the host molecule. However, no evidence of polymerization is observed within either co-crystal system.

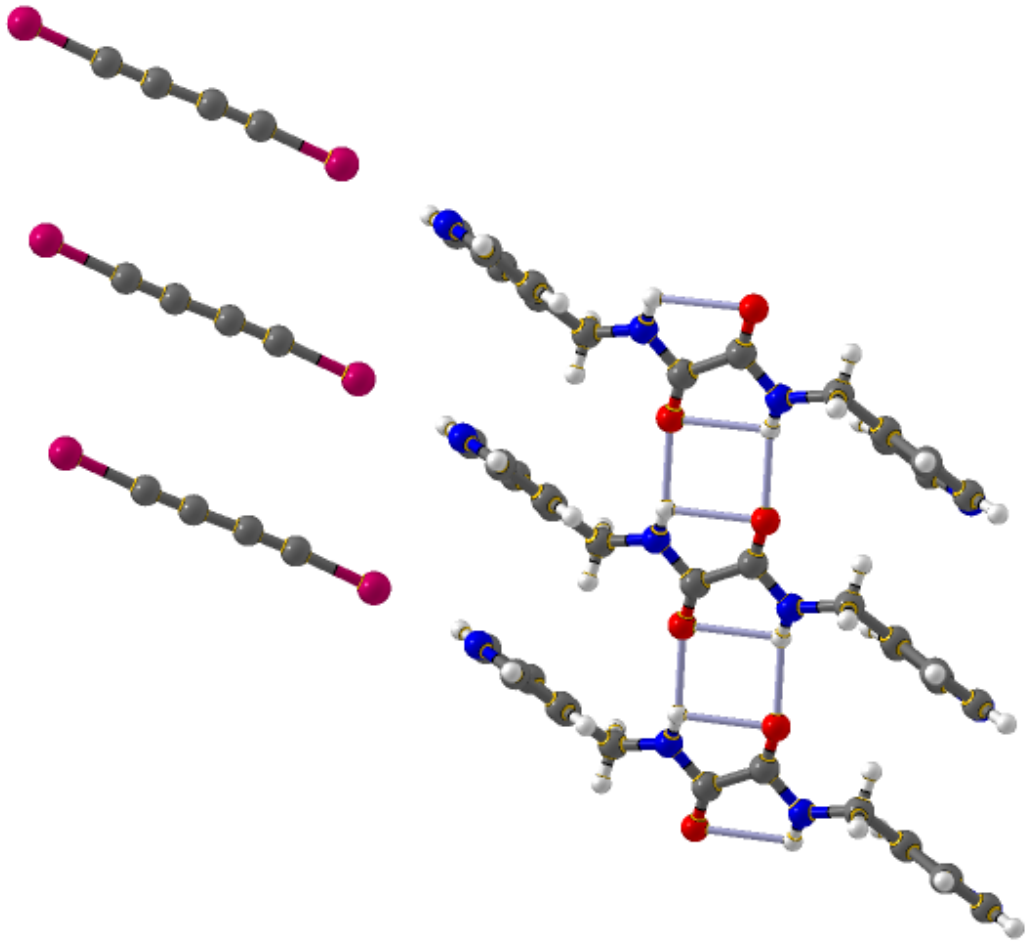

Figure 3.11 Single-crystal structure of blue phase **P1**/**1** co-crystal sample in blue phase, indicating absence of polymer **2**.

Powder samples were then taken from both batches of co-crystals, pressed in the MAP to >6 GPa, visually inspected, and observed to have entered the black crystal-phase. Single-crystal XRD and Raman scattering experiments performed on single-crystal black phase samples of both co-crystals give only amorphous results. However, when these powder samples are subject to ^{13}C CP MAS-NMR experiments the results are very clear. The ^{13}C CP MAS-NMR spectra of both the **M1**/**1** and **P1/1** co-crystal samples demonstrate a loss of intensity of the isotropic peaks attributed to the diiodobutadiyne monomer, and an increase in the intensity of the isotropic peaks attributed to 1,4-poly(diiododiacetylene). The **M1**/**1** co-crystal system demonstrates ~90% polymerization and the **P1**/**1** co-crystal system demonstrates ~55% polymerization after integration. Both samples demonstrate the same isotropic chemical shifts as those produced by the C1/C4 and C2/C3 nuclei in the **M2**/**2** co-crystals, as shown in Chapter 2 of this dissertation.

Figure 3.12 depicts the ^{13}C CP MAS-NMR spectrum measured from the powder sample of **M1**/**2** co-crystals. The blue arrow indicates the carbon peak produced by the C2/C3 carbon nuclei of the monomer (only about 10% monomer remains), while the inherent broadness of the C1/C4 isotropic shift prevents it from being discerned at all. The two isotropic peaks attributed to the polymer, occurring at ~90 and 110 ppm, are indicated by the red arrows. These co-crystals demonstrate ~90% polymerization at ~6 GPa of pressure.

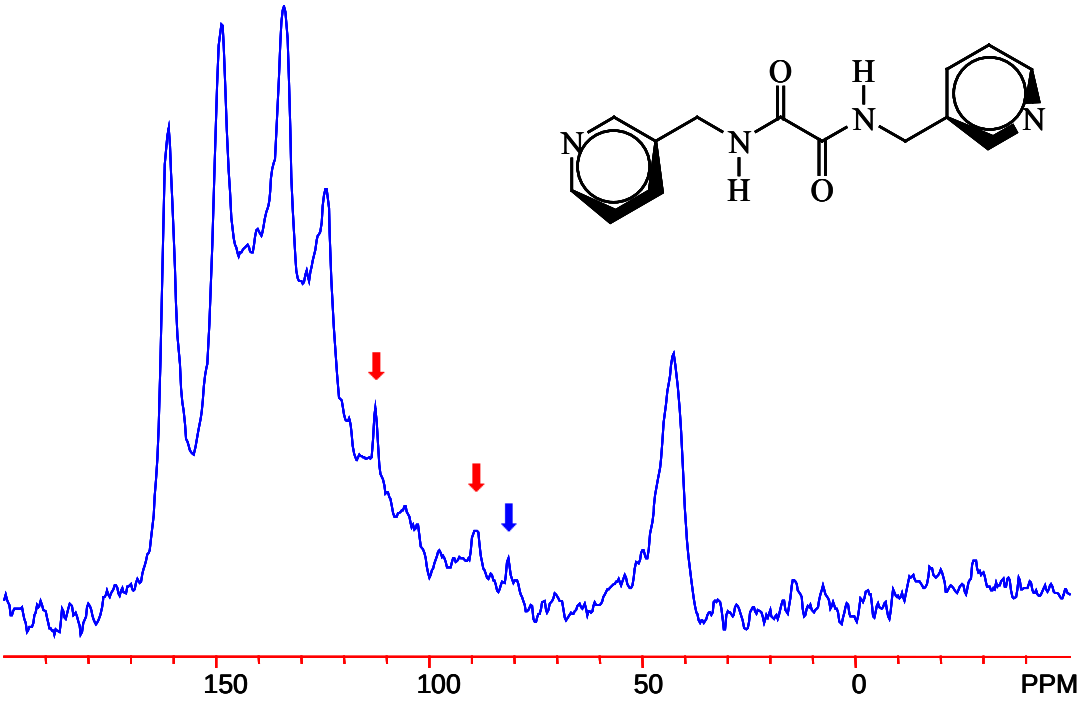

Figure 3.12 RAMP ^{13}C CP MAS-NMR spectrum of black phase **M1/2** co-crystal sample, monomer and polymer isotropic peaks are indicated, all other peaks are due to host molecule or spinning sidebands; Experiment was performed at 500 MHz with a 15 kHz spinning speed.

Figure 3.13 depicts the spectrum collected from a powder sample of black phase **P1**/**2** and **1** co-crystals. This co-crystal system demonstrates a far lesser degree of total polymerization, only ~55%, which is consistent with the poorer alignment of the starting material. The isotropic peaks produced by the monomer are indicated by blue arrows, and the isotropic peaks produced by the polymer are indicated by red arrows.

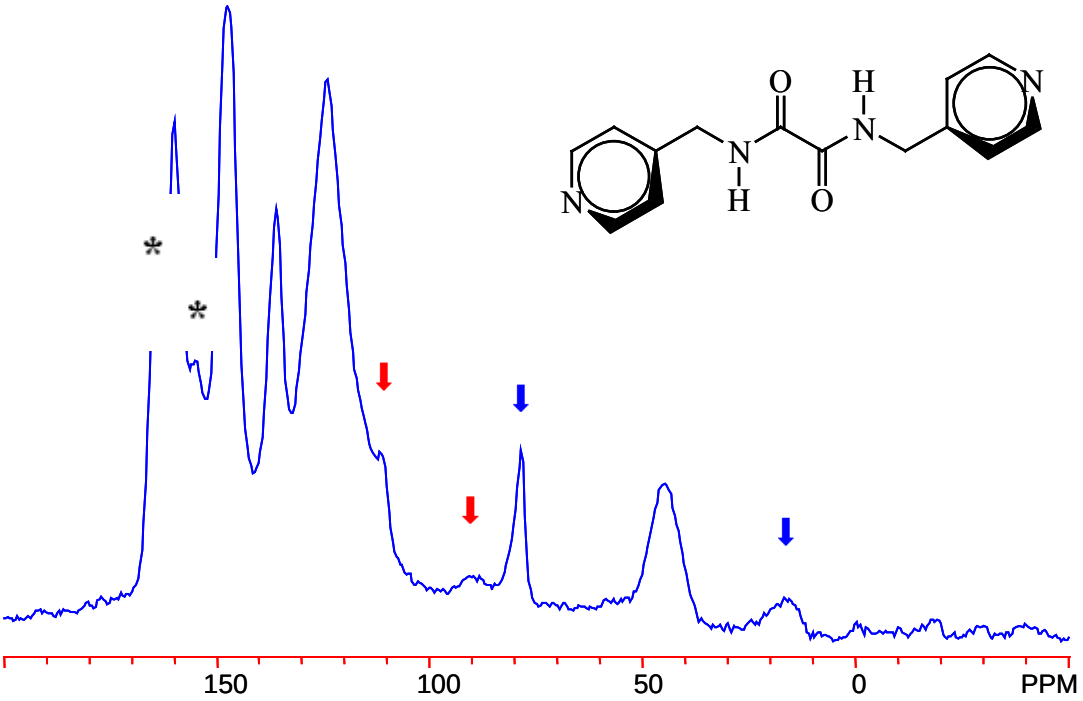

Figure 3.13 RAMP ^{13}C CP MAS-NMR spectrum of black phase **P1/2** and **1** co-crystal sample, monomer and polymer isotropic peaks are indicated, all other peaks are due to host molecule, background, or spinning sidebands; Experiment was performed at 360 MHz with a 15 kHz spinning speed.

3.3 Partially Polymerized M1/1 Co-crystals

In collaboration with Dr. Donald Lindsley, powder samples of the **M1**/**1** co-crystal system were pressed to 2.5 GPa using a piston press. The samples were packed in a silver cell encased in a silver chloride sleeve and wrapped in a graphite sheet to reduce friction. A bismuth slug was also encased in the silver chloride sleeve as a means of calibrating the actual pressure felt by the sample. Bismuth undergoes a phase transition at 2.5 GPa, which can be observed, indicating when the exact pressure is reached.[55] The sample was pressed to 2.5

GPa and allowed to anneal for five days. The sample was then unpacked and studied using Raman spectroscopy and ^{13}C CP MAS-NMR.

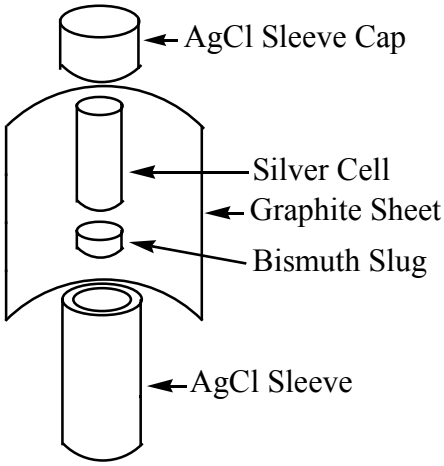

Figure 3.14 Cell assembly for partially polymerized **M1**/**1** pressure studies.

The sample, when unpacked, was visually inspected and was blue in color, consistent with a partially polymerized sample. The Raman spectrum, depicted in Figure 3.15 demonstrates the presence of the polymer within the crystal structure of the sample. The three characteristic peaks produced by the polymer can be clearly seen, and with good intensities. However, we know from single-crystal XRD experiments that samples exposed to similar pressures do not completely polymerize.

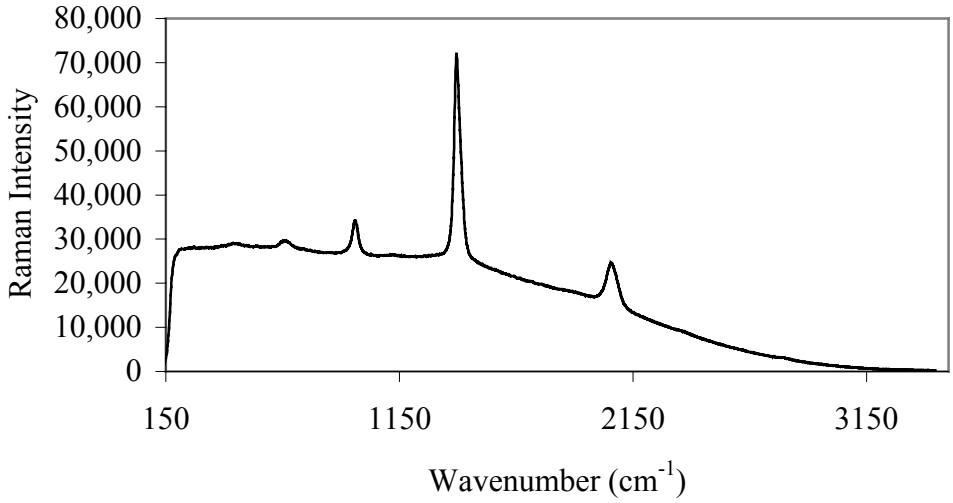

Figure 3.15 Raman spectrum of **M1**/**1** co-crystal sample pressed to 2.5 GPa.

After Raman spectroscopy, the powder sample was subject to a ^{13}C CP MAS-NMR experiment to confirm the total amount of polymerization. Figure 3.16 depicts the spectrum obtained from this experiment, blue arrows indicate the monomer isotropic peaks and red arrows indicate the polymer isotropic peaks. The integration of this spectrum indicates that this sample is ~10% polymerized after exposure to 2.5 GPa of pressure.

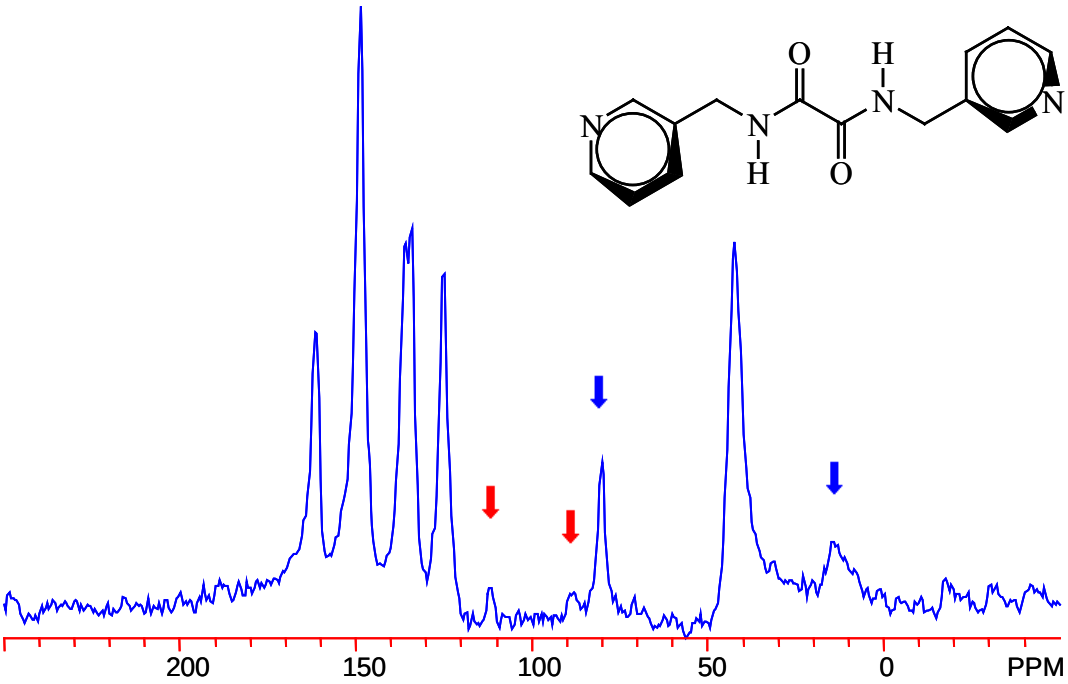

Figure 3.16 RAMP ^{13}C CP MAS-NMR spectrum of **M1/1** exposed to 2.5 GPa of pressure, monomer and polymer isotropic peaks are indicated, all other peaks are due to host molecule or spinning sidebands; Experiment was performed at 360 MHz with a 15 kHz spinning speed.

Finally, a small amount of the powder sample was dissolved in de-ionized water, and subject to a UV-visible experiment. The spectrum produced is depicted in Figure 3.17. This spectrum shows a maximum absorption at 680 nm, which indicates a higher energy absorption than the known polymeric co-crystals exhibit, but is consistent with the presence of shorter oligomer chains expected to absorb at a higher energy wavelength.

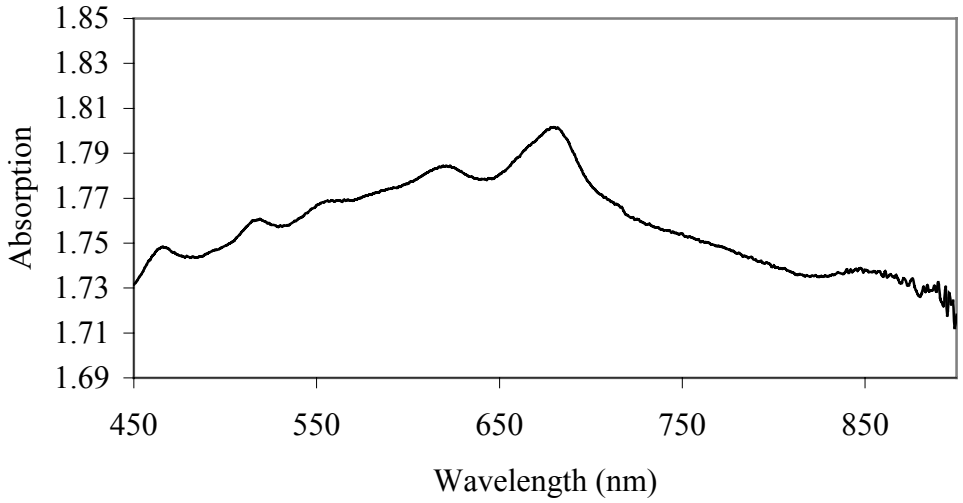

Figure 3.17 UV-visible spectrum produced by a **M1**/**1** co-crystal sample pressed to 2.5 GPa.

3.4 Conclusions

These experiments have demonstrated that a topochemical polymerization of diiodobutadiyne can be induced via mechanical pressure to produce 1,4-poly(diiododiacetylene) within the crystal lattice of co-crystal samples of **M1**/**1** and **P1**/**1**. The polymer has been identified using Raman spectroscopy and ^{13}C CP MAS-NMR, even though single-crystal XRD experiments have yielded no positive results. These experiments have further demonstrated the importance of proper alignment of the monomer in the starting material, as can be seen in the increased amount of polymerization when the **M1**/**1** co-crystal system is compared to the **P1**/**1** co-crystal system.

It has also been demonstrated that visual inspection of the color change is a reliable indication of polymerization, and that partially polymerized samples stable enough for further study can be produced reliably. Chapter 5 of this dissertation discusses the production of partially polymerized powder samples of the **M1**/**1** co-crystal system for the purpose of studying the polymerization intermediates.

Finally, the scientific value of our characterization techniques is clearly been established. ^{13}C MAS-NMR can demonstrate the simultaneous presence of monomer and polymer, Raman spectroscopy can clearly identify the presence of as little as 10% polymer, and single-crystal XRD will not produce structural information on samples that do not undergo a single-crystal-to-single-crystal transformation.

3.5 Experimental

Compounds and Co-Crystals

Compound 1

Diiodobutadiyne was synthesized according to the previously published procedure.[38]

Compounds M1 and P1

Bis-pyridyl oxalamides **M1** and **P1** were synthesized by Lei Li, according to the previously published procedure.[14,56]

Co-crystals

Co-crystals of **M1**/**1** and **P1/1** were prepared by dissolving compounds **M1** or **P1** and **1** in warm methanol in a 1:1 ratio. The solution was then cooled to -40 °C and the resulting solid was collected by vacuum filtration.

Single-Crystal X-Ray Diffraction

Crystals were obtained as described, and then selected with an optical microscope and epoxied on thin glass fibers. The crystal was centered and the x-ray intensity data were measured on a Bruker AXS diffractometer. The data were collected using graphite-monochromated Mo radiation and then structures were solved by direct methods and refined using full matrix least squares methods (SHELX97). SHELX97 – Programs for Crystal Structure Analysis (Release 97-2): G.M. Sheldick, SHELX-98, Program for the Solution of Crystal Structures, University of Göttingen, Göttingen (Germany), 1998.

Raman Spectroscopy

Raman spectroscopy was performed using a Thermo Nicolet Almega dispersive Raman spectrometer coupled with an infinity corrected, confocal design microscope. The spectrometer uses a 785 nm class I laser, and the data were collected in the reflection mode of the microscope at a slit width of 25 μm. The data were collected and analyzed using the Omnic software suite (Nicolet, USA).

RAMP ^{13}C CP MAS-NMR

All RAMP ^{13}C CP MAS-NMR spectra were taken at room temperature using either a Varian Infinity Plus 500 NMR spectrometer or a Varian Infinity Plus 360 NMR spectrometer (as noted in the Results section), with either the 5 mm double resonance probe or 4 mm double resonance probe, (as noted in the Results section), with the 5 mm or 4 mm zirconia rotor respectively. The probe was tuned to 125.7 MHz for ^{13}C and 499.8 MHz for ^{1}H on the Varian Infinity Plus 500 NMR spectrometer and 90.5 MHz for ^{13}C and 360.0 MHz for ^{1}H on the Varian Infinity Plus 360 NMR spectrometer (as noted in the Results section). The ^{13}C MAS-NMR spectra were collected using a CP RAMP pulse program with a contact time of 2ms, a pulse delay of 2s.[46] The number of steps in the CP RAMP ranged from 8-12 and the amplitude step size ranged from .001 to .01. These parameters lead to an X channel amplitude range of .2050-.6500 for the Varian Infinity Plus 500 NMR spectrometer and .3100-.4000 for the Varian Infinity Plus 360 NMR spectrometer. Over 1000 scans were acquired. Hexamethylbenzene (HMB) was used to set the Hartman-Hahn match condition, the 131 ppm resonance acting as a secondary reference.

UV-visible Spectroscopy

All UV-visible spectroscopy were taken at room temperature using a Cary 100 UV/Visible Scan Spectrophotometer scanning from 450 to 900 nm with a resolution of 1 nm.

Pressure Studies (performed by C. Martin, C. Tarabrella, and C. Wilhelm)

A modified Merrill-Bassett diamond-anvil cell (600 culet diamond size) was used in this pressure study in the pressure range of 0.0-7.0 GPa. Flourinert was used as the hydrostatic pressure-transmitting medium. For calibration purposes both co-crystals, together with a small ruby chip, were loaded into a 200 μm hole in a steel gasket. The pressure was calibrated by measuring the shift of the R^1 fluorescence line of the ruby for the initial run of each sample. Subsequent studies relied on the co-crystal color change for an approximate estimate of the pressure.[38,53]
A 2000 ton uniaxial split sphere apparatus fitted with a multi-anvil cell was used in this pressure study to obtain pressures from 0.0 to 10.0 GPa. The cell, which holds a 3 mm specimen, uses tungsten carbide anvils and boron epoxy as the pressure-transmitting medium. The press was not calibrated, but was estimated based on past experiments by observing the color change of the 3-pyridyl-oxalamide/diiodobutadiyne co-crystalline powder.[54]

3.6 References

14. Nguyen, T.L.; Scott, A.; Dinkelmeyer, B.; Fowler, F.W.; and Lauher, J.W. Design of Molecular Solids: Utility of the Hydroxyl Functionality as a Predictable Design Element. *New J. Chem.* **1998**, *22*, 129-135.

37. Goroff, N.S.; Curtis, S.M.; Webb, J.A.; Fowler, F.W.; and Lauher, J.W. Designed Cocrystals Based on the Pyridine-Iodoalkyne Halogen Bond. *Org. Lett.* **2005,** *7*, 1891-1893.

38. Webb, J.A. Small Molecule Carbon-Rich Compounds: from Polymerization to NMR Studies. PhD. Dissertation. SUNY Stony Brook, 2004.

46. Metz, G.; Wu, X.; and Smith, S. Ramped-Amplitude Cross Polarization in Magic-Angle-Spinning NMR. *J. Mag. Res. A*, **1994,** (110), 219-227.

47. Wilhelm, C.; Boyd, S.A.; Chawda, S.; Fowler, F.W.; Goroff, N.S.; Halada, G.P.; Grey, C.P.; Lauher, J.W.; Luo, L.; Martin, C.D.; Parise, J.B.; Tarabrella, C.; Webb, J.A. Pressure-Induced Polymerization of Diiodobutadiyne in Assembled Co-crystals. *J. Am. Chem. Soc.*, **2008**, *130*, 4415-4420.

53. Jephcoat, A.P.; Finger, L.W.; and Cox, D.E. High Pressure, High Resolution Synchrotron X-ray Powder Diffraction with a Position-Sensitive Detector. *High Press. Res.*, **1992**, *8*, 667-676.

54. Gwanmesia, G.D. Hot-Pressing of Polycrystals of High-Pressure Phases of Mantle Minerals in Multi-Anvil Apparatus. *Pure Appl. Geophys.*, **1993,** 2-4, (141), 467-484.

55. Boyd, F.R.; and England, J.L. Apparatus for phase-equilibrium measurements at pressures up to 50 kilobars and temperatures up to 1750 °C. *J. Geophys. Res.*, **1960**, *65*, 741-748.

56. Fowler, F.W.; and Lauher, J.W. A Rational Design of Molecular Materials. *J. Phys. Org. Chem.* **2000,** 13, 850-857.

Chapter 4. New Host Molecules and the Odd-Even Effect

4.1 Introduction to the Odd-Even Effect

In 1998 Tam Nguyen, a graduate student working for Frank Fowler and Joseph Lauher, discovered that the effectiveness of a series of host molecules at catalyzing a diyne polymerization followed an odd-even pattern.[57] Nguyen found that when a host molecule with an odd number of methylene groups in the alkyl-chain tether was co-crystallized with a diyne monomer, the resulting product was a high-quality crystal, indicating that this material had undergone a single-crystal-to-single-crystal transition during the topochemical polymerization reaction. However, when the host molecule had an even number of methylene groups in the alkyl-chain tether, the polymerization did not occur in a single-crystal-to-single-crystal fashion, and the degree of polymerization was not determined.[57]

Similar results were found by Sun and Luo when studying the production of 1,4-poly(diiododiacetylene) in co-crystals containing the bis-nitrile oxalamide hosts.[39,44] In expanding the library of bis-nitrile oxalamide hosts to include compounds **N5** and **N6**, Luo found host molecules containing an even number of methylene groups in the alkyl-chain tether between the oxalamide and nitrile functionalities led to the spontaneous polymerization of diiodobutadiyne to 1,4-poly(diiododiacetylene). Furthermore, the polymerization tended towards a highly ordered crystalline product, as is the case with the **N4** host molecule.[39,44]

When using a host molecule with an odd number of carbon atoms in the alkyl-chain tether, N3 and N5, there is no spontaneous polymerization to a high-quality co-crystal product.[39,44] Host molecules **N5** and **N6** are discussed in more detail in Chapter 5.

The host molecules with an odd number of methylene groups in the alkyl-chain tether, **N3** and **N5**, form co-crystals with diiodobutadiyne in a different ratio than the host molecules with an even number of methylene groups in each tether, **N4** and **N6**. Host molecules **N4** and **N6** form co-crystals with diiodobutadiyne in a 1:2 ratio, where one end of the diiodobutadiyne rod forms a halogen bond with the nitrile group of one host and the other end is in close contact a carbonyl of the neighboring host.[39,44] However, hosts **N3** and **N5** form co-crystals with the more expected 1:1 ratio, where both ends of the diiodobutadiyne rod form halogen bonds with the host nitriles. These different packing types are depicted in Figure 4.1.[39,44]

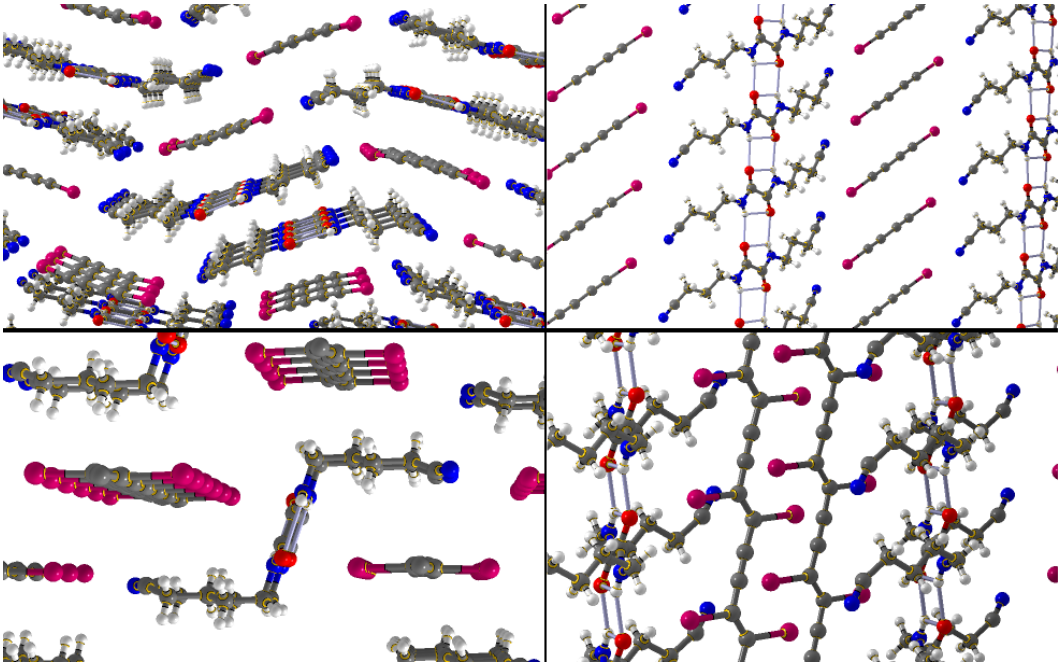

Figure 4.1 Illustration of the 1:1 host-guest ratio of the **N3**/**1** co-crystals (top) and 1:2 host-guest ratio of the **N4**/**2** co-crystals (bottom).[39,44]

4.2 New Bis-Pyridyl Hosts

Since this pattern was well established by Luo in the bis-nitrile system, it was hypothesized that a similar pattern may also be true of the bis-pyridyl systems.[44] An expansion of the current library of bis-pyridyl functionalized oxalamide hosts was begun to test this hypothesis. Figure 4.2 depicts the hosts that were synthesized to further the study of this odd-even effect. Two, three, and four-carbon alkyl-chain tethers were used to link the 3- or 4-pyridyl Lewis-base functionalities to the oxalamide moiety, expanding the known library of bis-pyridyl host compounds. These compounds will be referred to as compounds **M2**-**M4** and **P2**.

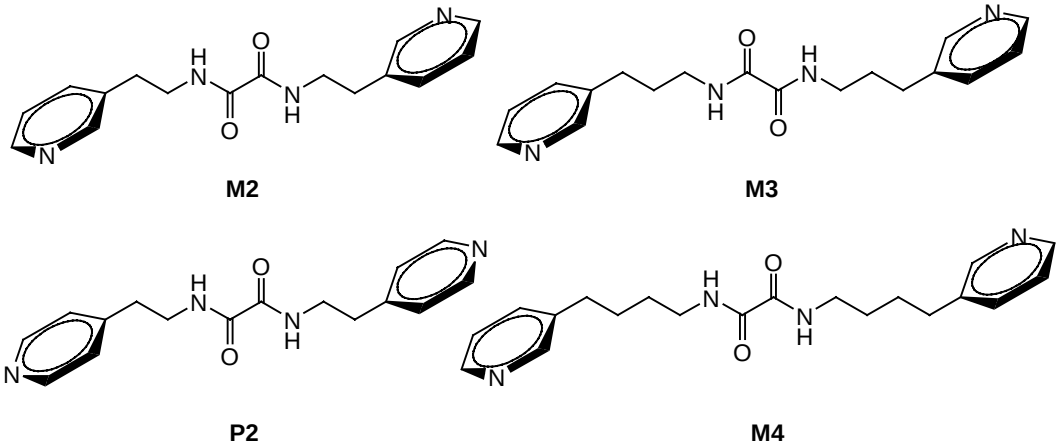

Figure 4.2 New host compounds for the study of the odd-even effect in the single-crystal quality of co-crystal samples; 2-methylene-3-pyridyl (**M2**), 3-methylene-3-pyridyl (**M3**), 4-methylene-3-pyridyl (**M4**), and 2-methylene-4-pyridyl (**P2**).

Scheme 4.1 depicts the general synthetic route used in preparing these new host molecules. A pyridyl-functionalized amine reacts with diethyl oxalate (2:1 ratio) to form the desired oxalamide.[16] The length of the alkyl-chain tether within the amine can be selected to afford the desired host molecule.

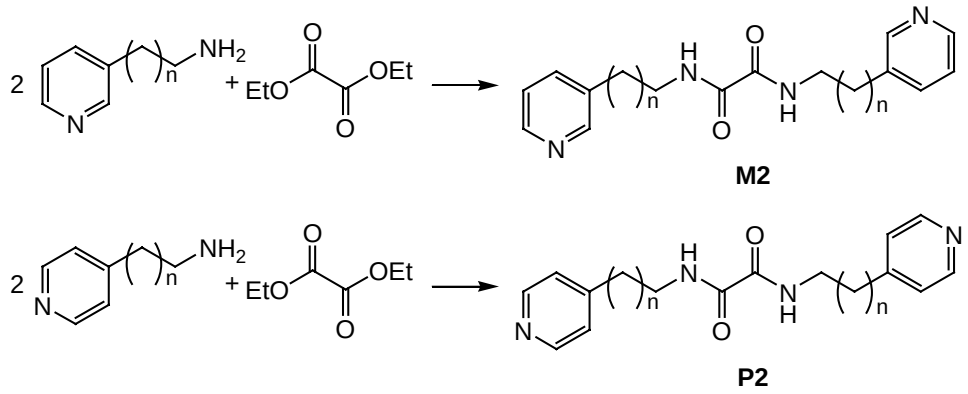

Scheme 4.1 General route to preparing new host molecules.[16]

4.3 Host Molecule M2

The first host molecule synthesized in this series was compound **M2**, prepared form commercially available 3-(2-aminoethyl)pyridine hydrochloride and diethyl oxalate, as shown in Scheme 4.2. The hydrochloride salt is deprotonated with sodium hydroxide, and amine **2a** is extracted with dichloromethane and concentrated under vacuum, yielding a yellow oil. Amine **2a** reacts subsequently with diethyl oxalate in ethanol (2:1 ratio), yielding a white powder. Host **M2** is purified by recrystallization in methanol, yielding nearly colorless crystals.

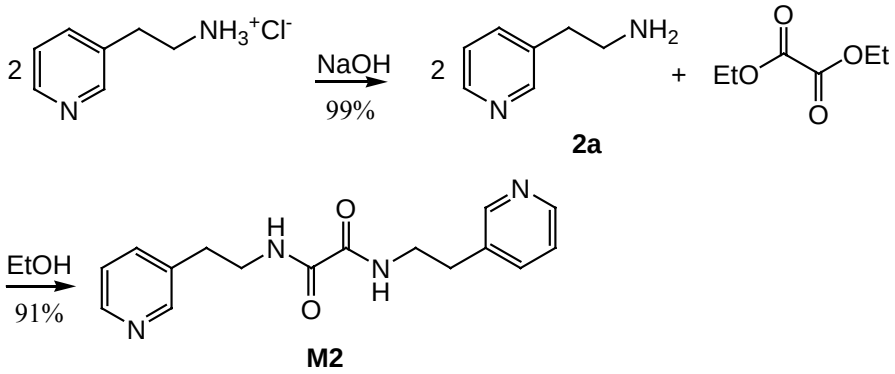

Scheme 4.2 Synthetic route to host compound **M2**.

The crystal structure of host **M2** is shown in Figure 4.3. As expected, in the crystal the oxalamide forms a 1-dimensional hydrogen-bonding network. However, the repeat distance along this network is longer than expected, at ~5.2 Å, instead of the desired repeat distance of ~5.0 Å, the ideal for the topochemical polymerization reaction.

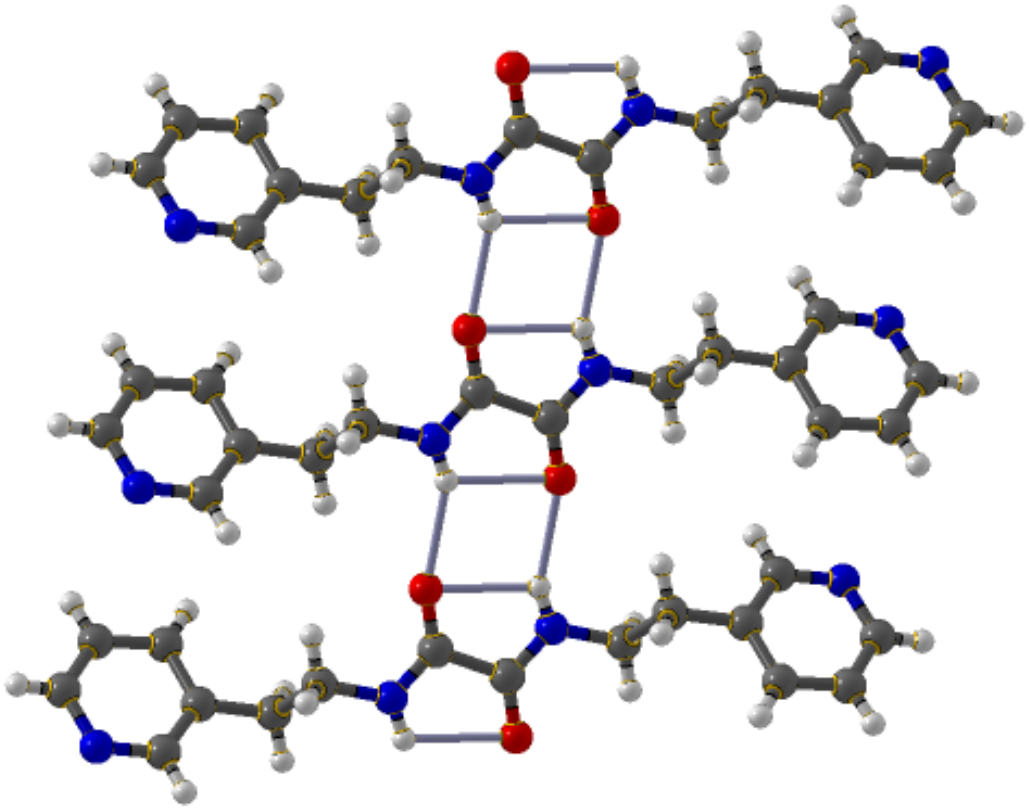

Figure 4.3 Crystal packing of compound **M2**, as determined single-crystal XRD.

Despite the long repeat distance of the monomer crystal structure, host molecule **M2** was co-crystallized with compound **1** by dissolving both in warm methanol with a 1:1.5 host-to-guest ratio. The solution was then subjected to centrifugation to remove any insoluble material, and decanted into a crystallization dish. Slow evaporation of the solvent led to the growth of coppery colored co-crystals. Similar coloring is found in co-crystal samples of **N4**/**2** and **N6**/**2,** an indication that these co-crystals also contains polymer **2**.[39,44] The initial co-crystal mixture yielded ~10% polymer containing product by mass. Figure 4.4

depicts the crystal structure of these co-crystals as resolved by single-crystal XRD.

Improvements in the co-crystallization procedure have increased the yield of the **M2**/**2** system to ~20%, but the co-crystallization of molecules **M2** and **1** have not proven as reliable as the **N6**/**2** system to-date. This may be the result of the solubility of molecule **M2**. However, the **M2**/**2** system does demonstrate benefits over the bis-nitrile systems. First, as discussed below, this system is the only system that has been fully characterized by the methods developed in this course of study. This characteristic should make the **M2**/**2** co-crystal system the most useful system for studying the topochemical polymerization reaction. Second, a synthetic pathway that is shorter and easier than the route to the bis-nitrile hosts, saving time and money, can be used to obtain the **M2** host molecule.

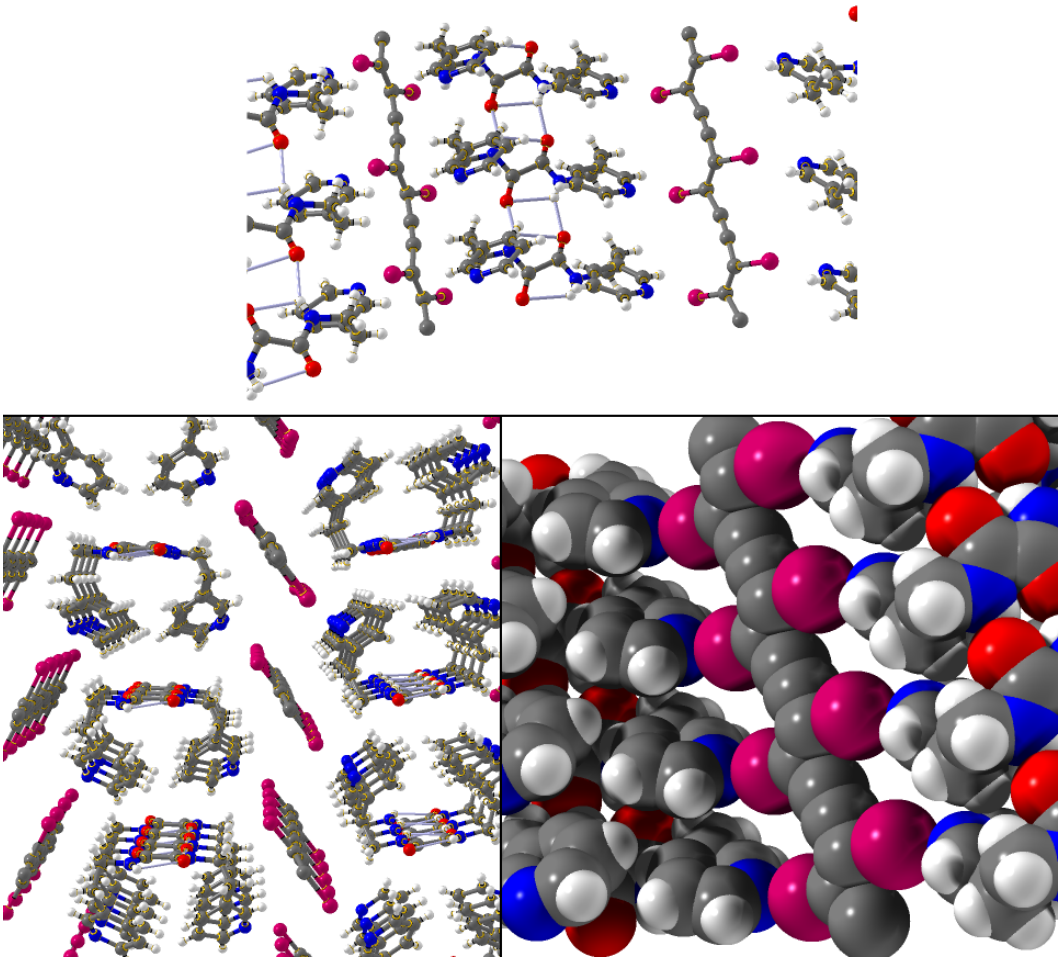

Figure 4.4 Crystal structure of co-crystal **M2**/**2**, packing shown (bottom).

The crystal structure of the **M2**/**2** co-crystals demonstrates a successful co-crystallization of compounds **M2** and **1**, and the successful topochemical polymerization of the diyne. This polymerization occurs spontaneously, under ambient conditions in the crystallization dish. The 4.9 Å repeat distance of the **M2**/**2** co-crystal system demonstrates a decrease along the oxalamide network of 0.2 Å from the **M2** crystal structure, demonstrating the ability to form polymer **2**

within a crystal lattice that may not be ideal, and the dimensions of this polymer neatly fit the structural parameters of the polymer described in Chapter 1, Figure 1.12. As expected, the halogens bonds within this system are shorter than in other polymer containing co-crystals, ~2.9 and 3.0 Å (the two sides of the polymer are not equivalent) compared to ~3.2 Å for the **N4**/**2** system, but longer than in the **M1**/**1** and **P1**/**1** co-crystal systems (~2.8 Å).

The Raman spectrum collected from a sample of **M2**/**2** co-crystals is shown in Figure 4.5. As expected, this spectrum consists of 3 peaks of high intensity that occur at ~900, 1400, and 2100 cm^{-1}. This spectrum matches nicely with Raman spectra collected from other PIDA containing samples.

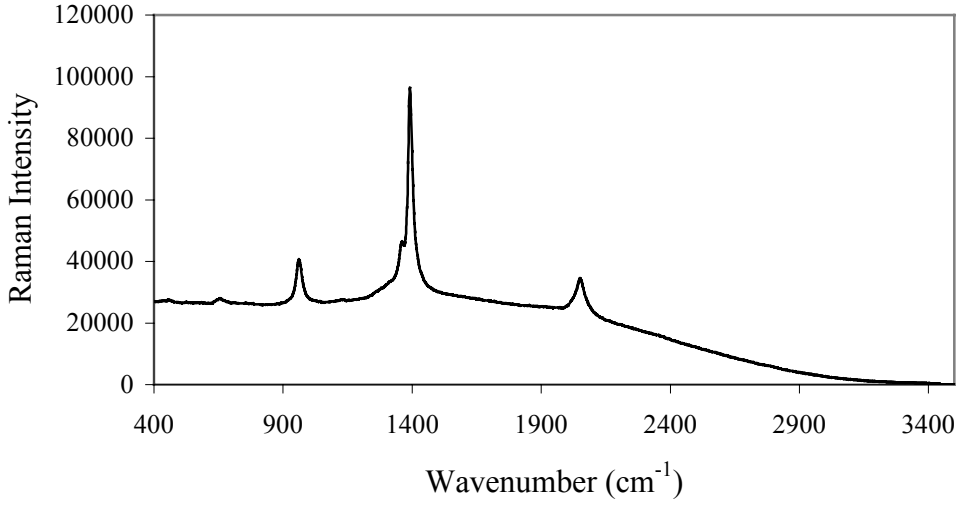

Figure 4.5 Raman spectrum produced by **M2**/**2** co-crystal sample.

A powder sample of **M2**/**2** co-crystals was then sonicated in deionized water, and a UV-visible spectrum was collected. This spectrum, shown in Figure 4.6 demonstrates a maximum of ~710 nm, consistent with other PDAs. Furthermore, it contains smaller local maxima consistent with the presence of the conjugated backbone of a polydiacetylene.

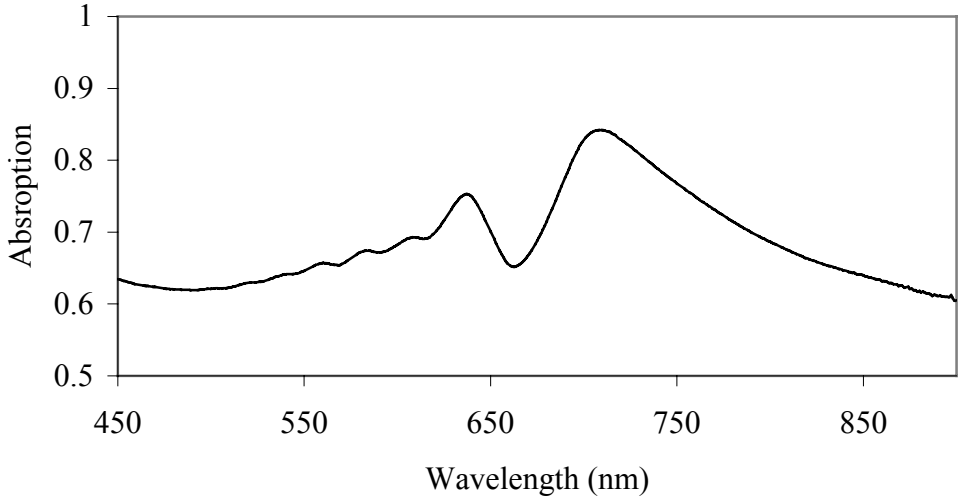

Figure 4.6 UV-visible spectrum produced by a sample of **M2**/**2** co-crystals.

Figure 4.7 depicts a ^{13}C NMR spectrum collected in chloroform$_d$ of compound **M2** before co-crystallization with diyne **1**. When this spectrum is compared with the MAS-NMR of a powder sample of **M2**/**2** co-crystals, shown in Figure 4.8, the peaks attributed to polymer **2** become easily identifiable. The isotropic peaks seen in both spectra are those of the host molecule.

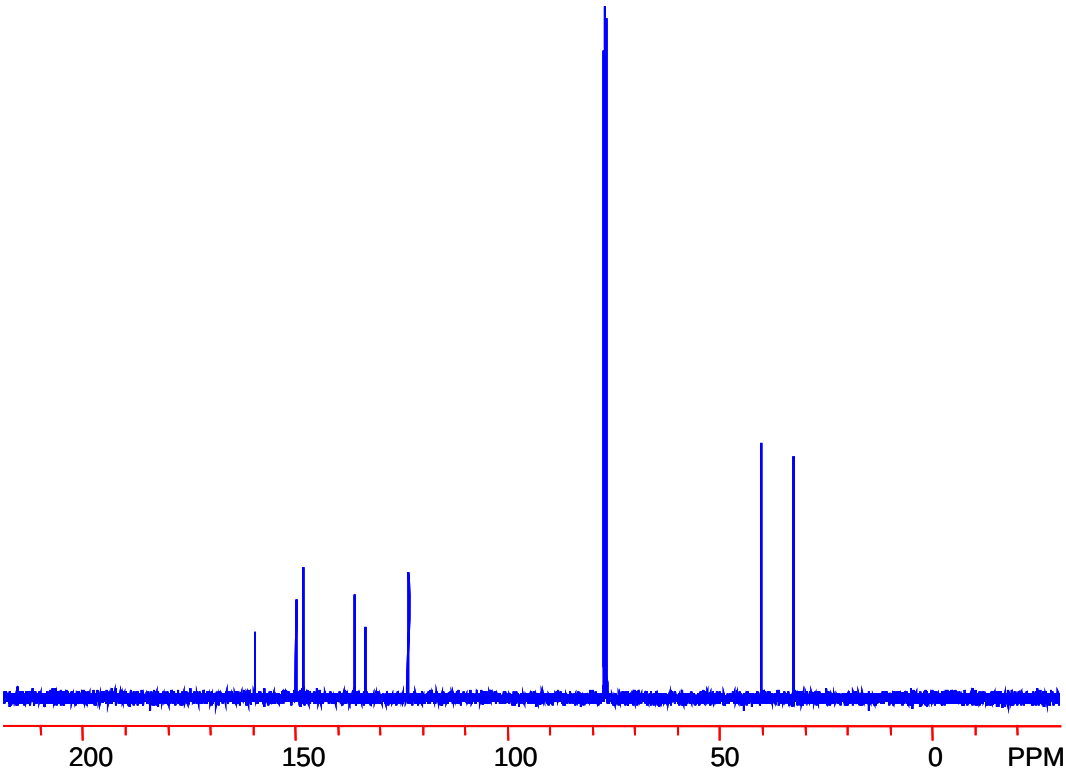

Figure 4.7 ^{13}C NMR of compound **M2**, experiment was performed at 400 MHz.

The MAS-NMR spectrum shown in Figure 4.8 clearly shows the presence of polymer **2**. It also confirms the lack of any unreacted monomer, demonstrating a degree of polymerization that approaches 100% within this sample. Co-crystal **M2**/**2** represents the first PIDA containing material to be analyzed by all four of these techniques.

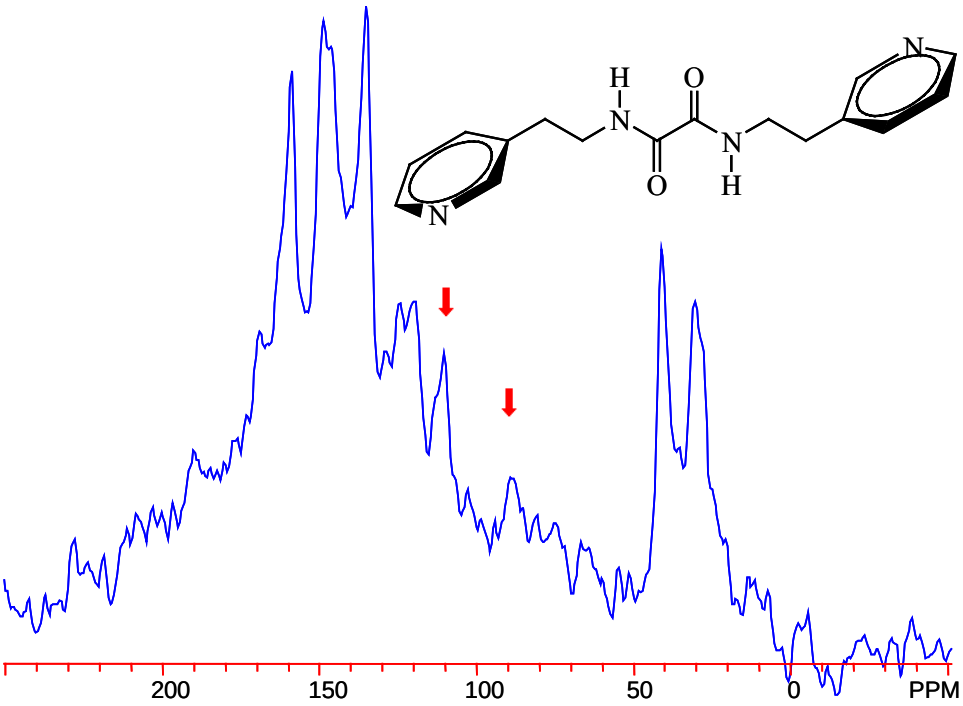

Figure 4.8 RAMP ^{13}C CP MAS-NMR spectrum of **M2/2**, polymer isotropic peaks are indicated, all other peaks are due to host molecule or spinning sidebands; Experiment was performed at 360 MHz with a 15 kHz spinning speed.

4.4 Host Molecule P2

The amine required to synthesize host **P2**, 4-(2-aminoethyl)pyridine (**2b**), is commercially available. Allowing amine **2b** to react with diethyl oxalate in a 2:1 ratio (see Scheme 4.3), yields a white powder, that can be purified by recrystallization in methanol. Figure 4.9 contains the crystal structure of this compound as resolved by single-crystal XRD.

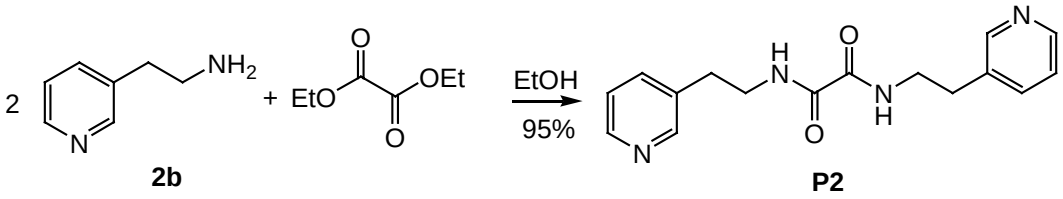

Scheme 4.3 Synthetic route to host compound **P2**.

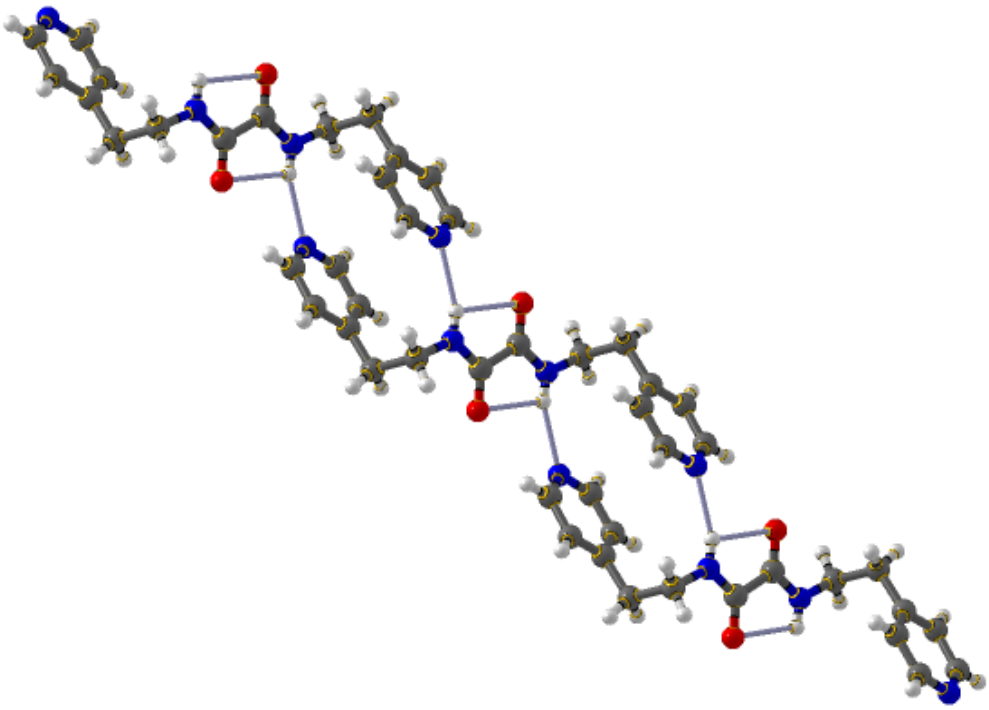

Figure 4.9 Crystal packing of compound **P2**.

As the crystal packing demonstrates, compound **P2** does not form the expected hydrogen bonded network between oxalamide moieties. Instead, neighboring molecules interact by the formation of a hydrogen bond between the pyridyl ring of one and the oxalamide functionality of the other. This packing pattern is

analogous to the published crystal structure of compound **P0**, shown in Figure 4.10, an oxalamide with no alkyl-chain tether.[58]

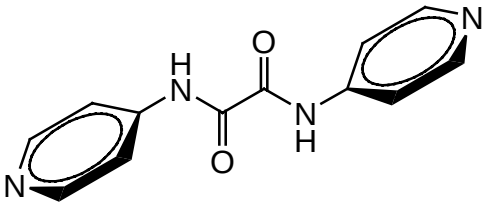

P0

Figure 4.10 Bis-pyridyl functionalized oxalamide with no alkyl-chain tether.

Several attempts were made to prepare co-crystals of host **P2** with compound **1**. A variety of solvents and crystallization conditions were studied, but in all cases only the starting materials were recovered. Unlike host molecule **M2**, compound **P2** appears to lack the ability to form co-crystals with monomer **1**. This lack of success with host molecule **P2** has discouraged further pursuit of the para-substituted bis-pyridyl oxalamide family of host compounds.

4.5 Host Molecule M3

Undergraduate Alexander Ceballos and graduate student David Connors carried out the synthesis of compound **M3**. The required amine precursor, compound **3c**, is not commercially available. However, it can be prepared in 2 steps from 3-(pyridyl) propanol, compound **3a** (Scheme 4.4). First, a Mitsunobu reaction transforms the alcohol into phthalimide **3b**. Reaction of the compound **3b** with hydrazine produces compound **3c** in good yield.

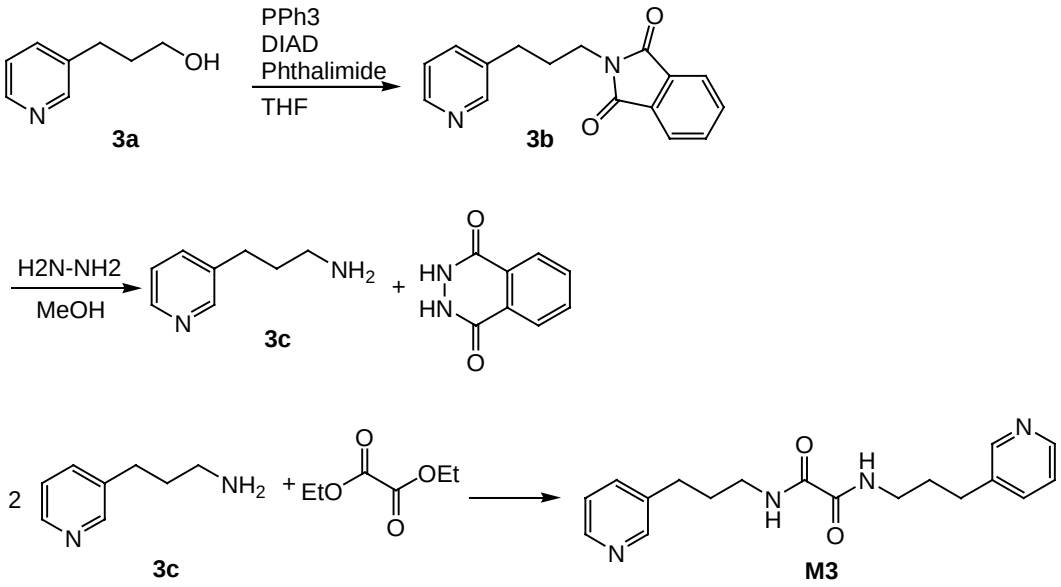

Scheme 4.4 Synthetic route to compound **M3**.[59]

The crystal structure of host **M3** is shown in Figure 4.11. Compound **M3** forms an α-network with a repeat distance of 5.2 Å. This repeat distance is longer than desired repeat distance of 5.0 Å, but comparable to the structure formed by host **M2**, which successfully templates monomer **1** for polymerization. Compound **M3** was tested as a possible host for topochemical polymerization of monomer **1** to produce polymer **2**.

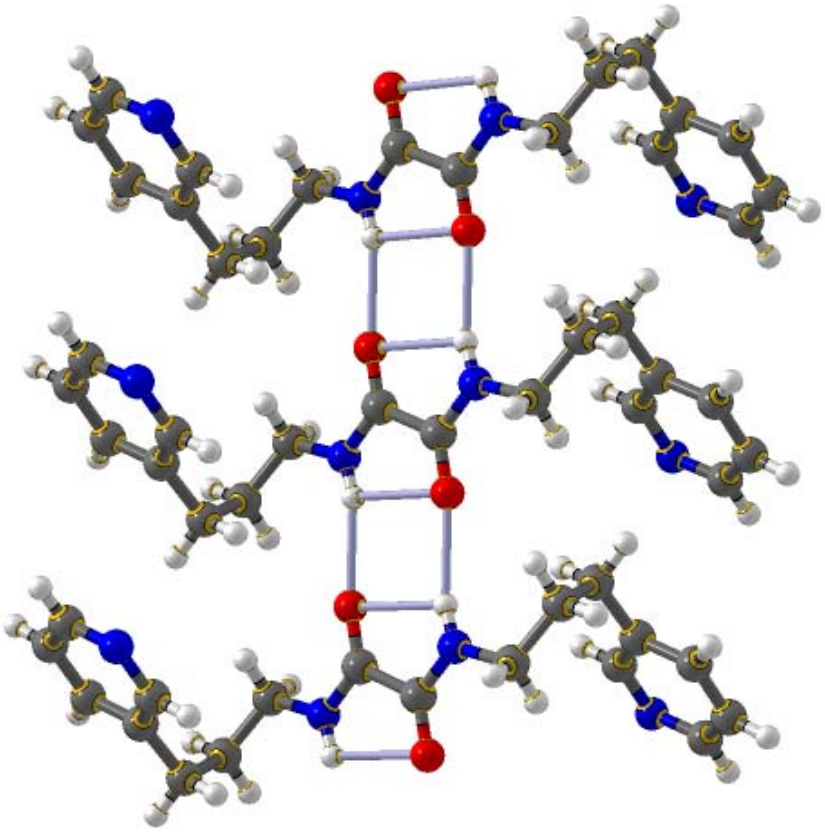

Figure 4.11 Crystal structure and packing of compound **M3**.

Compound **M3** was dissolved in warm methanol with compound **1** in a 1:1 ratio. The resulting solution was subjected to centrifugation and then decanted into a crystallization dish. Slow evaporation of the solvent produced colorless crystals. One of these crystals was studied by single-crystal XRD, and the resulting structure is shown in Figure 4.12. The crystal structure demonstrates the

presence of monomer **1** only, with no evidence of polymer **2**. The repeat distance in the co-crystal lattice is 5.1 Å, and the tilt angle of monomer **1** along the axis of translation is 62.5°. This large tilt angle leads to a C1 to C4 distance of 4.8 Å, far greater than the desired distance of 3.5 Å.

The orientation of monomer **1** within the co-crystal lattice demonstrates a similarity to both the **M1**/**1** and **P1**/1 co-crystal systems, as well as the halogen bond length (2.7 Å). The repeat distance of the **M3**/**1** sample is similar to that seen in the **M1**/**1** sample (5.1 Å). However, the large tilt angle of the **M3**/**1** system is more reminiscent of the **P1**/**1** sample (64°), leading to a similar C1 to C4 distance, the C1 to C4 distance in the **P1**/**1** system is 4.9 Å. Therefore, it may be possible to induce topochemical polymerization within these co-crystals using pressure, as with the **M1**/**1** and **P1**/**1** co-crystals. However, this approach will not be pursued at this time due to the ability to grow this polymer in large quantities using other host molecules. The results of this co-crystallization are consistent, however, with the hypothesis of an odd-even effect within these materials.

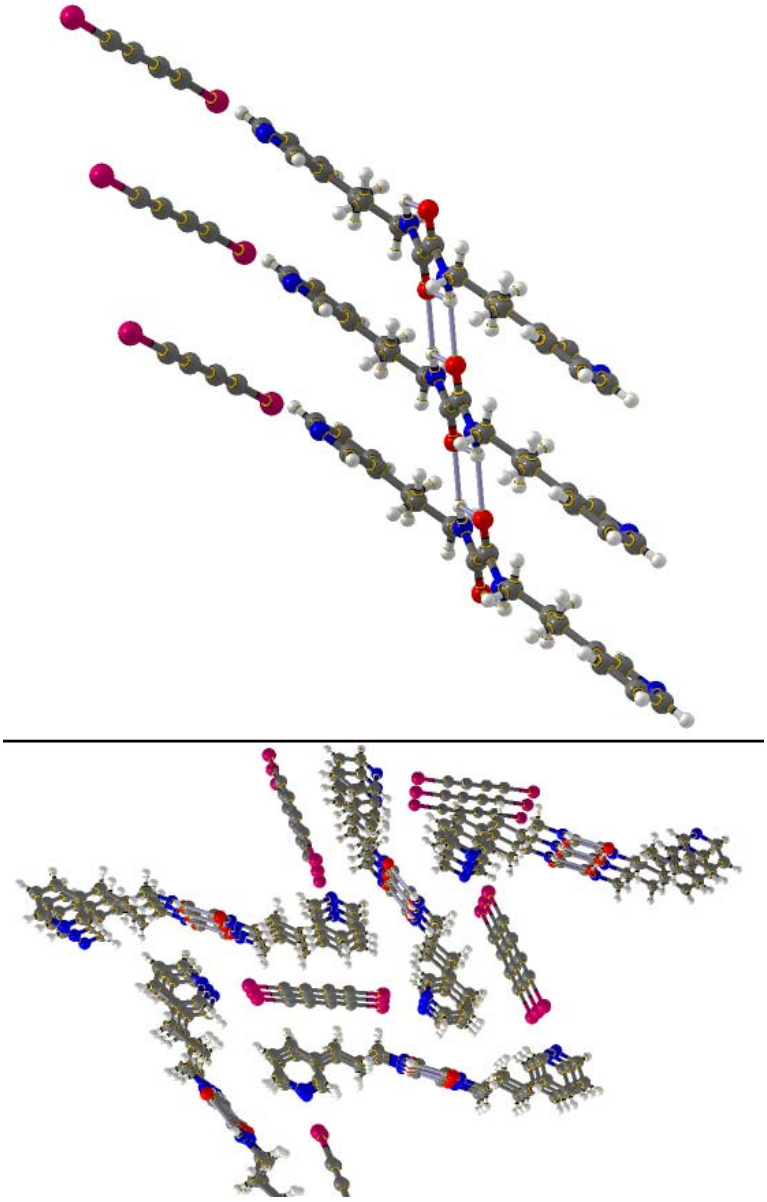

Figure 4.12 Structure and packing of co-crystal **M3/1**, packing shown (bottom).

4.6 Host Molecule M4

The production of 3-pyridinebutanamine was carried out using a modified version of Hawes and Davis's synthesis of the same molecule in 1973, as depicted

in Scheme 4.5.[60] Commercially available 3-pyridinepropanol reacts with an excess of thionyl chloride in dichloromethane to produce 3-(3-chloropropyl)pyridine (**4a**).[60,61]

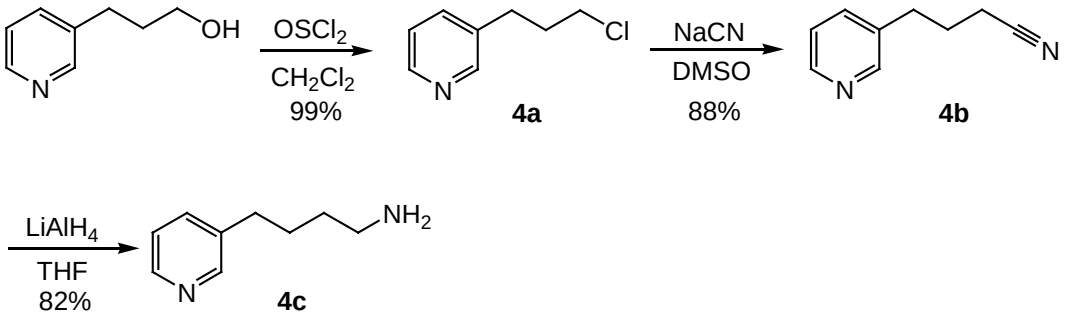

Scheme 4.5 Modified version of Hawes and Davis's synthesis of 3-pyridinebutanamine.[60]

4a then reacts with an excess of sodium cyanide in dimethyl sulfoxide to produce 4-pyridin-2-yl-butyronitrile (**4b**).[60,62] Reduction of compound **4b** with lithium aluminum hydride in dry tetrahydrofuran produces 3-pyridinebutanamine (**4c**) in good yield. The amine is a thick oil, and therefore is difficult to purify, as reported in the literature.[60]

To prepare host **M4**, compound **4c** reacts with diethyl oxalate in a 2:1 ratio in ethanol (Scheme 4.6a). This reaction yielded a mixture of mono- and di-substitution products that were separated on silica. After purification, compound **M4** was obtained not as the expected solid, but rather as a thick, brown oil. Several attempts to purify compound **M4** by recrystallization in a variety of

solvents have been attempted, but all have failed to produce a solid crystalline product, but the ^{13}C NMR is shown in Figure 4.13.

Following this procedure, compound **M4** was synthesized by reaction of 3-pyridinebutanamine (**4c**) with oxalyl chloride in a 2:1 ratio (Scheme 4.6b). While this reaction proceeds more quickly, it also yields a thick brown oil as the product. Based on these results it appears that compound **M4** does not form the necessary α-network required for the production of a crystal lattice. This may be an indication that host **M4** will not be able to form co-crystals with monomer **1**.

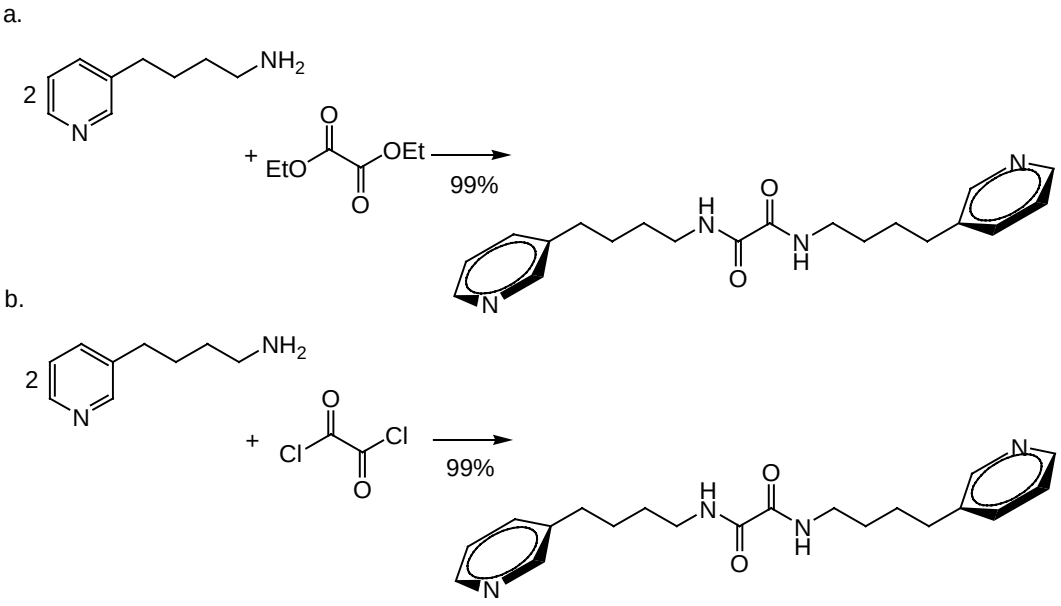

Scheme 4.6 Synthesis of host molecule **M4**.

Although compound **M4** is not crystalline, attempts were still made to form co-crystals of host **M4** with monomer **1**. Compound **M4** and monomer **1** were dissolved in warm methanol in a 1:1 ratio. The solution was decanted into a crystallization dish, and subjected to slow evaporation. However, this process yielded only an oily mixture of molecules **M4** and **1**, without the production of any crystalline species.

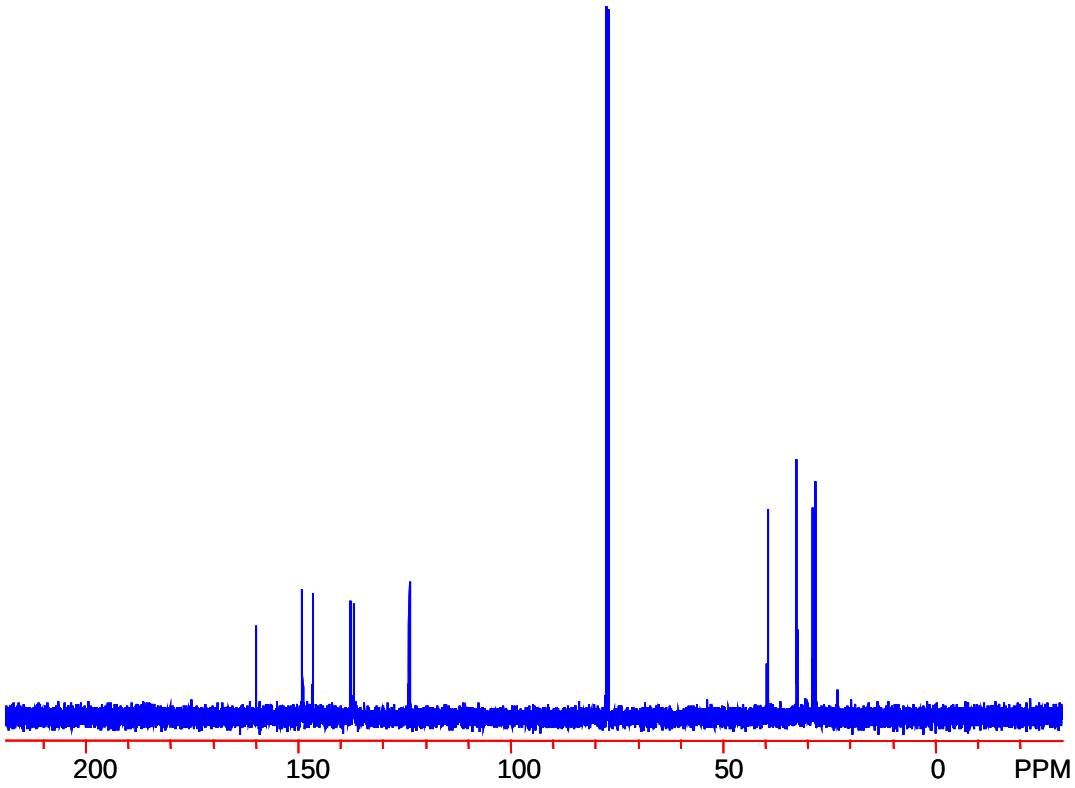

Figure 4.13 ^{13}C NMR of molecule **M4**, experiment was performed at 400 MHz.

4.7 Conclusions

It has been demonstrated that polymer **2** can be reliably produced using bis-pyridyl oxalamide host **M2**. These co-crystals can spontaneously polymerize at STD, while co-crystals with other hosts in the bis-pyridyl oxalamide series do not polymerize spontaneously. Furthermore, these samples undergo a single-crystal-to-single-crystal transformation. The rest of the family of para-functionalized bis-pyridyl compounds developed here indo not make viable hosts for inducing a single-crystal-to-single-crystal polymerization reaction.

The polymer grown in the **M2**/**2** co-crystal system neatly fits the structural parameters of the polymer grown in the **N4**/**2** co-crystal system, within the error of the crystal structure. The Lewis basic interactions within the **M2**/**2** co-crystal systems appears to be stronger, according to the MAS-NMR data and the halogen bonding lengths seen in the crystal structure, than those seen in the **N4**/**2** system, but the fact that these bonds are longer and weaker than those seen in other bis-pyridyl co-crystal systems may contribute to the ability of monomer **1** to form long chain polymers. The fact that the iodine side-chains of the polymer in the **M2** system are not equivalent may also be significant. We do not yet fully understand why this co-crystal system results in the spontaneous polymerization of monomer **1**, while the other bis-pyridyl systems do not, and therefore more investigation is necessary.

Disappointingly, however, the odd-even effect has not been fully demonstrated within this library of host molecules. It appears that bis-pyridyl-oxalamides with long alkyl-chain tethers may not reliably form an α-network along the oxalamide functionality. However, we now have a library of viable host molecules, and reliable synthetic route to new host precursors has been established.

4.8 Experimental

Compounds and Co-Crystals

Compound 1
Diiodobutadiyne was synthesized according to the previously published procedure.[38]

N,N'-bis-3-pyridylehtanyl oxalamide (**M2**)

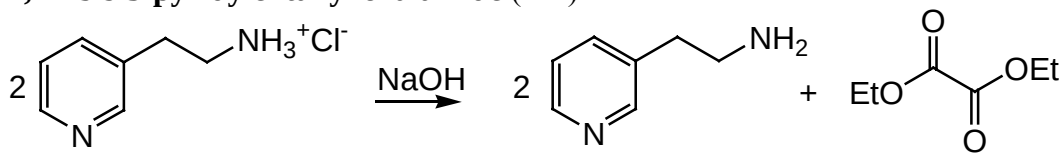

2a

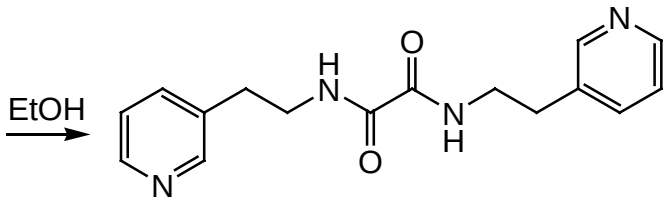

M2

Scheme 4.2 Synthetic route to host compound **M2**.

3-pyridineethylamine (**2a**)

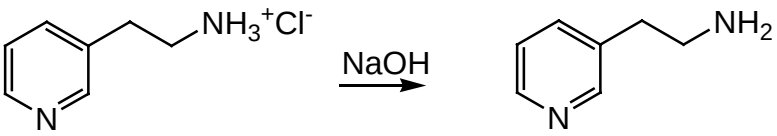

In a seperatory funnel 0.5157 g (3.25 mm) of 3-(2-aminoethyl)pyridine hydrochloride is mixed with 30 mL of dichloromethane. Enough 1M sodium hydroxide is added to make the pH of the resulting solution basic. The solution is mixed thoroughly and the organic layer collected. The remaining aqueous layer is washed twice more with 10 mL of dichloromethane and the three organic fractions are combined. The organic solution is then concentrated under vacuum yielding 0.3984 g of yellow oil (~99%). ^{13}C NMR (400 MHz CDCl3): δ150, 147, 136, 135, 123, 43, 37.

N,N'-bis-3-pyridylehtanyl oxalamide (**M2**)

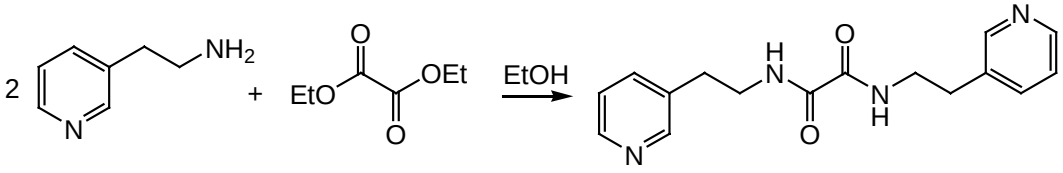

Too a rapidly stirring solution of 0.3894 g (3.26 mmol) of 3-pyridineethylamine (**2a**) in 10 mL of ethanol was added 0.2344 g of diethyl oxalate drop-wise. After stirring at room temperature for 12 hours the mixture was condensed under vacuum and a white powder was recovered. The white powder was dissolved in a minimum amount of methanol. The solvent was allowed to evaporate producing 0.4379 g of nearly colorless crystals (91%). Mp 187-188 °C; ^{1}H NMR (400 MHz CDCl3): δ2.9 (t 2H), 3.6 (q 2H), 7.2 (t 1H), 7.5 (d 1H), 7.5 (bs 1H), 8.5(s 1H), 8.5(d 1H), the singlet at ~1.7 ppm is from water in the NMR solvent; ^{13}C NMR (400 MHz CDCl3): δ160, 150, 148, 136, 134, 124, 40, 33.

N,N'-bis-4-pyridylehtanyl oxalamide (**P2)**

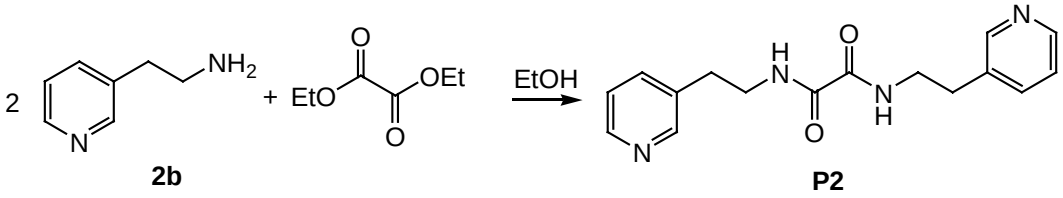

Scheme 4.3 Synthetic route to host compound **P2.**

Too a rapidly stirring solution of 1.2670 g (10.4 mmol) of 4-pyridineethylamine (**2b**) in 10 mL of ethanol was added 0.7301 g of diethyl oxalate drop-wise. After stirring at room temperature for 12 hours the mixture was condensed under vacuum and a white powder was recovered. The white powder was dissolved in a minimum amount of methanol. The solvent was allowed to evaporate producing 1.4220 g of nearly colorless crystals (95%). Mp 165-166 °C; ^{1}H NMR (400 MHz CDCl3): δ2.9 (t 2H), 3.6 (q 2H), 7.1 (d 2H), 7.5 (bs 1H), 8.5(d 2H), the singlet at ~1.6 ppm is from water in the NMR solvent; ^{13}C NMR (400 MHz CDCl3): δ160, 150, 147, 124, 40, and 35.

N,N'-bis-3-pyridylpropanyl oxalamide (M3)

Bis-pyridyl oxalamide **M3** was synthesized by Alex Ceballos and David Connors from the commercially available 3-pyridinepropanol via a Mitsunobu reaction followed by reaction with diethyl oxalate following Scheme 4.4.[59] The details of this reaction are reported elsewhere.

N,N'-bis-3-pyridylbutanyl oxalamide (**M4)**

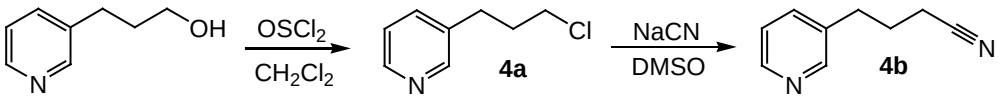

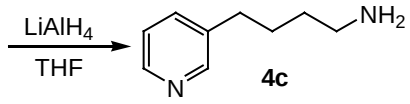

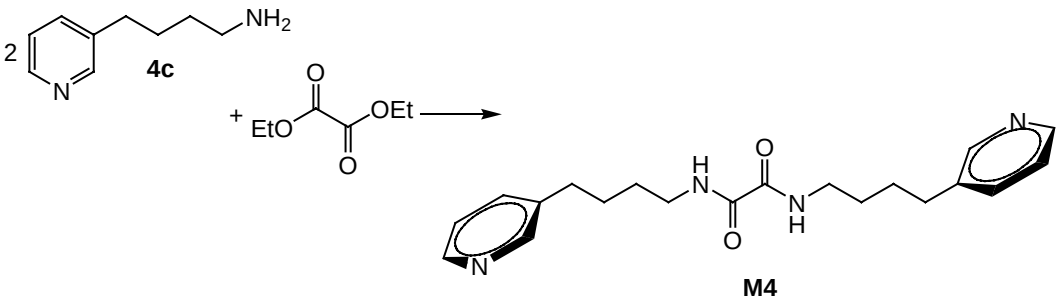

Scheme 4.5 and **Scheme 4.6** Modified version of Hawes and Davis's synthesis of 3-pyridinebutanamine with synthesis of host molecule **M4**.[60]

3-(3-chloropropyl)pyridine (4a)

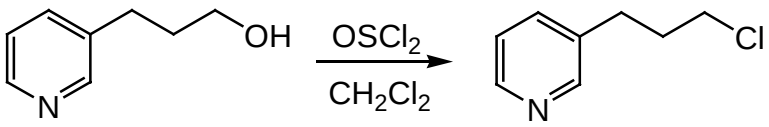

To a rapidly stirring solution of 2.0323 g 3-pyridinepropanol (14.94 mmol) in 30 mL of dichloromethane placed in an ice-bath, was added 1.9879 g of thionyl chloride drop wise. The mixture was allowed to stir for 15 minutes at 0 °C and

then for 4 hours at room temperature. The resulting solution was concentrated under vacuum and yielded 2.3121 g of a brown oil (99%). ^{13}C NMR (400 MHz CDCl3): δ146, 142, 141, 139, 127, 43, 33, 30.

4-pyridin-2-yl-butyronitrile (4b)

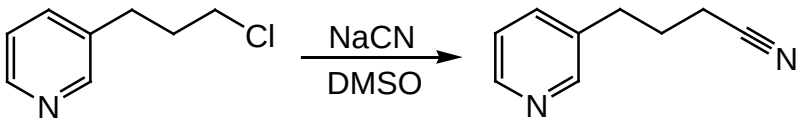

0.8277 g of sodium cyanide (19.9 mmol) was dissolved in 20 mL of dimethyl sulfoxide with rapid stirring and the temperature was brought to 80° C in an oil-bath. To this mixture 2.3121 g of compound **4a** (14.9 mmol) in 10 mL of dimethyl sulfoxide was added drop-wise, and the solution temperature was raised to ~130° C. This mixture was allowed to stir for 12 hours. The reaction was quenched with 100 mL of DI and poured into a 500 mL speratory funnel. 30 mL of dichloromethane was added, the mixture was agitated and then the organic layer was collected in a 250 mL round bottom flask. The aqueous layer was then washed three more times in this manner. The organic fractions were combined, and concentrated under vacuum yielding 1.9049 g of a brown oil (88%). ^{13}C NMR (400 MHz CDCl3): δ150, 148, 136, 135, 124, 119, 32, 27, 17.

3-pyridinebutanamine (4c)

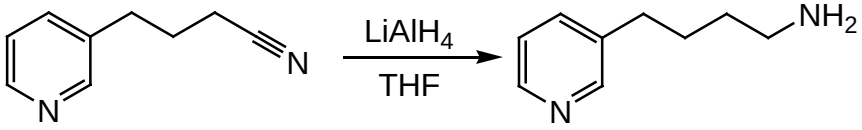

1.0215 g of lithium aluminum hydride (26.9 mmol) was added to 10 mL of and dry tetrahydrofuran and stirred rapidly at 0 °C in an ice-bath under an argon atmosphere. To this 1.9049 g of compound 4b (13.0 mmol) dissolved in 20 mL of dry tetrahydrofuran was added drop-wise. The mixture was stirred for an additional 20 minutes and then brought up to room temperature. The mixture was allowed to stir for an additional 2 hours at room temperature. The reaction was then quenched with a minimum of water and filtered via vacuum filtration. The filtrate was washed with 30 mL of dichloromethane and the resulting aqueous/organic mixture was separated using a 250 mL separatory funnel. The aqueous layer was then washed three more times with 10 mL of dichloromethane. The organic fractions were combined and concentrated under vacuum yielding a brown oil (82%). ^{13}C NMR (400 MHz CDCl3): δ150, 147, 137, 136, 123, 42, 33, 33, 28.

N,N'-bis-3-pyridylbutanyl oxalamide (**M4)**

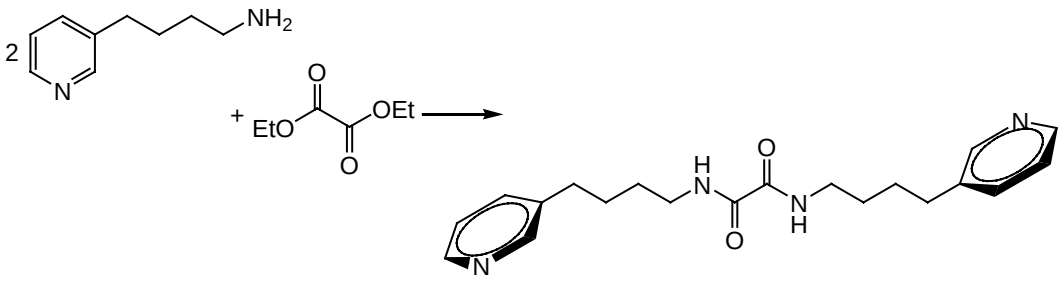

Too a rapidly stirring solution of 0.3324 g (2.2 mmol) of 4c in 1 mL of ethanol was added 0.1600 g of diethyl oxalate drop-wise. After stirring at room temperature for 12 hours the mixture was condensed under vacuum and a brown oil was recovered. The sample was purified over silica gel. No percent yield could be obtained because the sample could not fully purified. ^{13}C NMR (400 MHz CDCl3): δ60, 149, 147, 138, 137, 124, 39, 33, 29, 28.

Co-crystals

Co-crystals of **2M**/**1**, and **3M/1** were prepared by dissolving compounds **2M** or **3M** and **1** in warm methanol in a 1:1.5 or 1:1 ratio. The solution was then subjected to centrifugation and decanted into a crystallization dish. The solvent was then subjected to slow evaporation.

Single-Crystal X-Ray Diffraction

Crystals were obtained as described, and then selected with an optical microscope and epoxied on thin glass fibers. The crystal was centered and the x-ray intensity data were measured on a Bruker AXS diffractometer. The data were collected using graphite-monochromated Mo radiation and then structures were solved by direct methods and refined using full matrix least squares methods (SHELX97). SHELX97 – Programs for Crystal Structure Analysis (Release 97-2): G.M. Sheldick, SHELX-98, Program for the Solution of Crystal Structures, University of Göttingen, Göttingen (Germany), 1998.

Raman Spectroscopy

Raman spectroscopy was performed using a Thermo Nicolet Almega dispersive Raman spectrometer coupled with an infinity corrected, confocal design microscope. The spectrometer uses a 785 nm class I laser, and the data were

collected in the reflection mode of the microscope at a slit width of 25 μm. The data were collected and analyzed using the Omnic software suite (Nicolet, USA).

RAMP ^{13}C CP MAS-NMR

All RAMP ^{13}C CP MAS-NMR spectra were taken at room temperature using a Varian Infinity Plus 360 NMR spectrometer with a 4 mm double resonance probe and 4 mm zirconia rotor. The probe was tuned to 90.5 MHz for ^{13}C and 360.0 MHz for ^{1}H. The ^{13}C MAS-NMR spectra were collected using a CP RAMP pulse program with a contact time of 2ms, a pulse delay of 2s.[4] The number of steps in the CP RAMP ranged from 8-12 and the amplitude step size ranged from .001 to .01. These parameters lead to an X channel amplitude range of .3100-.4000. Over 1000 scans were acquired. Hexamethylbenzene (HMB) was used to set the Hartman-Hahn match condition, the 131 ppm resonance acting as a secondary reference.

Solution State NMR

Solvents were used as purchased without further purification. Host molecules were dissolved in $CDCl_3$. NMR spectra were collected at 25° C using a Varian 400 operating at 100.5 MHz for ^{13}C.

UV-visible Spectroscopy

All UV-visible spectroscopy were taken at room temperature using a Cary 100 UV/Visible Scan Spectrophotometer scanning from 450 to 900 nm with a resolution of 1 nm.

4.9 References

16. Schauer, C.L.; Matwey, E.; Fowler, F.W.; and Lauher, J.W. Controlled Spacing of Metal Atoms via Ligand Hydrogen Bonds. *J. Am. Chem. Soc.* **1997**, *119*, 10245-10246.

38. Webb, J.A. Small Molecule Carbon-Rich Compounds: from Polymerization to NMR Studies. PhD. Dissertation. SUNY Stony Brook, 2004.

39. Sun, A.; Lauher, J.W.; and Goroff, N.S. Preparation of Poly(diiododiacetylene), an Ordered Conjugated Polymer of Carbon and Iodine. *Science* **2006**, *312*, 1030-1034.

44. Luo, L.; Wilhelm, C.; Sun, A.; Grey, C.P.; Lauher, J.W.; and Goroff, N.S. Poly(diiododiacetylene): Preparation, Isolation, and full Characterization of a Very Simple Poly(diacetylene). *J. Am. Chem. Soc.*, **2008**, *130*, 7702-7709.

57. Nguyen, T.N. PhD Dissertation. Hydrogen Bonded Networks. SUNY Stony Brook, 1998.

58. Tzeng, B.-C.; Chen, Y.-F.; Wu, C.-C.; Hu, C.-C.; Chang, Y.-T.; Chen, C.-K. Anion-Recognition Studies of a Re(I)-Based Square Containing the Dipyridyl-Amide Ligand. *New J. Chem.*, **2007**, *31*, 202-209.

59. Mitsunobu, O.; Wada, M.; Sano, T. Stereospecific and Stereoselective Reactions. I. Preparation of Amines from Alcohols. *J. Am. Chem. Soc.*, **1972**, *94*, 679-680.

60. Hawes, E.M.; and Davis, H.L. Intramolecular Nucleophilic Cyclization of 3-Substituted Pyridylalkylamines onto the 2-Position of the Pyridine Ring. *J. Heterocycl. Chem.* **1973**, *10*, 39-42.

61. Eisch, J.J.; Gopal, H.; and Russo, D.A. Preparation and Aluminum Chloride Induced Rearrangement of Cyclopropylpyridines. *J. Org. Chem.* **1974**, *39*, 3110-3114.

62. Friedman, L.; and Shechter, H. Preparation of Nitriles from Halides and Sodium Cyanide. Advantageous Nucleophilic Displacement in Dimethyl Sulfoxide. *J. Org. Chem.* **1960**, *25*, 877-879.

Chapter 5. NMR Studies of the Bis-Nitrile Host Molecules, PIDA, and other Related Studies

5.1 Introduction and Background

MAS-NMR has proven to be a powerful tool for the study of polymer **2**. This method has been useful in identifying the starting materials and products in these studies, even when they co-exist within the same sample, while other methods have demonstrated a propensity to give falsely positive or negative results. Furthermore, NMR is a flexible and convenient analytical tool. For these reasons MAS-NMR has been used for the purposes of identifying samples suitable for studies of the polymerization reaction intermediates and high field NMR has been used to study of polymer **2** after it has been isolated from the co-crystal lattice.

The studies of polymer **2** reported here were performed on PIDA that was isolated from the **6N**/**2** co-crystal system by Liang Luo. Luo has developed a method for extracting the polymer from the co-crystal lattice by sonication in various solvents. This extraction process can be followed, in-situ, by UV-visible spectroscopy, and Luo has studied the isolated polymer using a variety of imaging techniques.[63]

Polymer **2** has been predicted to be a semi-conductor according to a study by Wang and Huang using self-consistent crystal and molecular orbital (SCF-CO and SCF-MO) calculations.[64] Studies performed on the co-crystal system by both Luo and Sun have supported this prediction.[63,65] However, isolated PIDA may prove

to behave differently, and isolated PIDA may be doped, whereas there is no obvious route to dope PIDA while it is contained in a co-crystal lattice. For these reasons, the ability to isolate PIDA from the co-crystal lattice has become important from a materials perspective.

5.2 High-Field NMR Studies of the Nonequivalent Lewis Base Interactions in the Bis-Nitrile Hosts

The single-crystal structure of the bis-nitrile co-crystal **N4**/**2**, and the likely packing of co-crystal **N6**/**2**, demonstrate two nonequivalent interactions at the acidic iodine atomic positions. One type of iodine atom is associated via a halogen bond with the terminal nitrile group of the host molecule, while the other is in close contact with the π-bond of the oxalamide system, as demonstrated in Figure 5.1.[39] Both of these interactions are weaker than the Lewis base interaction within the bis-pyridyl co-crystals, lowering the chemical shift of C1/C4 in polymer **2** by ~10 ppm according to MAS-NMR.[39,44]

High-field MAS-NMR studies of the **N4**/**2** co-crystal system may be able to resolve the two different C1/C4 chemical shifts. If the resolution is great enough, and the different carbon shifts can be clearly seen, then this same methodology can be applied to the **N6**/**2** co-crystal system to prove that it packs in a similar manor. To-date, a single-crystal structure of the **N6**/**2** co-crystal system has not been resolved, although the dimensions of the unit cell support a 2:1 guest to host ratio. If this nonequivalent Lewis base interaction can be identified within the

MAS-NMR spectrum of the **N6**/**2** co-crystal sample, this will be further evidence that both the **N6**/**2** and **N4**/**2** co-crystal pack with a similar 2:1 guest to host ratio. Furthermore, we should be able to identify the approximate amount of polymerization within this co-crystal system.

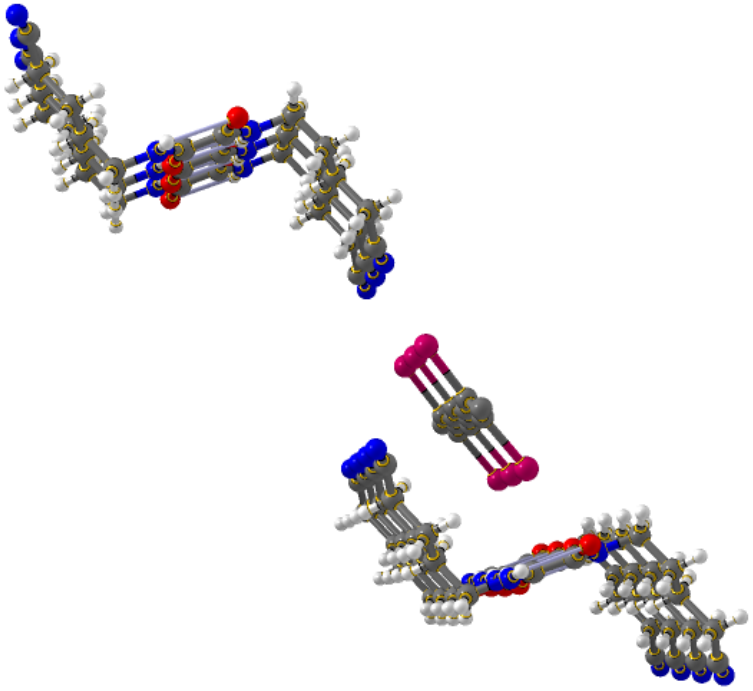

Figure 5.1 Crystal packing of **N4**/**2** co-crystal.[39]

A powder sample of **N4**/**2** co-crystals was packed in a 1.8 mm rotor and subject to a RAMP CP MAS NMR experiment in a 750 (rel. ^{1}H) MHz magnetic field. Figure 5.2 shows this high-field spectrum compared to a spectrum collected at 360 MHz (rel. ^{1}H). The red arrows in the Figure indicate the isotropic shifts of polymer **2**. The improved resolution at the higher field is demonstrated by the obvious splitting of the nonequivalent C1/C4 chemical shifts, with two peaks

appearing at ~86 and 81 ppm. In this material, the difference in these interactions is significant, resulting in the further splitting of the C2/C3 chemical shifts by ~2 ppm.

From both of these spectra we can see not only this nonequivalent interaction, but also the absence of the monomer peak, at ~ 79 ppm. This is further evidence that the **N4/2** co-crystal system approaches 100% polymerization. The peak at ~79 ppm becomes important because the second monomer peak, ~18 ppm, will be hidden under the alkyl-chain resonances. This methodology can be exploited to gain insight on the packing and percent polymerization of the **6N**/**2** co-crystal system.

A similar experiment was performed on a sample of **N6**/**2** co-crystals at 700 MHz (rel. ^{1}H), and the spectrum acquired is depicted in Figure 5.3. Again the splitting of the C1/C4 chemical shifts is easily resolved in this sample. There is no visible splitting of the C2/C3 isotropic peaks in this sample, but the C1/C4 splitting of ~4 ppm is readily observable. This data provides strong evidence that the **N4** and **N6** co-crystals pack in a similar manner, with a 2:1 guest to host ratio. This packing pattern is evidently beneficial for the spontaneous production of PIDA within co-crystal samples of the bis-nitrile type.

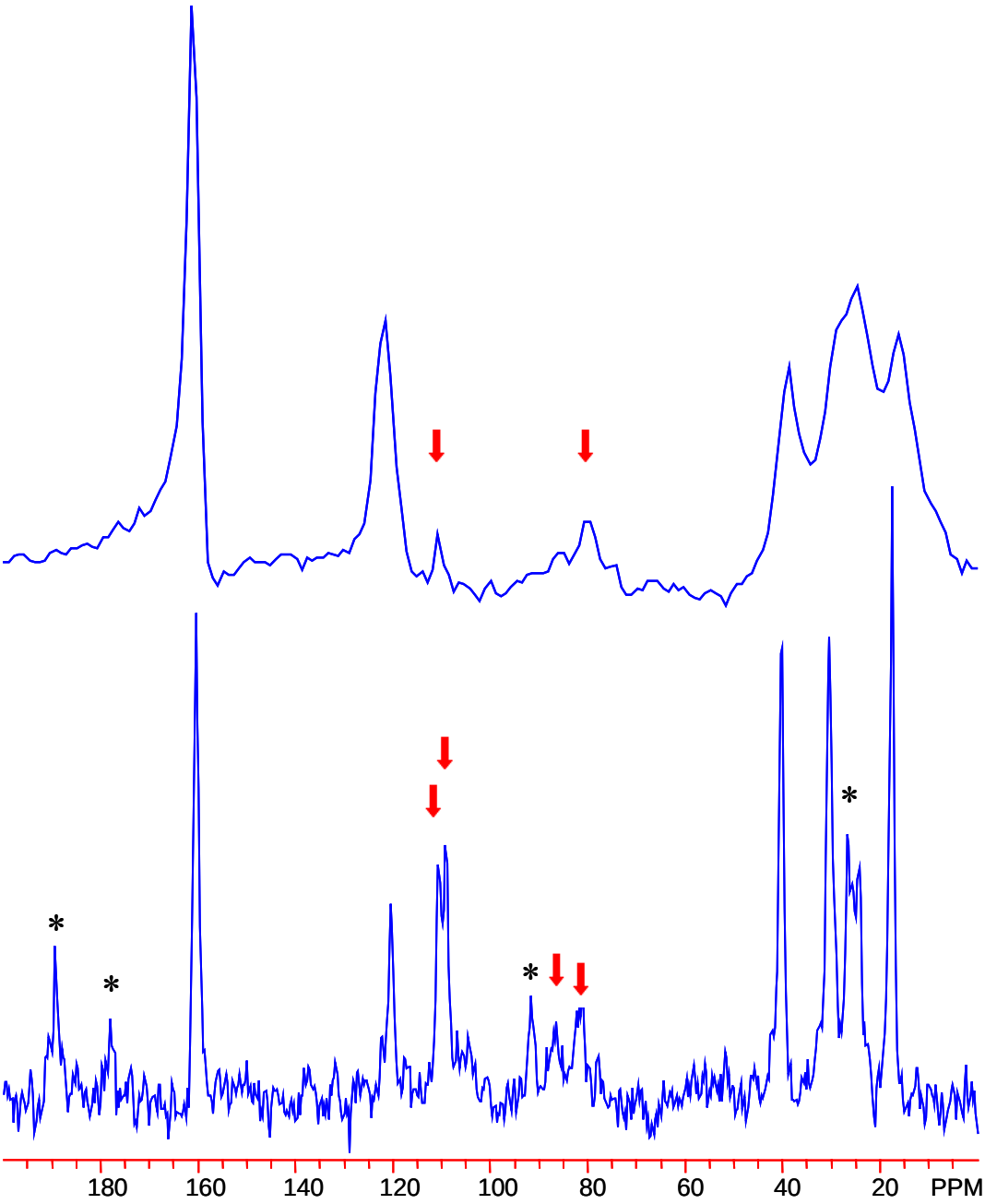

Figure 5.2 (top) RAMP ^{13}C CP MAS-NMR spectrum of **N4/2**, isotropic polymer peaks are indicated by arrows; Experiment was performed at 360 MHz with a 15 kHz spinning speed. (bottom) RAMP ^{13}C CP MAS-NMR spectrum of **N4/2**, isotropic polymer peaks are indicated by arrows, spinning sidebands are marked; Experiment was performed at 750 MHz with a 15 kHz spinning speed.

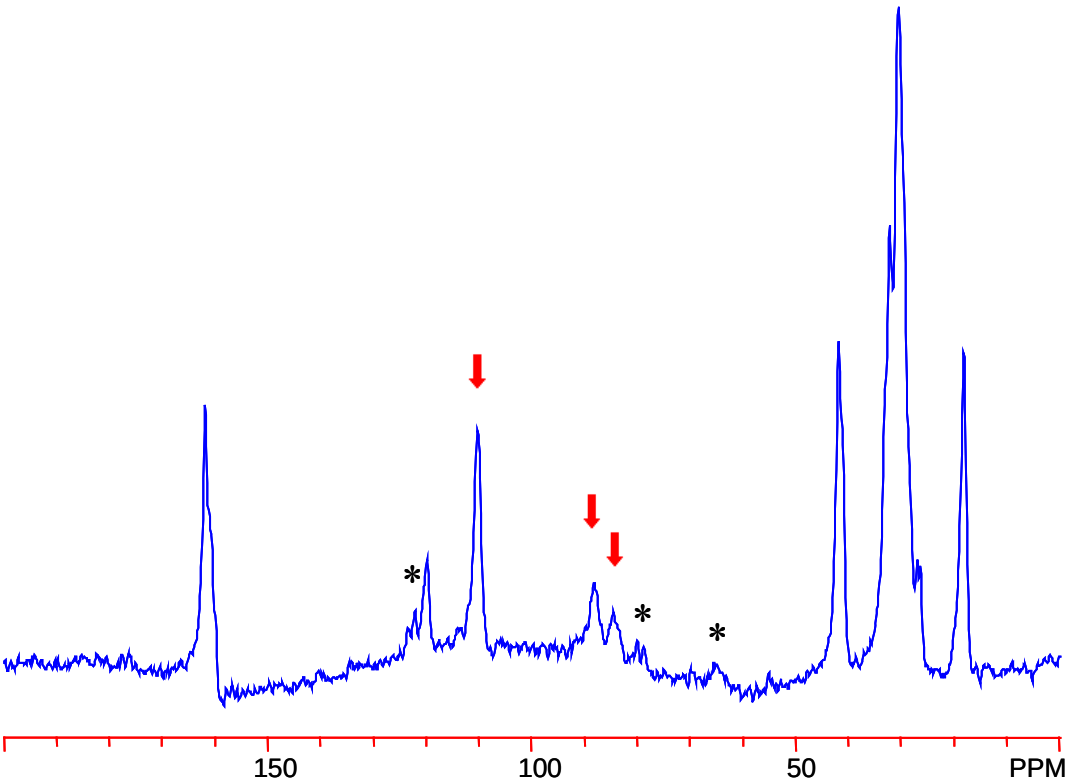

Figure 5.3 RAMP ^{13}C CP MAS-NMR spectrum of **N6/2**, isotropic polymer peaks are indicated by arrows, spinning sidebands are marked; Experiment was performed at 700 MHz with a 17 kHz spinning speed.

The spectrum in Figure 5.3 also indicates that this co-crystal system approaches 100% polymerization. It is possible that there is a small amount of unreacted monomer present, there is a small peak at ~79 ppm. However the two peaks at ~88 and 84 ppm both integrate in a 1:2 ratio with the peak at ~110 ppm, demonstrating that they result from the C1 and C4 nuclei of the polymer.

5.3 MAS-NMR Identification of a Possible In-Situ Reaction Sample

In order to perform the proper experiments for identifying the reactive intermediates produced during the topochemical polymerization reaction of diiodobutadiyne, samples must be identified that can be studied in-situ. Two such samples were discussed in Chapter 3 of this dissertation, co-crystals **M1**/**1** and **P1**/**1**. However, the practicality of performing high-pressure studies in-situ is limited. It is now possible to perform high-pressure single-crystal diffraction, however single-crystal XRD is not the most efficient way of identifying these reactive intermediates.[66] ESR has been used to study these intermediates, but literature searches indicate that the technology necessary for placing a DAC in the magnetic field of an ESR spectrometer has not been developed. Therefore, it is beneficial to identify co-crystals containing monomer in which the topochemical reaction can be induced under milder conditions. One such sample is the co-crystals formed by host compound **5N** and **1**. Compound **5N** is depicted in Figure 5.4.

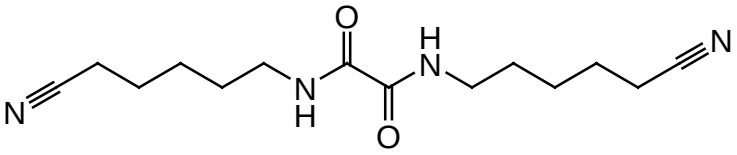

Figure 5.4 Host molecule **N5**.

Upon co-crystallization via the slow evaporation of methanol, co-crystals of **N5**/**1** appear pale blue in color, and do not visually appear to polymerize

spontaneously or to contain PIDA. Unlike the **N4** and **N6** co-crystal samples, single-crystal XRD indicates that host molecule **N5** co-crystallizes in a 1:1 ratio with diiodobutadiyne.[63] This difference in packing maybe the reason that PIDA does not polymerize in the **N5**/**1** co-crystals under ambient conditions. However, MAS-NMR experiments indicate that the co-crystals produced do not contain a large percentage of monomer either, see Figure 5.5. This NMR spectrum does not contain any significant or sharp peak in the region of ~70 – 100 ppm. Since both monomer **1** and polymer **2** are expected to produce carbon signals within this region it can be concluded that neither exists in a significant amount. This is not unreasonable since the reactive species are expected to be NMR silent.

When this sample is heated to 40 °C for a short period of time (24 - 72 hours), the co-crystals grow dark, eventually turning black. These dark co-crystals, as demonstrated by MAS-NMR in Figure 5.6, now contain the isotropic peaks of polymer **2**. These peaks are most likely the result of the presence of long oligomer chains of polymer **2** within the crystal lattice. This co-crystal system demonstrates a means of polymerizing diiodobutadiyne under conditions that are gentle enough to be used in-situ with almost all standard analytical techniques.

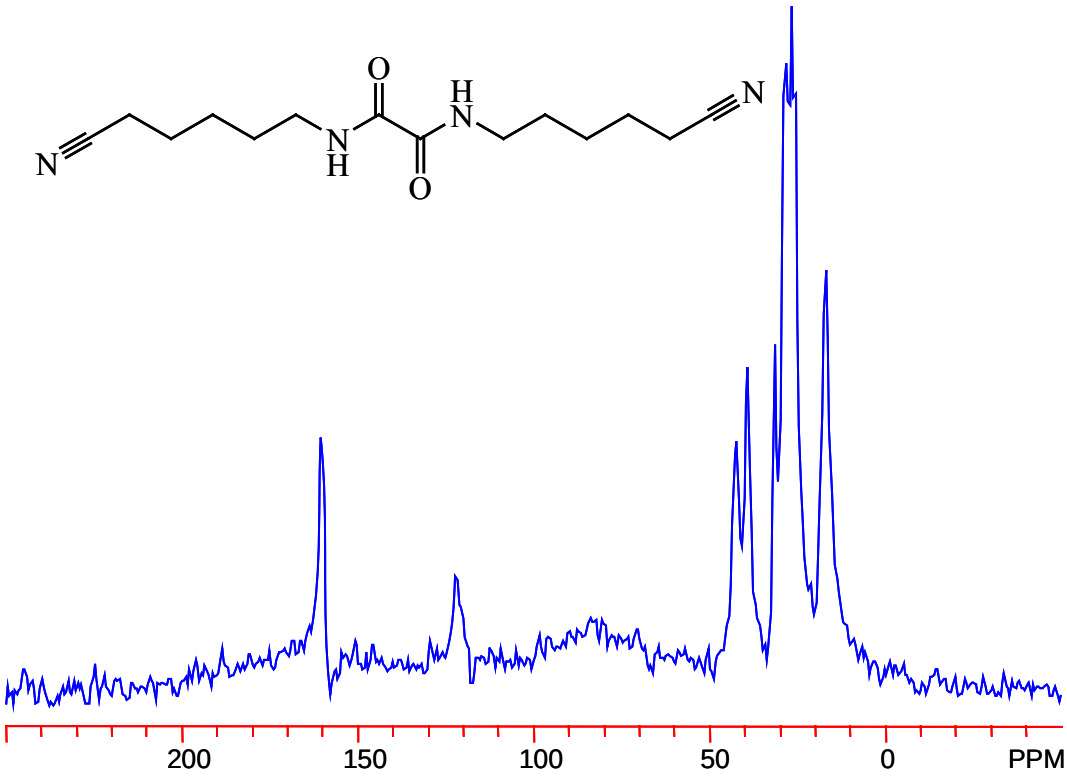

Figure 5.5 RAMP ^{13}C CP MAS-NMR spectrum of **N5/1**, indicating no monomer or polymer chemical shifts; Experiment was performed at 360 MHz with a 15 kHz spinning speed.

This system should prove to be an almost perfect material for studying the topochemical polymerization of diiodobutadiyne. Co-crystal samples can be produced as monomeric materials and polymerized in-situ in a variety of analytical instruments. ESR, MAS-NMR, and UV-visible spectra can all be acquired in real time during polymerization. This may not only allow for a greater understanding of the topochemical reaction, but may also lead to improvements in the design of host materials.

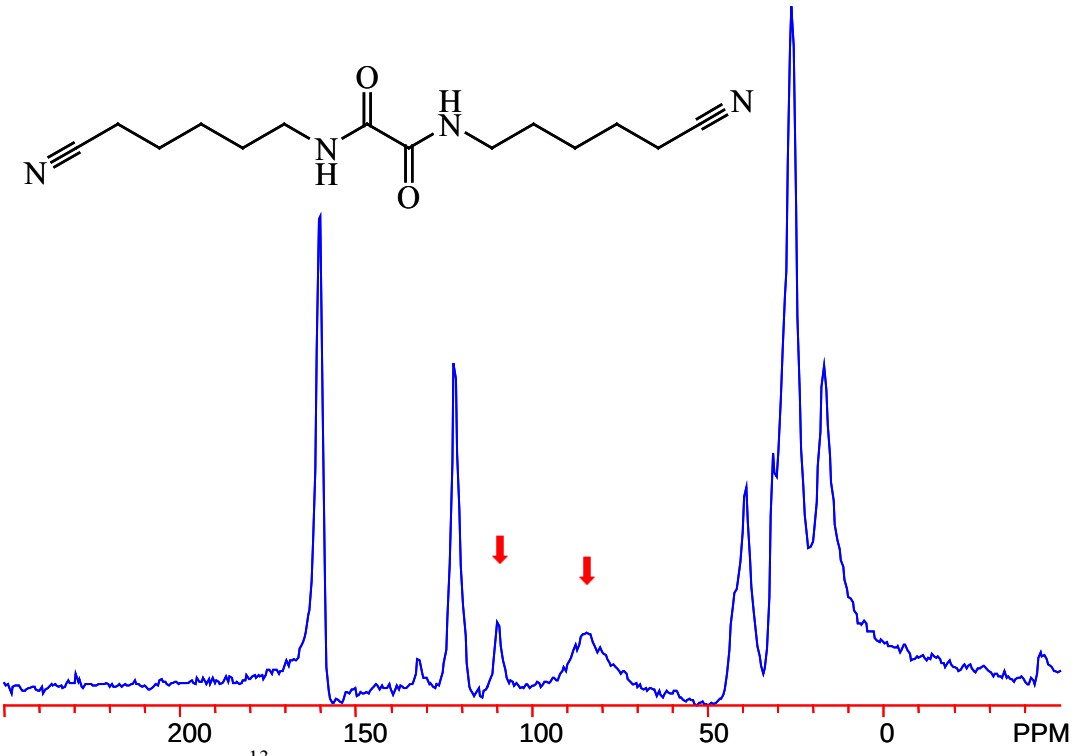

Figure 5.6 RAMP ^{13}C CP MAS-NMR spectrum of **N5/1** after heating to 40 °C for 72 hours, polymer isotropic peaks are indicated, all other peaks are due to the host molecule or spinning sidebands; Experiment was performed at 360 MHz with a 15 kHz spinning speed.

5.4 NMR Studies of Isolated PIDA

Recently, Luo has successfully isolated polymer **2** from the co-crystal lattice, making it possible to study the properties of the polymer when it is not supported by the host scaffold.[63] It is possible that once removed from this support PIDA loose the rigid ene-yne bonding structure that it maintains within the co-crystal lattice. The ene-yne bonding structure is lower in energy than the cumulenic

bonding structure, however it may not be exclusive when the polymer is allowed to fold or coil.[2]

Isolated PIDA was subjected to a 1-pulse ^{13}C MAS-NMR experiment, and the resulting spectrum is shown in Figure 5.7. A carbon 1-pulse experiment was used because of PIDA does not contain hydrogen atoms, as explained in Chapter 2.7. As this section also explains, these sample were also diluted , < 0.01 g of sample were used in these experiments. Both the small sample size and decreased efficiency of the ^{13}C 1-pulse experiments, with a 10 second pulse delay, result in the large signal-to-noise observed in the spectra reported here.

The spectrum shown in Figure 5.7 clearly shows the isotropic chemical shifts of polymer **2**, and these are consistent with the chemical shifts demonstrated in all of the co-crystal systems. Furthermore, there is a clear absence of any other carbon signals, indicating that PIDA has successfully been removed from the co-crystal lattice. The signal-to-noise ratio in this spectrum is quite high, due to the diluteness of the sample within the NMR rotor. During the work-up to this experiment it was discovered that PIDA is a contact explosive, and can combust during spinning in the NMR or during the packing of the rotor. For this reason the sample was diluted with sodium nitrate. This allowed for a small amount of matted sample (< 0.01 g) to placed within the center of the rotor, while the salt could be packed around it, preventing the sample from being compressed. The explosive properties were confirmed by controlled tests in the laboratory. PIDA

was combusted with both with pressure on the bench top and by agitation in a test tube.

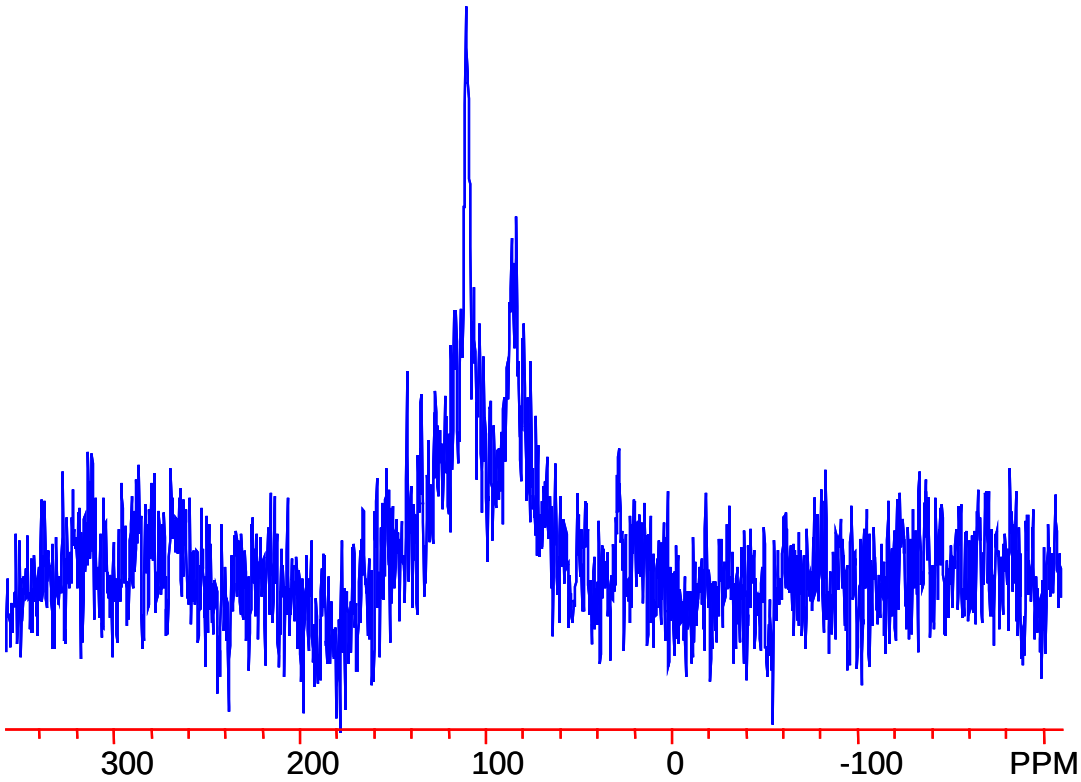

Figure 5.7 ^{13}C 1-Pulse MAS-NMR spectrum of **2** demonstrating isotropic shifts at ~110 and 85 ppm; Experiment was performed at 700 MHz with a 31 kHz spinning speed.

Following this experiment, Luo treated polymer **2** with pyrrolidine.[63] An excess of Pyrrolidine was added to a blue suspension of PIDA in methanol. This mixture was subjected to centrifugation, the solvent decanted, and the remaining black solid was allowed to dry.[63] According to Luo's UV-visible studies of PIDA, treatment with a Lewis base may change the bonding structure of the polymer. Luo prepared a sample of polymer **2** treated with Pyrrolidine (the

solvent was decanted and the solid allowed to dry) and it was subject to an identical MAS-NMR experiment.[63] Difficulty was encountered in spinning this sample within the magnetic field, a property associated with eddy currents and a possible indication that this material may be conductive, so the sample was again diluted with sodium nitrate.[67-69] The spectrum acquired is depicted in Figure 5.8.

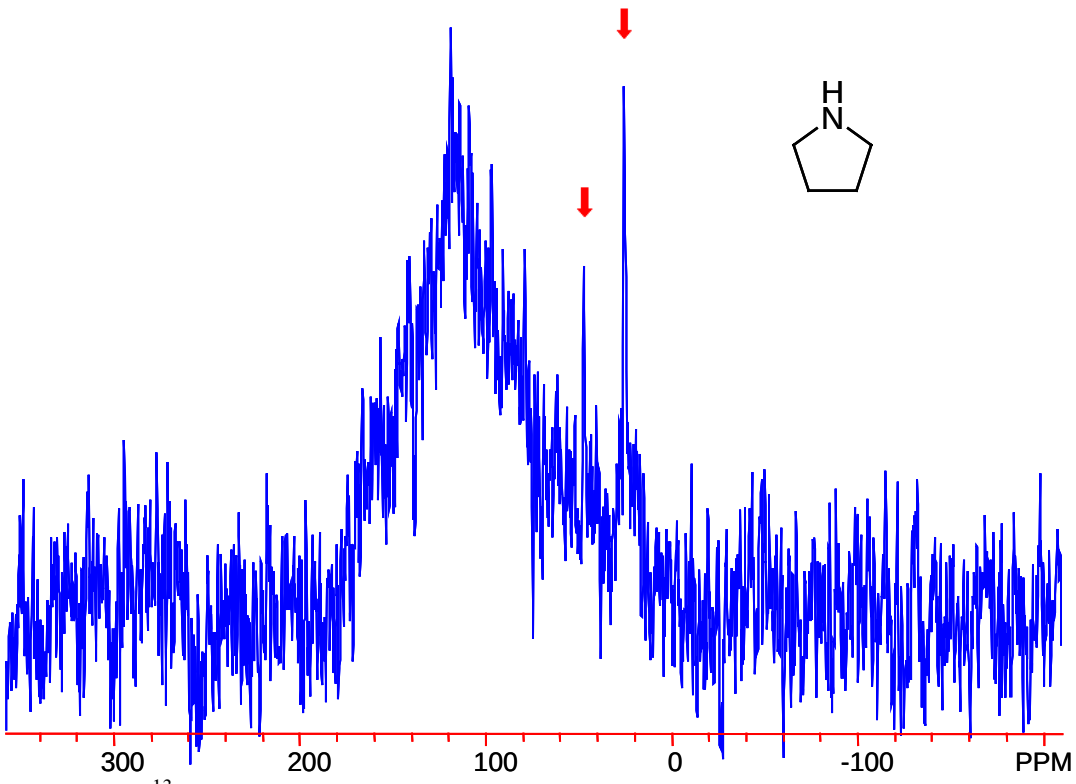

Figure 5.8 ^{13}C 1-Pulse MAS-NMR spectrum of **2** treated with pyrrolidine (inset) demonstrating isotropic shifts at ~47 and 25 ppm marked with arrows, consistent with Pyrrolidine; Experiment was performed at 700 MHz with a 31 kHz spinning speed.

This spectrum depicts two isotropic chemical shifts consistent with the presence of Pyrrolidine (~48 and 25 ppm). However, the isotropic shifts of

polymer **2** appear as one broad peak centered at ~120 ppm. This phenomenon is also consistent with conductivity.[70-72] As a means to further explore the possibility that PIDA becomes conductive when treated with a Lewis base, Luo next treated a sample of polymer **2** with pyridine, a weaker Lewis base, in a similar manner.[63] A dried sample of isolated PIDA was dispersed in pyridine. This solution was then subjected to centrifugation, the solvent was decanted, and the remaining black solid was allowed to dry.[63] This sample was also subject to a 1-pulse ^{13}C MAS-NMR experiment, the spectrum acquired is shown in Figure 5.9.

Again, this sample had to be diluted with sodium nitrate in order to allow for the rotor to spin within the magnetic field. The presence of the base can easily be seen by the isotropic shifts observed (~146, 145, and 128 ppm), but they are not consistent with the spectrum of a PIDA sample that has been saturated with pyridine (~149, 139, and 125 ppm), shown in Figure 5.10. The isotropic peaks shown in Figure 5.9 are consistent however, with a pyridine molecule associated with an iodine molecule, see Table 5.1.[73] The isotropic resonances assigned to PIDA again present as one broad peak centered at ~130 ppm. This further supports the hypothesis that polymer **2** becomes conducting upon treatment with a Lewis base.

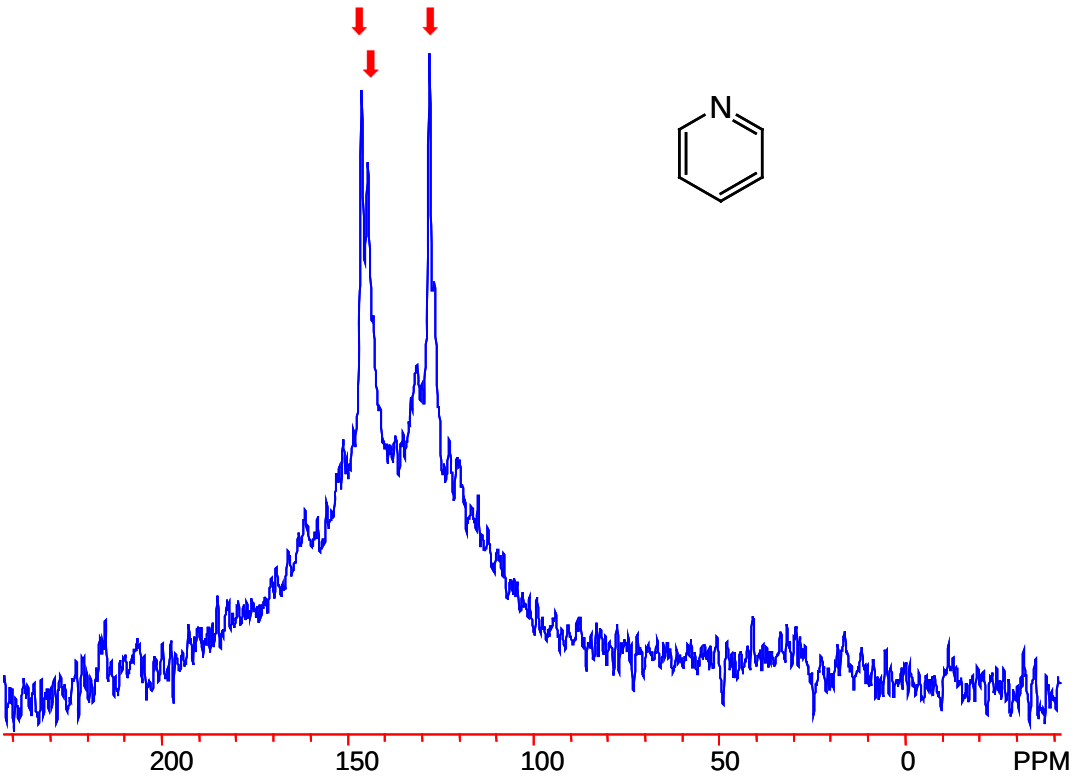

Figure 5.9 ^{13}C 1-Pulse MAS-NMR spectrum of **2** treated with pyridine (inset) demonstrating isotropic shifts at ~146, 145 and 128 ppm marked with arrows, consistent with pyridine-iodine complex; Experiment was performed at 500 MHz with a 30 kHz spinning speed.

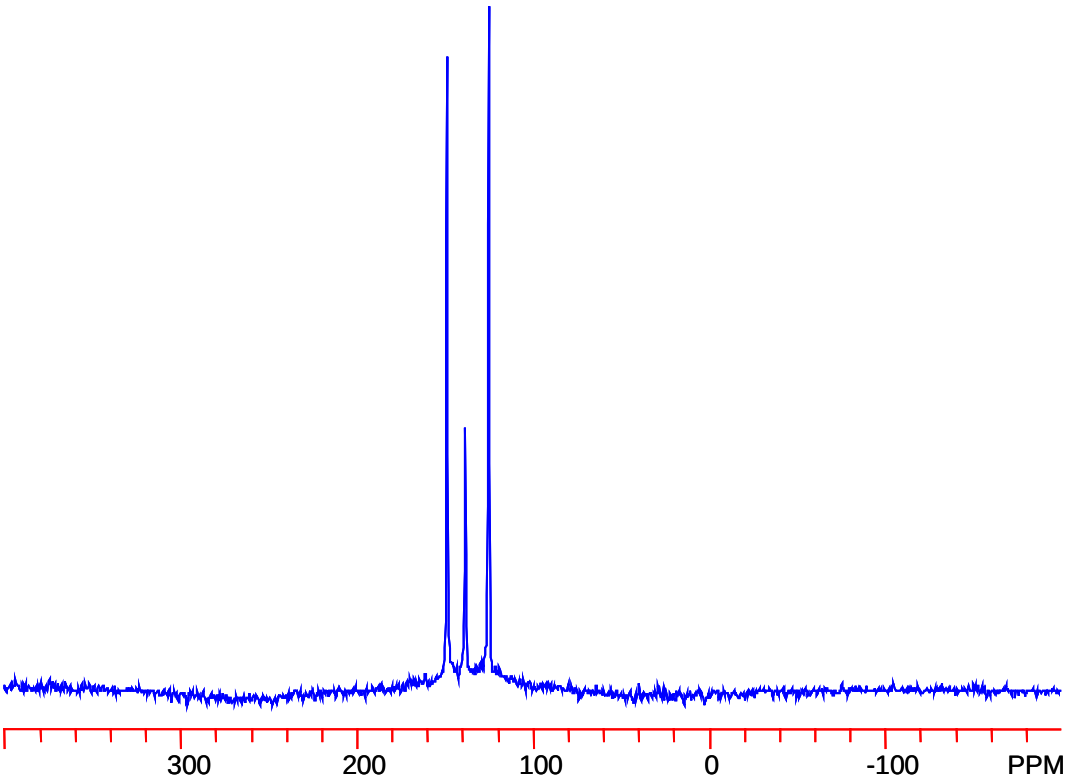

Figure 5.10 ^{13}C 1-Pulse MAS-NMR spectrum of **2** saturated with Pyridine (inset) demonstrating isotropic shifts at ~149, 139 and 125 ppm, consistent with Pyridine; Experiment was performed at 600 MHz with a 31 kHz spinning speed.

The change in the ^{13}C NMR resonances is shown in Table 5.1. The pyridine saturated sample (P.S. PIDA) was not dried, and has carbon peaks near that of pyridine in solution, 150, 136, and 124 ppm. However, the pyridine treated sample (P.T. PIDA) was allowed to air-dry before the MAS-NMR experiment was performed, and contains a lower concentration of pyridine. These NMR shifts are more consistent with those reported by Larkindale and Simkin in the solution state NMR of a pyridine-iodine complex (P.-I Complex).[73]

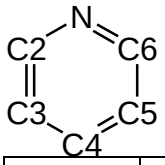

^{13}C δ	P.S. PIDA	P.T. PIDA	Observed Δ	P.-I. Complex[73]
C2 and C6	146	149	-3	-1
C3 and C5	145	139	-6	-3
C4	128	125	-3	-5

Table 5.1 Comparison of MAS-NMR shifts.

More recent TEM studies performed by Luo demonstrate that the ratio of carbon to iodine atoms has increased as a result of treatment with a Lewis base.[63] This new material may be an iodine-depleted polymer, or it may have a new, non-PDA bonding system. The broad peaks observed in the base-treated MAS-NMR results support the conductivity of the base treated samples, and are also similar to the reported MAS-NMR spectrum of graphite, a broad peak centered at ~125 ppm, but no definitive conclusions have be reached as to the bonding-structure or conductivity of these samples.[70-72,74]

5.5 Isolation of PIDA from the M2 Co-crystal Lattice

Liang Luo has previously demonstrated that PIDA can be isolated from the co-crystal lattice.[63] MAS-NMR experiments confirming Luo's results were described in Chapter 5.4. It is prudent then to attempt an isolation of PIDA from the **M2**/**2** co-crystal system as well. As stated earlier, polymer **2** is a contact explosive, and as such MAS-NMR was not attempted to prove that PIDA has been successfully extracted from the **M2** co-crystal. However, the Raman studies

presented here do support the successful isolation of polymer **2** from the **M2** co-crystal lattice.

Following Luo's successful isolation of polymer **2**, a sample of **M2**/**2** co-crystals was subjected to sonication in methanol for a period of ~15 hours.[63] The UV-visible absorption spectra of the suspension was collected after 15 hours and was found to be similar to the results observed by Luo, confirming the isolation of polymer **2**.[63] Figure 5.11 illustrates this spectrum. This spectrum demonstrates a broad shoulder at ~750 nm, but the multiple maxima seen in the co-crystal spectrum are absent.

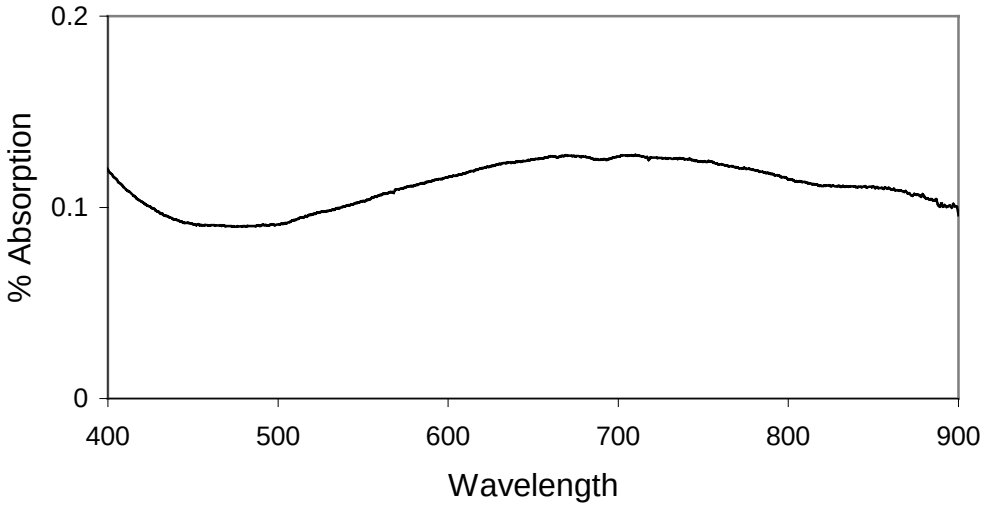

Figure 5.11 UV-visible spectrum of **M2**/**2** after fifteen hours of sonication in methanol.

The sample was then subjected to centrifugation and the blue colored solvent was decanted. The solid that remained was subject to a series of Raman

spectroscopy experiments, the results of which are almost identical to those seen by Luo.[63] The results of these experiments are shown in Figures 5.12 through 5.14. The first spectrum was acquired using an excitation wavelength of 785 nm, and demonstrates three peaks, consistent with those produced by co-crystal samples of **M2**/**2**, see Figure 5.13.

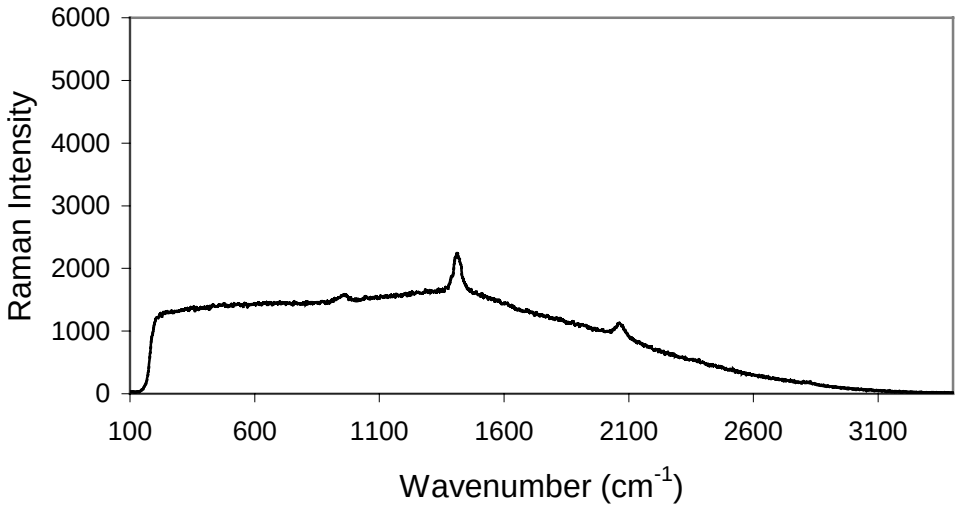

Figure 5.12 Raman spectrum of polymer **2**, excitation wavelength of 785 nm.

A spectrum was then collected using an excitation wavelength of 532 nm. Consistent with Luo's results, the spectrum of polymer **2** has changed, and no longer shows peaks consistent with the double and triple bonds of the ene-yne structure of PIDA.[63] Instead, Figure 5.13 demonstrates a broad peak at ~1600 cm^{-1} with a shoulder, a signal more indicative of fluorescence. This structural

change remains after laser excitation is removed, as demonstrated in Figure 5.14 a third spectrum collected using an excitation wavelength of 785 nm.

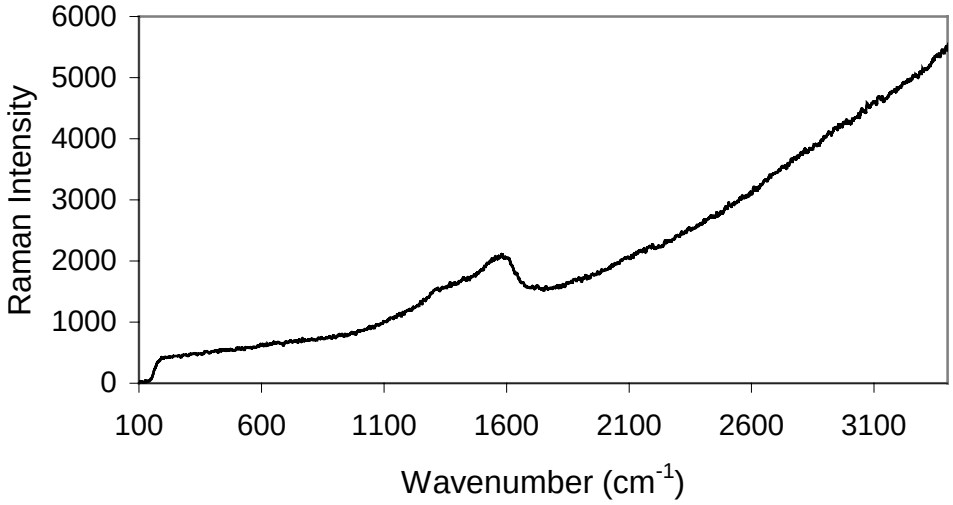

Figure 5.13 Raman spectrum of sample depicted in Figure 5.12, collected using an excitation wavelength of 532 nm.

The structural change occurring when polymer **2** is exposed to the higher energy, shorter wavelength laser, is still being investigated using a variety of analytical methods.[63] It is also unclear if this change is due to the loss of iodine. It can be determined though, by comparing these experimental results to those seen by Luo, that polymer **2** is being successfully isolated from the **M2** supra-structure.[63]

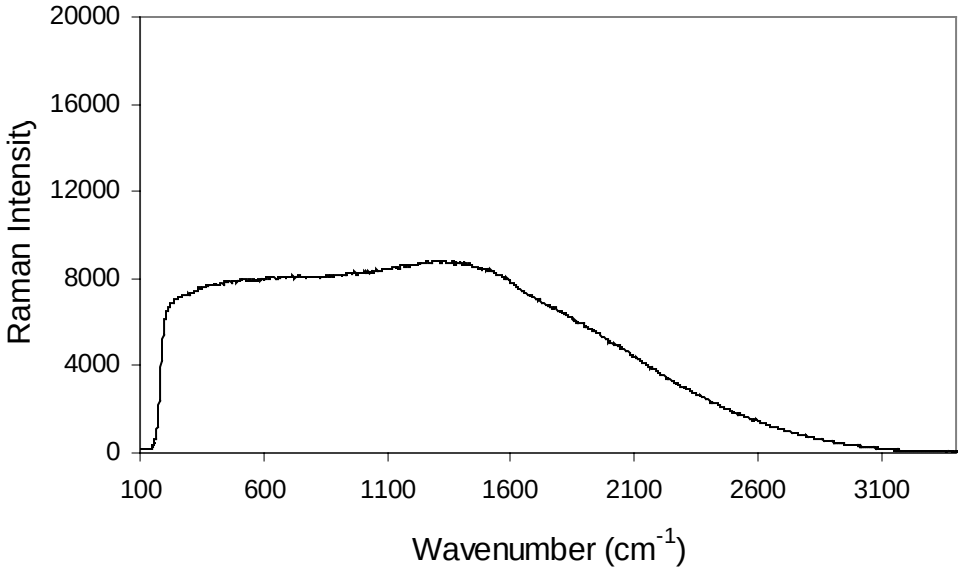

Figure 5.14 Raman spectrum of sample depicted in Figure 5.13, collected using an excitation wavelength of 785 nm.

5.6 ESR Studies of the Polymerization Intermediates

As stated in Chapter 2.7, ESR should be an appropriate means of analyzing the intermediate species produced during the topochemical polymerization reaction. Previous work on other PDA systems indicates that the reactive species will contain unpaired electrons, and therefore they will be NMR silent.[2] ESR should therefore be able to identify these intermediate structures. Much work has been done on other PDAs using single crystal samples where the orientation of the polymer backbone within the magnetic field is known. The work reported here was performed in collaboration with Professor Paul Lahti of the University of Massachusetts at Amherst, using powdered crystalline samples, and therefore

hyperfine splitting, if any is present in these reactive species, will not be detectable.[75]

A single crystal sample placed at a known orientation within a magnetic field can demonstrate hyperfine coupling to nuclei that are near the unpaired electron. This information can be interpreted to decipher structural information about the location of the unpaired spin. However, in a powder sample the observed spectrum is a sum of the hyperfine patterns in all random orientations, this can lead to line broadening and overlap, preventing the determination of structural information.[75]

However, these experiments serve as a precursor to single-crystal studies, and provide useful information supporting the viability of future experiments. Samples of both **M1**/**1** and **N5**/**1** co-crystals were grown. Both samples are known not to contain polymer **2**. The **M1**/**1** samples were annealed in a piston press under a mechanical strain of 2.5 GPa for 5 days prior to these experiments. ESR spectra were then collected from both the **M1**/**1** and **N5**/**1** samples, see Figures 5.15 and 5.16 respectively. While no hyperfine splitting is observed, the *g* shift of both spectra indicate a radical located on a carbon atom near a hetero-atom. The *g* values of the spectra are 2.0041 and ~1.99 respectively.

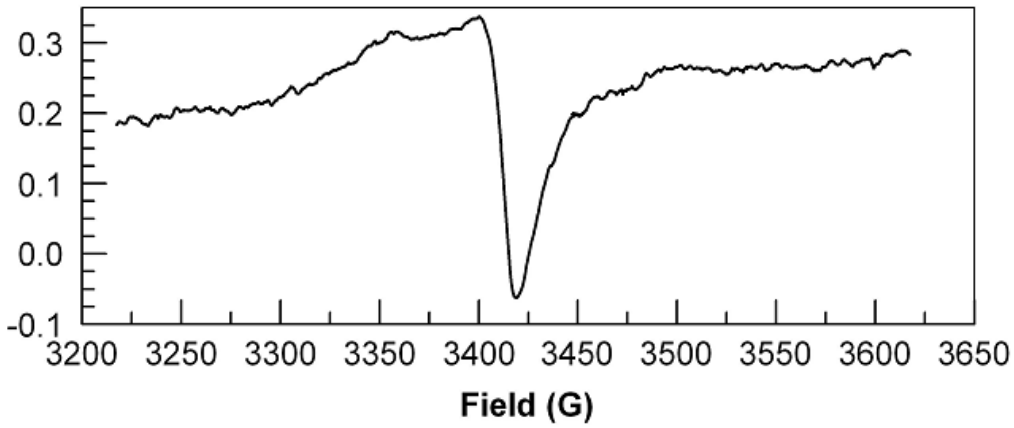

Figure 5.15 ESR spectrum of **M1**/**1** powder sample.

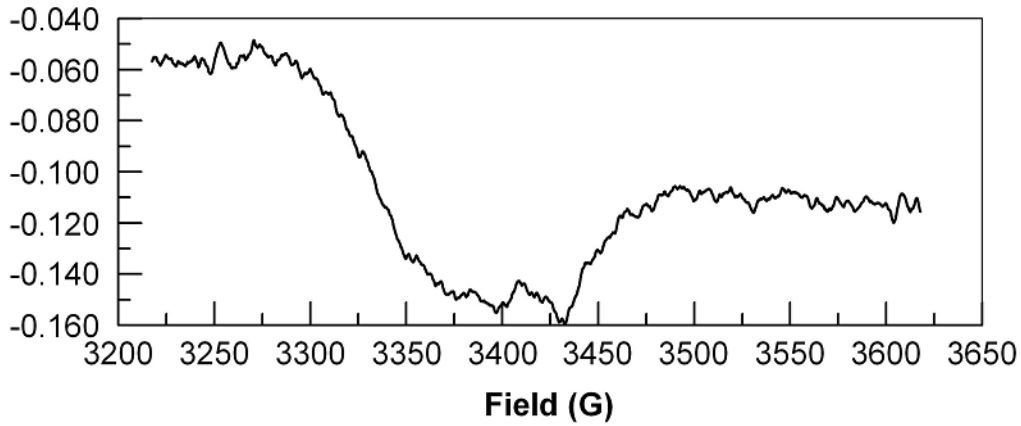

Figure 5.16 ESR spectrum of **N5**/**1** powder sample.

These samples were then allowed to sit at STP in ambient conditions. Spectra were then collected after three weeks time, and demonstrated a dramatic change in line shape. The line shapes of both spectra apparently become more symmetrical, with values of g = 1.999 and 2.0042 respectively. These g values are approximately those of a free electron (g = 2.0023).[2] These later spectra,

shown in Figures 5.17 and 5.18, are consistent with literature reports of the spectra produced by other PDAs containing high polymer percents.

The **M1**/**1** sample is already known to contain ~10% polymer after being exposed to 2.5 GPa of mechanical stress, refer to Chapter 3.3 of this dissertation. However, the **N5**/**1** sample was subject to a RAMP ^{13}C CP MAS-NMR experiment to determine the percent polymerization within this sample. Figure 5.19 depicts this spectrum. Clearly the peaks associated with PIDA (at ~110 and 80 ppm) are present. However the broadness of these peaks likely indicates the presence of long chain oligomers of polymer **2**, and does not indicate full polymerization of the monomer.

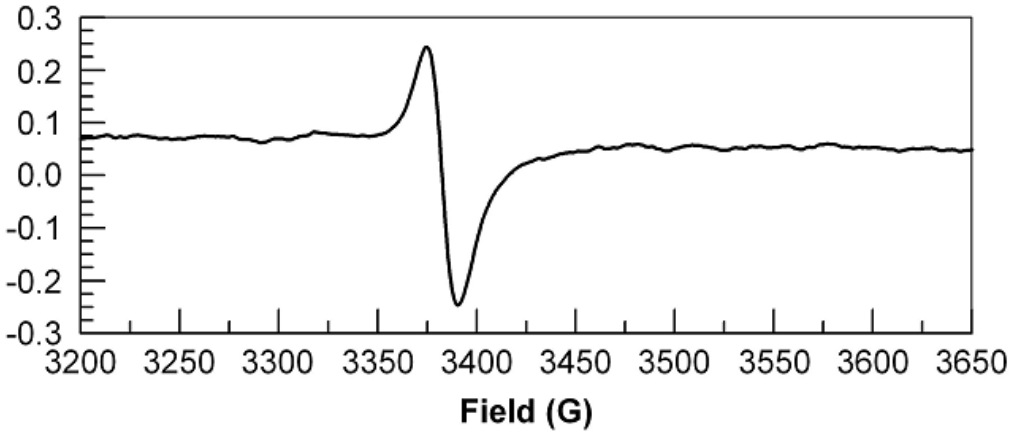

Figure 5.17 ESR spectrum of aged **M1**/**1** powder sample.

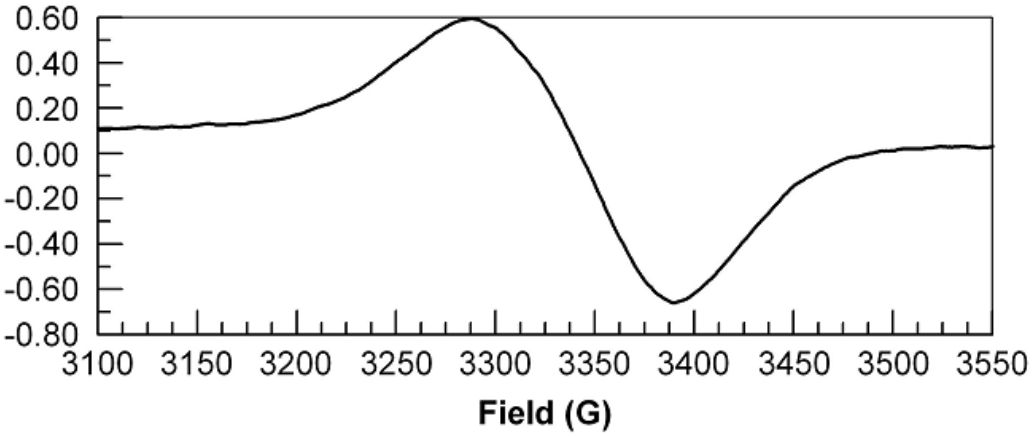

Figure 5.18 ESR spectrum of aged **N5**/**1** powder sample.

While these experiments are not sufficient to identify the structure of any reactive intermediates, they do provide important information. They confirm the presence of unpaired electron spins in both co-crystal samples. They also demonstrate the change of the ESR signal as the percent of polymerization increases. Finally, they tell us that further study of the ESR signals produced by these systems need to be study more in depth. A study of the **N4**/**2** system would be particularly beneficial, since single-crystal structures of both the monomeric and polymeric forms of the system have been resolved.[63]

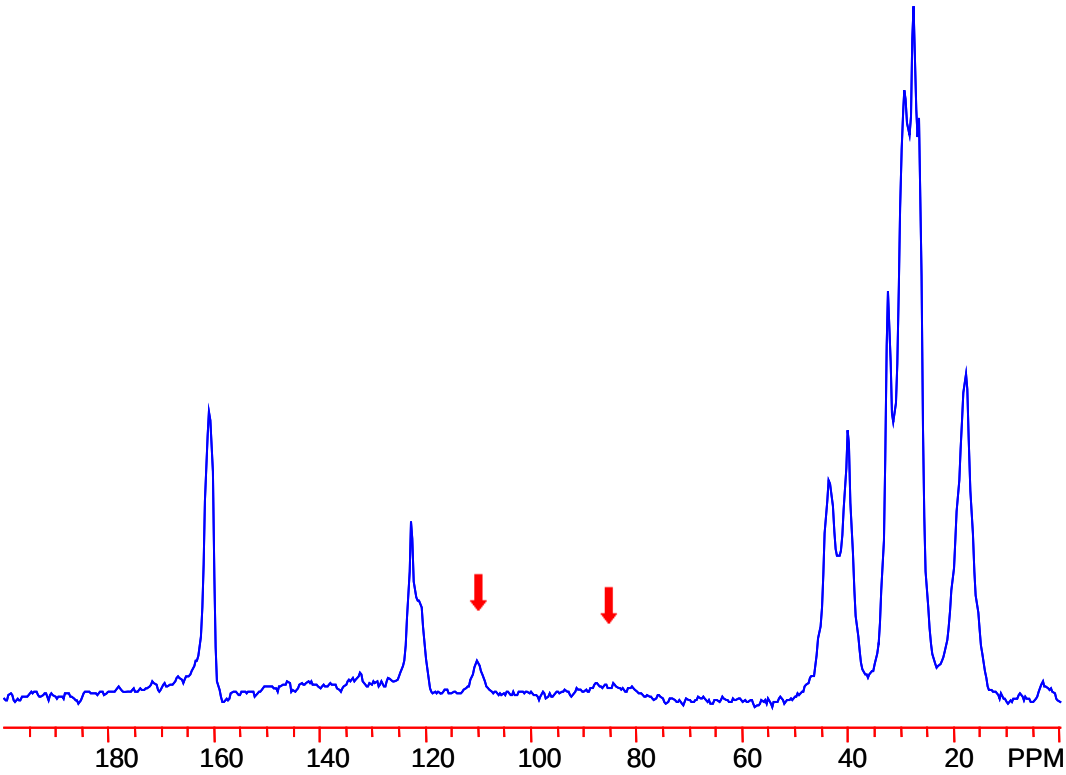

Figure 5.19 RAMP ^{13}C CP MAS-NMR spectrum of aged **N5**/**1** powder sample, polymer isotropic peaks are indicated, all other peaks are due to the host molecule or spinning sidebands; Experiment was performed at 360 MHz with a 15 kHz spinning speed.

5.7 Conclusions

This work has further demonstrated the usefulness of MAS-NMR in studying these systems. MAS-NMR can be used successfully to identify co-crystal systems, in which the polymerization reaction is not complete, as the types of models needed to study the intermediate species produced during the topochemical reaction. High-field NMR studies have been used to identify the packing behavior of samples that are not high-quality crystals, and have proven to

be of sufficient resolution to decipher the two different iodine interactions present in the bis-nitrile co-crystal systems.

High-field NMR has also been used to confirm the isolation of PIDA from the co-crystal lattice, and to begin studying the effects of base-doping PIDA. In fact, MAS-NMR studies have provided some evidence of eddy currents in base-treated samples of PIDA. This is a possible indication of conductive behavior.

Finally, ESR has been shown to be a useful method for following the topochemical polymerization reaction, and possibly identifying the reactive intermediates produced during polymerization. While the studies presented here are not of sufficient quality to determine these structures, they indicate that similar studies performed on single-crystal samples will be able to help in the assignment of the structures of these intermediates. There is clear evidence of unpaired spins during and after the topochemical reaction, as expected according to previous work.[2]

5.8 Experimental

Compounds and Co-Crystals

Compound 1
Diiodobutadiyne was synthesized according to the previously published procedure.[38]

Compounds N4, N5, N6
Bis-nitrile oxalamides **N4**, **N5**, and **N6** were synthesized by Liang Luo according to the previously published procedures.[61]

Compound M1
Bis-pyridyl oxalamide **M1** was synthesized by Lei Li, according to the previously published procedure.[14,56]

Compound M2
Bis-pyridyl oxalamide **M2** was synthesized from the commercially available 3-(2-aminoethyl)pyridine hydrochloride salt. The hydrochloride salt was dissolved in methylene chloride and washed with a concentrated solution of sodium hydroxide. The resulting mixture was separated, and the organic layer was concentrated under vacuum. The amine was isolated as a yellow oil. The amine was subsequently reacted with diethyl oxalate in a 2:1 ratio, at room temperature with stirring, in ethanol, and yielded a white powder. The powder was dissolved in warm methanol, and then subject to slow evaporation in a crystallization dish, yielding colorless crystals.

Co-crystals
Co-crystals of **N4**, **N5**, and **N6** with **1** were synthesized by Liang Luo according to the previously published procedures.[61]

Co-crystals of **M2**/**1** were prepared by dissolving compounds **M2** and **1** in warm methanol in a 1:1.5 ratio. The solution was subjected to centrifugation and decanted into a crystallization dish. The dish was covered with perforated aluminum foil and the solvent was allowed to evaporate.

Co-crystals of **M1**/**1** were prepared by dissolving compounds **M1** and **1** in warm methanol in a 1:1 ratio. The solution was then cooled to -40 °C and the resulting solid was collected by vacuum filtration.

Single-Crystal X-Ray Diffraction

Crystals were obtained as described, and then selected with an optical microscope and epoxied on thin glass fibers. The crystal was centered and the x-ray intensity data were measured on a Bruker AXS diffractometer. The data were collected using graphite-monochromated Mo radiation and then structures were solved by direct methods and refined using full matrix least squares methods (SHELX97). SHELX97 – Programs for Crystal Structure Analysis (Release 97-2): G.M. Sheldick, SHELX-98, Program for the Solution of Crystal Structures, University of Göttingen, Göttingen (Germany), 1998.

Raman Spectroscopy

Raman spectroscopy was performed using a Thermo Nicolet Almega dispersive Raman spectrometer coupled with an infinity corrected, confocal design microscope. The spectrometer uses a 785 nm class I laser, and the data were collected in the reflection mode of the microscope at a slit width of 25 μm. The data were collected and analyzed using the Omnic software suite (Nicolet, USA).

RAMP ^{13}C CP MAS-NMR

All RAMP ^{13}C CP MAS-NMR spectra were taken at room temperature using a Varian Infinity Plus 360 NMR spectrometer with a 4 mm double resonance probe and 4 mm zirconia rotor. The probe was tuned to 90.5 MHz for ^{13}C and 360.0 MHz for ^{1}H. The ^{13}C MAS-NMR spectra were collected using a CP RAMP pulse program with a contact time of 2ms and a pulse delay of 2s.[4] The number of steps in the CP RAMP ranged from 8-12 and the amplitude step size ranged from .001 to .01. These parameters lead to an X channel amplitude range of .3100-.4000. Over 1000 scans were acquired.

High-Field RAMP ^{13}C CP MAS-NMR

High-Field RAMP ^{13}C CP MAS-NMR spectra were taken at NYSBC, at room temperature using a Bruker 750 MHz NMR spectrometer with a 1.8 mm double resonance probe and 1.8 mm zirconia rotor. The probe was tuned to 188.7 MHz for ^{13}C and 750.0 MHz for ^{1}H. Spectra were also collected at SUNY Stony Brooking using a Bruker Advance 700 NMR spectrometer , with the 2.5 mm double resonance probe, with the 2.5 mm zirconia rotor spinning at 17 kHz. The probe was tuned to 176.1 MHz for ^{13}C and 700.1 MHz for ^{1}H. The ^{13}C MAS-NMR spectra were collected using a CP RAMP pulse program with a contact time of 2ms and a pulse delay of 2s.[4] The number of steps in the CP RAMP ranged

from 10-12 and the amplitude step size ranged from .001 to .01. Over 1000 scans were acquired.

^{13}C 1-Pulse MAS-NMR

^{13}C 1-Pulse MAS-NMR spectra, as noted, were taken at room temperature using a Bruker Advance 700 NMR spectrometer or a Bruker Advance 600 NMR spectrometer, with the 2.5 mm double resonance probe, with the 2.5 mm zirconia rotor spinning at 31 kHz. The probe was tuned to 176.1 MHz or 150.9 MHz for ^{13}C respectively. The ^{13}C MAS-NMR spectra were collected using a ^{13}C 1-Pulse pulse program with decoupling, and a pulse delay of 10s. Over 1000 scans were acquired.

^{13}C 1-Pulse MAS-NMR spectra, as noted, were also taken at room temperature using a Varian Infinity Plus 500 NMR spectrometer, with the 1.8 mm double resonance probe, with the 2 mm zirconia rotor spinning at 30 kHz. The probe was tuned to 125.6 MHz for ^{13}C. The ^{13}C MAS-NMR spectra were collected using a ^{13}C 1-Pulse pulse program with decoupling, and a pulse delay of 10s. Over 1000 scans were acquired.

The rotor was packed using < 0.01 g of isolated PIDA. The MAS-NMR rotor was filled halfway with $NaNO_3$. PIDA was allowed to gently fall into the rotor and was not tamped down. Then the remainder of the rotor was filled with $NaNO_3$. The rotor was then allowed to settle while spinning and the spinning speed gradually raised.

UV-visible Spectroscopy

All UV-visible spectroscopy were taken at room temperature using a Cary 100 UV/Visible Scan Spectrophotometer scanning from 450 to 900 nm with a resolution of 1 nm.

Electron Spin Resonance

Powder samples of **M1**/**1** and **N5**/**1** co-crystals were placed in standard 4.0 mm ESR tubes. The samples were then exposed to liquid nitrogen in an ESR X-band cavity finger Dewar. The Dewar was placed into the ESR cavity and the spectrum obtained at 9.5 GHz over a field range of 3100 to 3700 gauss.

5.9 References

2. Bassler, H.; Sixl, H.; and Enkelmann, V. *Adv. Polymer Sci. 63: Polydiacetylenes*.; 63; H.-J. Cantow: Springer-Verlag, 1984.

38. Webb, J.A. Small Molecule Carbon-Rich Compounds: from Polymerization to NMR Studies. PhD. Dissertation. SUNY Stony Brook, 2004.

39. Sun, A.; Lauher, J.W.; and Goroff, N.S. Preparation of Poly(diiododiacetylene), an Ordered Conjugated Polymer of Carbon and Iodine. *Science* **2006**, *312*, 1030-1034.

44. Luo, L.; Wilhelm, C.; Sun, A.; Grey, C.P.; Lauher, J.W.; and Goroff, N.S. Poly(diiododiacetylene): Preparation, Isolation, and full Characterization of a Very Simple Poly(diacetylene). *J. Am. Chem. Soc.*, **2008**, *130*, 7702-7709.

63. Luo, L. PhD. Dissertation. Preparation and Comprehensive Characterization of Poly(diiododiacetylene) and Spectroscopic Studies of Its Reactions with Lewis Bases. SUNY Stony Brook, 2009.

64. Wang, G.; and Huang Y. Theoretical Study on the Co-crystal Composed of Poly(diiododiacetylene) and Bis(nitrile) Oxalamide. *J. Phys. Chem. Solid.* **2007**, *68*, 2003-2007.

65. Sun, A. PhD. Dissertation. Design, Synthesis and Characterization of an Ordered Conjugated Polymer of Carbon and Iodine. SUNY Stony Brook, 2007.

66. Mao, H.-K.; Shu, J.; Shen, G.; Hemley, R.J.; Li, B.; and Singh, A.K. Elasticity and Rheology of Iron Above 220 GPa and the Nature of the Earth's Inner Core. *Nature*, **1998**, *396*, 741-743.

67. Isogai, H. An Analysis of the Effects of Eddy Currents on the Accuracy of a Spinning Rotor Gauge. *Vacuum*, **1997**, *48*, 175-179.

68. Xiong, J.; Lock, H.; Tao, T.; Keeler, C.; and Maciel, G.M. NMR of Samples Containing Metal Foils. *Solid State NMR*, **1999**, *14*, 95-103.

69. Bonavolonta, C.; Peluso, G.; Pepe, G.P.; and Valentino, M. Detection of Early Stage Damage in Carbon Fiber Reinforced Polymers for Aeronautical Applications Using an HTS SQUID Magnetometer. *E. Phys. J. B*, **2004**, *42*, 491-496.

70. Swager, T.M.; and Grubbs, R.H. Synthesis and Properties of a Novel Cross-Conjugated Conductive Polymer Precursor: Poly(3,4-diisopropylidenecyclobutene) *J. Am. Chem. Soc.*, **1987**, *109*, 894-896.
71. Kababya, S.; Appel, M.; Haba, Y.; Titelman, G.I.; and Schmidt, A. Polyaniline-Dodecylbenzene Sulfonic Acid Polymerized from Aqueous Medium: A Solid-State NMR Characterization. *Macromol.*, **1999**, *32*, 5357-5364.

72. Carrasco, P.M.; Grande, H.J.; Cortazar, M.; Alberdi, J.M.; Areizaga, J.; and Pomposo, J.A. Structure-Conductivity Relationships in Chemical Polypyrroles of Low, Medium, and High Conductivity. *Synthetic Met.*, **2006**, *156*, 420-425.

73. Larkindale, J.P.; and Simkin, D.J. Carbon-13 Magnetic Resonance Studies on Charge Transfer Complexes: Pyridine-Iodine. *J. Chem. Phys.*, **1971**, *55*, 5048-5052.

74. Freitas, J.C.C.; Emmerich, F.G.; Cernicchiaro, G.R.C.; Sampaio, L.C.; and Bonagamba, T.J. Magnetic Suceptibility Effects on 13C MAS NMR Spectra of Carbon Materials and Graphite. *Solid State Nucl. Magn. Reson.*, **2001**, *20*, 61-73.

75. Poole, C.P. *Electron Spin Resonance: A Comprehensive Treatise on Experimental Techniques*, John Wiley and Sons: New York, 1983.

Chapter 6. Discussion and Conclusions

6.1 Discussion and Conclusions

The research presented in this dissertation has proven the chemist's ability to produce and identify 1,4-poly(diiododiacetylene), and expanded the library of useable host molecules. Several analytical methods have been developed here in, and their specific identifiers for the presence of 1,4-poly(diiododiacetylene) have also been established and discussed. Furthermore, the strengths and weaknesses of these various analytical techniques have been identified.

Since Sun's report of the first production of 1,4-poly(diiododiacetylene) in 2006, chemists now have easier access to this polymer through a variety of host molecules. Furthermore, the affordability and reliability of the host molecules in use have been improved. 1,4-poly(diiododiacetylene) can be made within a variety of co-crystal lattices and by using different Lewis base functionalities to suit the chemists needs.

This research has demonstrated the ability of mechanical stress to induce a topochemical polymerization among a series of poorly aligned diacetylene functionalities. While this is not novel, it does demonstrate the chemist's ability to use large amounts of pressure to polymerize even very poorly aligned monomers. This may lead to the production of other novel polydiacetylenes in the future.

The study of the topochemical polymerization of 1,4-poly(diiododiacetylene) and the reactive species produced during this reaction has also begun during the course of this research. Two co-crystal systems were identified and proven to produce ESR signals throughout the process of polymerization. Furthermore, it has been demonstrated that the ESR signals produced by these samples change when the polymerization reaction proceeds.

High-field MAS-NMR has been developed as a tool for identifying the different types of packing within the co-crystal systems reported here. This technique can be used to identify the relative strengths of the halogen bonding within the co-crystal lattice. It can even be used to identify non-equivalent interactions within the same crystal lattice.

The isolation of 1,4-poly(diiododiacetylene) from the co-crystal lattice has also been successfully demonstrated. Isolated 1,4-poly(diiododiacetylene) has been identified by MAS-NMR, and has demonstrated a reactivity with Lewis bases. The product of this reaction (or doping) is likely to be conductive, but the mechanism with which carbon-iodine ratio is changed requires further study.

This research has been instrumental in producing and identifying a number of novel compounds, and describes their ability to produce 1,4-poly(diiododiacetylene) within a co-crystal system. While more physical studies of these materials are required, their usefulness in the fields of Chemistry and Materials Science is expected to be profound. The ability of 1,4-

poly(diiododiacetylene) to act a precursor to novel PDAs as well as carbyne, and its own unique electrical and optical properties is bound to have a broad impact in the science community.

7. Bibliography

1. Kaiser, J.; Wegner, G.; and Fischer, E.W. Topochemical Reactions of Monomers with Conjugated Triple Bonds. VII. Mechanism of Transition from Monomer to Polymer Phase During Solid-State Polymerization. *Isr. J. Chem.*, **1972**, *10*, 157-171.

2. Bassler, H.; Sixl, H.; and Enkelmann, V. *Adv. Polymer Sci. 63: Polydiacetylenes*.; 63; H.-J. Cantow: Springer-Verlag, 1984.

3. Charych, D.H.; Nagy, J.O.; Spevak, W.; and Bednarski, M.D. Direct Colorimetric Detection of a Receptor-Ligand Interaction by a Polymerized Bilayer Assembly. *Science* **1993**, *261*, 585-588.

4. Charych, D.H.; Cheng, Q.; Reichert, A.; Kuziemko, G.; Stroh, M.; Nagy, J.O.; Spevak, W.; and Stevens, R.C. A 'Litmus Test' for Molecular Recognition Using Artificial Membranes. *Chem. Biol.* **1996**, *3*, 113-120.

5. Geiger, E.; Hug, P.; and Keller, B.A. Chromatic Transitions in Polydiacetylene Langmuir-Blodgett Films due to Molecular Recognition at the Film Surface Studied by Spectroscopic Methods and Surface Analysis. *Macromol. Chem. Phys.* **2002**, *203*, 2422-2431.

6. Reichert, A.; Nagy, J.O.; Spevak, W.; and Charych, D. Polydiacetylene Liposomes Functionalized with Sialic Acid Bind and Colorimetrically Detect Influenza Virus. *J. Am. Chem. Soc.*, **1995**, *117*, 829-830.

7. Orynbayeva, Z.; Kolusheva, S.; Livneh, E.; Lichtenshtein, A.; Nathan, I.; Jelinek, R. Visualization of Membrane Processes in Living Cells by Surface-Attached Chromatic Polymer Patches. *Angew. Chem. Int. Ed.*, **2005**, *44*, 1092-1096.

8. Mech, A.; Orynbayeva, Z.; Irgebayev, K.; Kolusheva, S.; and Jelinek R. Screening Membrane Interactions of Pesticides by Cells Decorated with Chromatic Polymer Nanopatches. *Chem. Res. Toxicol.*, **2009**, *22*, 90-96.

9. Baughman, R.H. Solid State Polymerization of Diacetylenes. *J. Appl. Phys.* **1972**, *43*, 4362-4370.

10. Baughman, R.H. Solid-State Synthesis of Large Polymer Single Crystals. *J. Polym. Sci., Polym. Phys. Ed.* **1974**, *12*, 1511-1535.

11. Toledo, L.M.; Lauher, J.W.; and Fowler, F.W. Design of Molecular Solids. Application of 2-Amino-4(1H)-pyridones to the Preparation of Hydrogen Bonded α- and β- Networks. *Chem. Mater.* **1994**, *6*, 1222-1226.

12. Toledo, L.M.; Musa, K.; Lauher, J.W.; and Fowler, F.W. Development of Strategies for the Preparation of Designed Solids. An Investigation of the 2-Amino-4(1H)-pyrimidone Ring System for the Molecular Self-Assembly of Hydrogen Bonded α- and β- Networks. *Chem. Mater.* **1995**, *7*, 1639-1647.

13. Coe, S.; Kane, J.J.; Nguyen, T.L.; Toledo, L.M.; Wininger, E.; Fowler, F.W.; and Lauher, J.W. Molecular Symmetry and the Design of Molecular Solids: The Oxalamide Functionality as a Persistent Hydrogen Bonding Unit. *J. Am. Chem. Soc.* **1997**, *119*, 86-93.

14. Nguyen, T.L.; Scott, A.; Dinkelmeyer, B.; Fowler, F.W.; and Lauher, J.W. Design of Molecular Solids: Utility of the Hydroxyl Functionality as a Predictable Design Element. *New J. Chem.* **1998**, *22*, 129-135.

15. Kane, J.J.; Liao, R.-F.; Lauher, J.W.; and Fowler, F.W. Preparation of Layered Diacetylenes as a Demonstration of Strategies for Supramolecular Synthesis. *J. Am. Chem. Soc.* **1995**, *117*, 12003-12004.

16. Schauer, C.L.; Matwey, E.; Fowler, F.W.; and Lauher, J.W. Controlled Spacing of Metal Atoms via Ligand Hydrogen Bonds. *J. Am. Chem. Soc.* **1997**, *119*, 10245-10246.

17. Curtis, S.M.; Le, N.; Fowler, F.W.; and Lauher, J.W. A Rational Approach to the Preparation of Polydipyridyldiacetylenes: An Exercise in Crystal Design. *Crystal Growth and Design* **2005**, *5*, 2313-2321.

18. Hoang, T.; Lauher, J.W.; and Fowler, F.W. The Topochemical 1,6-polymerization of a Triene. *J. Am. Chem. Soc.*, **2002**, *124*, 10656-10657.

19. Stevens, G.C.; and Bloor, D. Solid-State Thermal Polymerization of bis(p-toluene sulfonate) of 2,4-hexadiyne-1,6-diol. III. ESR Study. *J. Poly. Sci. Poly. Phys. Ed.* **1975**, *13*, 2411-2427.

20. Stevens, G.C.; and Bloor, D. Observation of Paramagnetic Triplet Species During the Thermal Polymerization of bis(p-toluene sulfonate) of 2,4-hexadiyne-1,6-diol. *Chem. Phys. Lett.* **1975**, *40*, 37-40.

21. Bloor, D.; Koski, L.; Stevens, G.C.; Preston, F.H.; and Ando, D.J. Solid State Polymerization of bis(p-toluenesulfonate) of 2,4-hexadiyne-1,6-diol. 1. X-ray Diffraction and Spectroscopic Observations. *J. Mat. Sci.* **1975**, *10*, 1678-1688.

22. Eichele, H.; Schwoerer, M.; Huber, R.; and Bloor, D. ESR of a Diacetylene Polymer Single Crystal. *Chem. Phys. Lett.* **1976**, *42*, 342-346.

23. Chance, R.R.; and Sowa, J.M. An Examination of the Thermal Polymerization of a Crystalline Diacetylene Using Diffuse Reflectance Spectroscopy. *J. Am. Chem. Soc.* **1977**, *99*, 6703-6708.

24. Chance, R.R.; Patel, G.N.; Turi, E.A.; and Khanna, Y.P. Energetics of the Thermal Polymerization of a Diacetylene Crystal. *J. Am. Chem. Soc.* **1978**, *100*, 1307-1309.

25. Chance, R.R.; and Patel, G.N. Solid-State Polymerization of a Diacetylene Crystal. Thermal, Ultraviolet and Ray Polymerization of 2,4-hexadiyne-1,6-diol bis-(p-toluene sulfonate). *J. Poly Sci. Poly. Phys. Ed.* **1978**, *16*, 859-881.

26. Hori, Y.; and Kispert, L.D. An ESR Study of X-irradiated Diacetylene Single Crystals at 77 K. *J. Phys. Chem.* **1978**, *69*, 3826-3829.

27. Hori, Y.; and Kispert, L.D. ESR Evidence for a Biradical Dimer Initiator in Diacetylene Polymerization. *J. Am. Chem. Soc.* **1979**, *101*, 3173-3177.

28. Huber, R.; Schwoerer, M.; Bubeck, C.; and Sixl, H. The Sign of D in the Triplet Carbene of a Polydiacetylene Single Crystal (PTS). *Chem. Phys. Lett.* **1978**, *53*, 35-38.

29. Sixl, H.; Hersel, W.; and Wolf, H.C. Photopolymerization of Diacetylene Single Crystals. Optical Transmission Spectroscopy. *Chem. Phys. Lett.* **1978**, *53*, 39-44.

30. Bubeck, C.; Sixl, H.; and Wolf, H.C. ESR of the Low Temperature Photoproducts in a Diacetylene Single Crystal. *Chem. Phys.* **1978**, *32*, 231-237.

31. Bubeck, C.; Sixl, H.; and Neumann, W. ESR Analysis of the Initial Reaction Products in the Solid State Photopolymerization of Diacetylenes. *Chem. Phys.* **1980**, *48*, 269-275.

32. Neumann W.; and Sixl, H. The Kinetics of the Low-Temperature Photochemical Polymerization in a Diacetylene Single Crystal. *Chem. Phys.* **1980**, *50*, 273-280.

33. Neumann, W.; and Sixl, H. The Mechanism of the Low-Temperature Polymerization Reaction in Diacetylene Crystals. *Chem. Phys.* **1981**, *58*, 303-312.

34. Sixl, H.; and Neumann, W. The Mechanism of the Polymerization Reactions in Diacetylene Crystals: ESR Analysis of the Paramagnetic Reaction Intermediates. *Mol. Cryst. Liq. Cryst.* **1984**, *105*, 41-54.

35. Kudryavtsev, Y.P.; Sladkov, A.M.; Aseev, Y.G.; Nedoshivin, Y.N.; Kasatochkin, V.I.; and Korshak, V.V. Properties and Structure of Carbyne. *Dokl. Akad. Nauk SSSR* **1964,** *158*, 389-392.

36. Moss, W. N.; and Goroff, N.S. Theoretical Analysis of the 13C NMR of Iodoalkynes Upon Complexation with Lewis Bases. *J. Org. Chem.* **2005**, *70*, 802-808.

37. Goroff, N.S.; Curtis, S.M.; Webb, J.A.; Fowler, F.W.; and Lauher, J.W. Designed Cocrystals Based on the Pyridine-Iodoalkyne Halogen Bond. *Org. Lett.* **2005,** *7*, 1891-1893.

38. Webb, J.A. Small Molecule Carbon-Rich Compounds: from Polymerization to NMR Studies. PhD. Dissertation. SUNY Stony Brook, 2004.

39. Sun, A.; Lauher, J.W.; and Goroff, N.S. Preparation of Poly(diiododiacetylene), an Ordered Conjugated Polymer of Carbon and Iodine. *Science* **2006**, *312*, 1030-1034.

40. Baughman, R.H.; Witt, J.D.; Yee, K.C. Raman spectral shifts relevant to electron delocalization in polydiacetylenes. *J. Chem. Phys.*, **1974**, *60*, 4755-4759.

41. Exarhos, G.J.; Risen, W.M.; and Baughman, R.H. Resonance Raman Study of the Thermochromic Phase Transition of a Polydiacetylene. *J. Am. Chem. Soc.*, **1976**, *98*, 481-487.

42. Iqbal, Z.; Chance, R.R.; and Baughman, R.H. Electronic Structure Change at a Phase Transition in a Polydiacetylene Crystal. *J. Chem. Phys.*, **1977**, *66*, 5520-5525.

43. Galambos, A.F.; Stockton, W.B.; Koberstein, J.T.; Sen, A.; Weiss, R.A.; and Russell, T.P. Study of the Thermochromic Phase Transition of Polydiacetylene by Solid State ^{13}C NMR. *Macromol.*, **1987**, *20*, 3094-3097.

44. Luo, L.; Wilhelm, C.; Sun, A.; Grey, C.P.; Lauher, J.W.; and Goroff, N.S. Poly(diiododiacetylene): Preparation, Isolation, and full Characterization of a Very Simple Poly(diacetylene). *J. Am. Chem. Soc.*, **2008**, *130*, 7702-7709.

45. Duer, M. J. *Introduction to Solid State NMR Spectroscopy*, Blackwell Publishing Limited: Malden, 2004.

46. Metz, G.; Wu, X.; and Smith, S. Ramped-Amplitude Cross Polarization in Magic-Angle-Spinning NMR. *J. Mag. Res. A*, **1994,** (110), 219-227.

47. Wilhelm, C.; Boyd, S.A.; Chawda, S.; Fowler, F.W.; Goroff, N.S.; Halada, G.P.; Grey, C.P.; Lauher, J.W.; Luo, L.; Martin, C.D.; Parise, J.B.; Tarabrella, C.; Webb, J.A. Pressure-Induced Polymerization of Diiodobutadiyne in Assembled Co-crystals. *J. Am. Chem. Soc.*, **2008**, *130*, 4415-4420.

48. Gao, K.; and Goroff, N.S. Two New Iodine Capped Rods. *J. Am. Chem. Soc.* **2000**, (122), 9320-9321.

49. Webb, J.A.; Klijn, J.E.; Hill, P.A.; Bennett, J.L.; Goroff, N.S. Experimental Studies of the 13C NMR of Iodoalkynes in Lewis-Basic Solvents. *J. Org. Chem.* **2004**, *69*, 660-664.

50. Moss, W. N.; and Goroff, N.S. Theoretical Analysis of the 13C NMR of Iodoalkynes Upon Complexation with Lewis Bases. *J. Org. Chem.* **2005**, *70*, 802-808.

51. Wenz, G.; Müller, M.A.; Schmidt, M.; and Wegner, G. Structure of Poly(diacetylenes) in Solution. *Macromol.*, **1984**, *17*, 837-850.

52. Iqbal, Z.; Murthy, N.S.; Khanna, Y.P.; Szobota, J.S.; Dalterio, R.A.; and Owens, F.J. The Mechanism of the Solid State Phase Transitions in the Polydiacetylene, Poly-4BCMU: Thermal, X-ray Diffraction and Raman Scattering Studies. *J. Phys. C.: Solid State Phys.*, **1987**, *20*, 4283-4295.

53. Jephcoat, A.P.; Finger, L.W.; and Cox, D.E. High Pressure, High Resolution Synchrotron X-ray Powder Diffraction with a Position-Sensitive Detector. *High Press. Res.*, **1992**, *8*, 667-676.

54. Gwanmesia, G.D. Hot-Pressing of Polycrystals of High-Pressure Phases of Mantle Minerals in Multi-Anvil Apparatus. *Pure Appl. Geophys.*, **1993,** 2-4, (141), 467-484.

55. Boyd, F.R.; and England, J.L. Apparatus for phase-equilibrium measurements at pressures up to 50 kilobars and temperatures up to 1750 °C. *J. Geophys. Res.*, **1960**, *65*, 741-748.

56. Fowler, F.W.; and Lauher, J.W. A Rational Design of Molecular Materials. *J. Phys. Org. Chem.* **2000,** 13, 850-857.

57. Nguyen, T.N. Hydrogen Bonded Networks. PhD Dissertation. SUNY Stony Brook, 1998.

58. Tzeng, B.-C.; Chen, Y.-F.; Wu, C.-C.; Hu, C.-C.; Chang, Y.-T.; Chen, C.-K. Anion-Recognition Studies of a Re(I)-Based Square Containing the Dipyridyl-Amide Ligand. *New J. Chem.*, **2007**, *31*, 202-209.

59. Mitsunobu, O.; Wada, M.; Sano, T. Stereospecific and Stereoselective Reactions. I. Preparation of Amines from Alcohols. *J. Am. Chem. Soc.*, **1972**, *94*, 679-680.

60. Hawes, E.M.; and Davis, H.L. Intramolecular Nucleophilic Cyclization of 3-Substituted Pyridylalkylamines onto the 2-Position of the Pyridine Ring. *J. Heterocycl. Chem.* **1973**, *10*, 39-42.

61. Eisch, J.J.; Gopal, H.; and Russo, D.A. Preparation and Aluminum Chloride Induced Rearrangement of Cyclopropylpyridines. *J. Org. Chem.* **1974**, *39*, 3110-3114.

62. Friedman, L.; and Shechter, H. Preparation of Nitriles from Halides and Sodium Cyanide. Advantageous Nucleophilic Displacement in Dimethyl Sulfoxide. *J. Org. Chem.* **1960**, *25*, 877-879.

63. Luo, L. PhD. Dissertation. Preparation and Comprehensive Characterization of Poly(diiododiacetylene) and Spectroscopic Studies of Its Reactions with Lewis Bases. SUNY Stony Brook, 2009.

64. Wang, G.; and Huang Y. Theoretical Study on the Co-crystal Composed of Poly(diiododiacetylene) and Bis(nitrile) Oxalamide. *J. Phys. Chem. Solid.* **2007**, *68*, 2003-2007.

65. Sun, A. PhD. Dissertation. Design, Synthesis and Characterization of an Ordered Conjugated Polymer of Carbon and Iodine. SUNY Stony Brook, 2007.

66. Mao, H.-K.; Shu, J.; Shen, G.; Hemley, R.J.; Li, B.; and Singh, A.K. Elasticity and Rheology of Iron Above 220 GPa and the Nature of the Earth's Inner Core. *Nature*, **1998**, *396*, 741-743.

67. Isogai, H. An Analysis of the Effects of Eddy Currents on the Accuracy of a Spinning Rotor Guage. *Vacuum*, **1997**, *48*, 175-179.

68. Xiong, J.; Lock, H.; Tao, T.; Keeler, C.; and Maciel, G.M. NMR of Samples Containing Metal Foils. *Solid State NMR*, **1999**, *14*, 95-103.

69. Bonavolonta, C.; Peluso, G.; Pepe, G.P.; and Valentino, M. Detection of Early Stage Damage in Carbon Fiber Reinforced Polymers for Aeronautical Applications Using an HTS SQUID Magnetometer. *E. Phys. J. B*, **2004**, *42*, 491-496.

70. Swager, T.M.; and Grubbs, R.H. Synthesis and Properties of a Novel Cross-Conjugated Conductive Polymer Precursor: Poly(3,4-diisopropylidenecyclobutene) *J. Am. Chem. Soc.*, **1987**, *109*, 894-896.

71. Kababya, S.; Appel, M.; Haba, Y.; Titelman, G.I.; and Schmidt, A. Polyaniline-Dodecylbenzene Sulfonic Acid Polymerized from Aqueous Medium: A Solid-State NMR Characterization. *Macromol.*, **1999**, *32*, 5357-5364.

72. Carrasco, P.M.; Grande, H.J.; Cortazar, M.; Alberdi, J.M.; Areizaga, J.; and Pomposo, J.A. Structure-Conductivity Relationships in Chemical Polypyrroles of Low, Medium, and High Conductivity. *Synthetic Met.*, **2006**, *156*, 420-425.

73. Larkindale, J.P.; and Simkin, D.J. Carbon-13 Magnetic Resonance Studies on Charge Transfer Complexes: Pyridine-Iodine. *J. Chem. Phys.*, **1971**, *55*, 5048-5052.

74. Freitas, J.C.C.; Emmerich, F.G.; Cernicchiaro, G.R.C.; Sampaio, L.C.; and Bonagamba, T.J. Magnetic Suceptibility Effects on 13C MAS NMR Spectra of Carbon Materials and Graphite. *Solid State Nucl. Magn. Reson.*, **2001**, *20*, 61-73.

75. Poole, C.P. *Electron Spin Resonance: A Comprehensive Treatise on Experimental Techniques*, John Wiley and Sons: New York, 1983.

Appendix

Crystallographic Tables

Co-crystal M1/1 Blue Phase

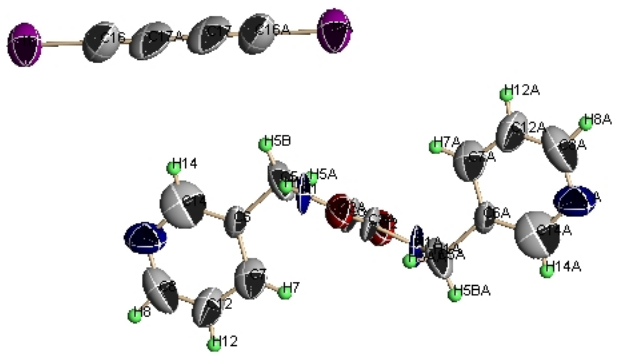

Table 1. Crystal data and structure refinement for cwax113.

Identification code	cwax113	
Empirical formula	C18 H14 I2 N4 O2	
Formula weight	572.13	
Temperature	273(2) K	
Wavelength	0.71073 Å	
Crystal system	Triclinic	
Space group	P-1	
Unit cell dimensions	a = 5.101(2) Å	α= 96.223(11)°
	b = 8.623(4) Å	β= 99.588(8)°
	c = 11.745(5) Å	γ = 103.610(9)°
Volume	489.2(4) $Å^3$	
Z	1	
Density (calculated)	1.942 Mg/m^3	
Absorption coefficient	3.234 mm^{-1}	
F(000)	272	
Crystal size	0.3 x 0.4 x 0.4 mm^3	
Theta range for data collection	1.78 to 28.69°.	
Index ranges	-6<=h<=6, -10<=k<=11, -6<=l<=14	
Reflections collected	3196	
Independent reflections	2193 [R(int) = 0.2649]	
Completeness to theta = 28.69°	87.0 %	
Absorption correction	None	
Refinement method	Full-matrix least-squares on F^2	
Data / restraints / parameters	2193 / 0 / 118	
Goodness-of-fit on F^2	0.703	
Final R indices [I>2sigma(I)]	R1 = 0.1046, wR2 = 0.2172	
R indices (all data)	R1 = 0.3263, wR2 = 0.3011	
Largest diff. peak and hole	0.828 and -1.042 e.$Å^{-3}$	

Table 2. Atomic coordinates (x 10^4) and equivalent isotropic displacement parameters ($Å^2$x 10^3) for cwax113. U(eq) is defined as one third of the trace of the orthogonalized U^{ij} tensor.

	x	y	z	U(eq)
I(1)	10741(4)	7998(2)	3943(2)	98(1)
N(1)	1530(30)	5700(20)	8865(16)	59(5)
C(3)	-370(50)	5410(30)	9437(18)	57(7)
O(2)	-2680(30)	5640(20)	9189(15)	84(5)
C(6)	2610(50)	8220(30)	7940(20)	61(7)
C(7)	1860(50)	9280(40)	8790(30)	82(9)
C(5)	1230(50)	6310(30)	7880(30)	100(11)
C(8)	4960(60)	11300(40)	8150(30)	103(11)
N(2)	5620(50)	10370(40)	7330(20)	96(8)
C(14)	4540(70)	8800(50)	7290(30)	115(11)
C(12)	3230(60)	10790(40)	8790(20)	86(9)
C(17)	3900(60)	4410(40)	5170(30)	113(13)
C(16)	8040(60)	6450(40)	4560(30)	107(12)

Table 3. Bond lengths [Å] and angles [°] for cwax113.

I(1)-C(16)	1.97(3)
N(1)-C(3)	1.26(2)
N(1)-C(5)	1.32(3)
C(3)-O(2)	1.23(2)
C(3)-C(3)#1	1.60(4)
C(6)-C(14)	1.38(3)
C(6)-C(7)	1.44(3)
C(6)-C(5)	1.62(3)
C(7)-C(12)	1.33(3)
C(8)-C(12)	1.28(3)
C(8)-N(2)	1.32(4)
N(2)-C(14)	1.33(4)
C(17)-C(16)#2	1.20(3)
C(17)-C(17)#2	1.47(6)
C(17)-C(16)	2.66(6)
C(16)-C(17)#2	1.20(3)
C(3)-N(1)-C(5)	122(2)
O(2)-C(3)-N(1)	127(2)
O(2)-C(3)-C(3)#1	119(2)
N(1)-C(3)-C(3)#1	114(2)
C(14)-C(6)-C(7)	121(3)
C(14)-C(6)-C(5)	123(3)
C(7)-C(6)-C(5)	116(2)
C(12)-C(7)-C(6)	109(3)
N(1)-C(5)-C(6)	117(2)
C(12)-C(8)-N(2)	125(3)
C(8)-N(2)-C(14)	114(3)
N(2)-C(14)-C(6)	122(3)

C(8)-C(12)-C(7)	128(3)
C(16)#2-C(17)-C(17)#2	174(4)
C(16)#2-C(17)-C(16)	176(2)
C(17)#2-C(17)-C(16)	2.9(17)
C(17)#2-C(16)-I(1)	170(3)
C(17)#2-C(16)-C(17)	4(2)
I(1)-C(16)-C(17)	172.5(16)

Symmetry transformations used to generate equivalent atoms:
#1 -x,-y+1,-z+2 #2 -x+1,-y+1,-z+1

Table 4. Anisotropic displacement parameters ($Å^2 x\ 10^3$) for cwax113. The anisotropic displacement factor exponent takes the form: $-2\pi^2[\ h^2\ a^{*2}U^{11} + ... + 2\ h\ k\ a^*\ b^*\ U^{12}\ ]$

	U^{11}	U^{22}	U^{33}	U^{23}	U^{13}	U^{12}
I(1)	74(1)	93(2)	138(2)	38(1)	28(1)	28(1)
N(1)	33(10)	76(14)	72(15)	45(12)	23(10)	-3(9)
C(3)	43(14)	73(17)	67(19)	26(14)	37(14)	12(13)
O(2)	52(10)	71(12)	132(16)	6(11)	37(10)	16(9)
C(6)	42(14)	80(20)	44(17)	1(15)	15(11)	-10(14)
C(7)	58(17)	90(20)	110(30)	30(20)	18(16)	32(17)
C(5)	71(19)	38(16)	190(40)	20(19)	50(20)	3(14)
C(8)	70(20)	70(20)	150(40)	30(20)	-10(20)	3(18)
N(2)	110(20)	70(20)	110(20)	-3(17)	26(16)	40(17)
C(14)	100(30)	120(30)	130(30)	40(30)	0(20)	50(20)
C(12)	90(20)	90(30)	100(30)	40(20)	48(19)	37(19)
C(17)	110(30)	120(40)	150(30)	10(30)	60(30)	70(30)
C(16)	80(20)	150(30)	80(20)	0(20)	16(18)	20(20)

Table 5. Hydrogen coordinates ($x\ 10^4$) and isotropic displacement parameters ($Å^2 x\ 10^3$) for cwax113.

	x	y	z	U(eq)
H(1)	3069	5492	9124	71
H(7)	622	8956	9272	98
H(5A)	-728	6100	7566	120
H(5B)	1992	5721	7322	120
H(8)	5812	12397	8270	124
H(14)	5099	8066	6810	138
H(12)	2893	11576	9309	103

Host Molecule M2

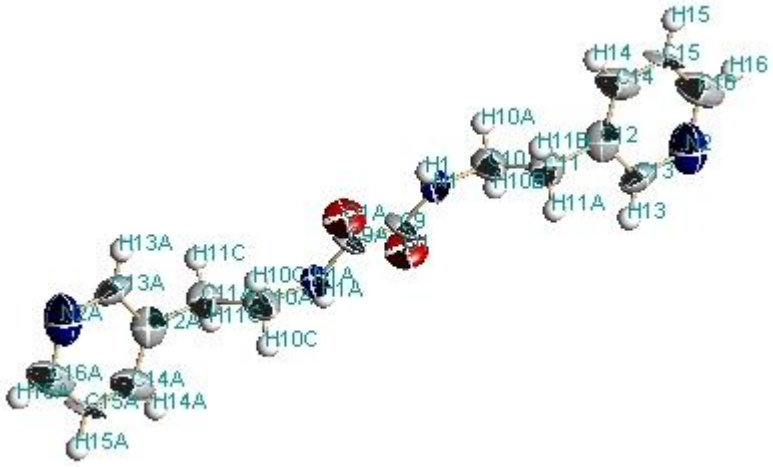

Table 1. Crystal data and structure refinement for cwcq102.

Identification code	cwcq102	
Empirical formula	C16 H18 N4 O2	
Formula weight	298.34	
Temperature	273(2) K	
Wavelength	0.71073 Å	
Crystal system	Triclinic	
Space group	P-1	
Unit cell dimensions	a = 5.031(5) Å	α= 89.92(2)°
	b = 5.238(5) Å	β= 89.76(2)°
	c = 30.25(3) Å	γ = 73.676(15)°
Volume	765.2(13) $Å^3$	
Z	2	
Density (calculated)	1.295 Mg/m^3	
Absorption coefficient	0.089 mm^{-1}	
F(000)	316	
Crystal size	0.5 x 0.6 x 0.2 mm^3	
Theta range for data collection	0.67 to 29.00°.	
Index ranges	-6<=h<=6, -7<=k<=6, -38<=l<=19	
Reflections collected	5008	
Independent reflections	3433 [R(int) = 0.4516]	
Completeness to theta = 29.00°	84.4 %	
Absorption correction	None	
Refinement method	Full-matrix least-squares on F^2	
Data / restraints / parameters	3433 / 0 / 199	
Goodness-of-fit on F^2	0.596	
Final R indices [I>2sigma(I)]	R1 = 0.0913, wR2 = 0.1466	
R indices (all data)	R1 = 0.5529, wR2 = 0.2524	
Largest diff. peak and hole	0.250 and -0.249 $e.Å^{-3}$	

Table 2. Atomic coordinates (x 10^4) and equivalent isotropic displacement parameters ($Å^2$x 10^3) for cwcq102. U(eq) is defined as one third of the trace of the orthogonalized U^{ij} tensor.

	x	y	z	U(eq)
O(2)	13307(14)	2902(13)	265(2)	74(3)
O(1)	8316(14)	2905(14)	4738(2)	75(3)
C(10)	10530(20)	7901(18)	671(4)	62(3)
N(3)	12652(17)	7442(17)	344(3)	63(3)
C(11)	11080(20)	9380(20)	1054(3)	64(3)
N(1)	7737(16)	7440(16)	4676(3)	49(2)
C(2)	5540(20)	7820(20)	4338(4)	66(3)
C(12)	8870(20)	9980(30)	1402(4)	51(3)
N(6)	4680(20)	12970(20)	1705(4)	82(4)
C(9)	13880(20)	5020(30)	166(3)	49(3)
C(8)	1830(30)	12320(30)	3610(4)	71(4)
N(2)	-310(20)	12987(18)	3322(4)	83(3)
C(3)	6140(20)	9280(20)	3931(4)	66(3)
C(6)	1330(30)	8940(30)	2964(3)	69(4)
C(4)	3790(30)	9970(30)	3593(4)	67(4)
C(1)	8873(19)	5050(20)	4821(3)	51(3)
C(16)	6690(30)	12360(20)	1396(4)	78(4)
C(7)	-570(30)	11260(30)	2996(5)	82(4)
C(5)	3650(30)	8110(20)	3245(4)	66(4)
C(13)	4470(30)	11220(40)	2001(5)	95(6)
C(15)	8590(30)	8240(20)	1724(6)	78(4)
C(18)	6430(40)	8870(30)	2033(4)	88(5)

Table 3. Bond lengths [Å] and angles [°] for cwcq102.

O(2)-C(9)	1.257(10)
O(1)-C(1)	1.258(10)
C(10)-N(3)	1.421(10)
C(10)-C(11)	1.466(10)
N(3)-C(9)	1.356(12)
C(11)-C(12)	1.496(12)
N(1)-C(1)	1.299(11)
N(1)-C(2)	1.480(10)
C(2)-C(3)	1.522(11)
C(12)-C(15)	1.366(13)
C(12)-C(16)	1.410(14)
N(6)-C(13)	1.306(12)
N(6)-C(16)	1.346(13)
C(9)-C(9)#1	1.503(17)
C(8)-C(4)	1.346(14)
C(8)-N(2)	1.358(12)
N(2)-C(7)	1.370(13)
C(3)-C(4)	1.530(12)
C(6)-C(7)	1.321(14)

C(6)-C(5)	1.415(12)
C(4)-C(5)	1.451(13)
C(1)-C(1)#2	1.564(17)
C(13)-C(18)	1.350(16)
C(15)-C(18)	1.397(14)
N(3)-C(10)-C(11)	113.3(8)
C(9)-N(3)-C(10)	123.7(8)
C(10)-C(11)-C(12)	115.3(9)
C(1)-N(1)-C(2)	118.3(8)
N(1)-C(2)-C(3)	112.4(8)
C(15)-C(12)-C(16)	113.6(11)
C(15)-C(12)-C(11)	124.7(13)
C(16)-C(12)-C(11)	121.4(14)
C(13)-N(6)-C(16)	120.8(12)
O(2)-C(9)-N(3)	125.1(9)
O(2)-C(9)-C(9)#1	120.1(14)
N(3)-C(9)-C(9)#1	114.8(14)
C(4)-C(8)-N(2)	122.4(12)
C(8)-N(2)-C(7)	120.8(12)
C(2)-C(3)-C(4)	114.4(8)
C(7)-C(6)-C(5)	124.1(12)
C(8)-C(4)-C(5)	118.8(12)
C(8)-C(4)-C(3)	120.5(13)
C(5)-C(4)-C(3)	120.7(13)
O(1)-C(1)-N(1)	130.2(9)
O(1)-C(1)-C(1)#2	116.9(13)
N(1)-C(1)-C(1)#2	112.7(13)
N(6)-C(16)-C(12)	123.0(11)
C(6)-C(7)-N(2)	118.8(13)
C(6)-C(5)-C(4)	115.1(11)
N(6)-C(13)-C(18)	120.4(14)
C(12)-C(15)-C(18)	122.4(13)
C(13)-C(18)-C(15)	119.2(14)

Symmetry transformations used to generate equivalent atoms:
#1 -x+3,-y+1,-z #2 -x+2,-y+1,-z+1

Table 4. Anisotropic displacement parameters ($Å^2 x\ 10^3$) for cwcq102. The anisotropic displacement factor exponent takes the form: $-2\pi^2[\ h^2\ a^{*2}U^{11} + ...\ + 2\ h\ k\ a^*\ b^*\ U^{12}\ ]$

	U^{11}	U^{22}	U^{33}	U^{23}	U^{13}	U^{12}
O(2)	92(6)	35(5)	104(7)	-2(4)	44(5)	-30(5)
O(1)	101(6)	37(5)	100(6)	-8(4)	-2(5)	-41(5)
C(10)	75(9)	30(7)	83(10)	-20(7)	42(8)	-21(7)
N(3)	58(7)	54(7)	68(7)	-35(6)	31(6)	0(6)
C(11)	80(9)	56(8)	51(8)	-29(7)	14(8)	-13(7)
N(1)	52(6)	36(6)	52(7)	12(5)	-10(5)	1(5)
C(2)	73(9)	41(8)	78(10)	-2(7)	-7(8)	-8(7)
C(12)	66(9)	35(8)	66(10)	-14(7)	26(8)	-37(8)
N(6)	62(7)	72(9)	114(11)	-47(8)	58(7)	-22(7)
C(9)	45(8)	79(10)	27(8)	-4(8)	25(5)	-24(8)
C(8)	46(9)	55(11)	110(12)	0(8)	-6(8)	-13(8)
N(2)	70(8)	37(7)	140(11)	-3(7)	4(7)	-12(7)
C(3)	81(9)	61(9)	67(9)	12(7)	-1(8)	-36(8)
C(6)	82(10)	92(12)	45(9)	5(8)	-30(8)	-42(9)
C(4)	61(9)	66(10)	83(11)	8(9)	-2(8)	-33(9)
C(1)	47(8)	38(7)	63(9)	-3(7)	-9(6)	-1(8)
C(16)	115(12)	28(9)	93(12)	2(8)	-8(10)	-22(9)
C(7)	74(11)	46(9)	127(13)	0(9)	6(9)	-19(9)
C(5)	98(11)	52(8)	53(9)	-20(7)	36(8)	-28(8)
C(13)	117(15)	79(13)	119(15)	-38(11)	73(11)	-79(13)
C(15)	73(10)	55(10)	108(13)	-51(10)	20(10)	-21(9)
C(18)	115(13)	65(12)	93(12)	-38(10)	29(11)	-38(11)

Table 5. Hydrogen coordinates (x 10^4) and isotropic displacement parameters ($Å^2$x 10^{3}) for cwcq102.

	x	y	z	U(eq)
H(10A)	10334	6203	770	74
H(10B)	8792	8884	539	74
H(11A)	11343	11049	951	76
H(11B)	12803	8369	1188	76
H(2A)	3788	8823	4467	79
H(2B)	5361	6098	4250	79
H(8)	1955	13537	3828	85
H(3A)	7798	8191	3788	79
H(3B)	6513	10917	4025	79
H(6)	1124	7782	2742	83
H(16)	6648	13568	1169	94
H(7)	-2053	11711	2801	98
H(5)	4985	6481	3210	80
H(13)	2948	11601	2192	114
H(15)	9884	6581	1738	94
H(18)	6353	7683	2258	106

Co-crystal M2/2

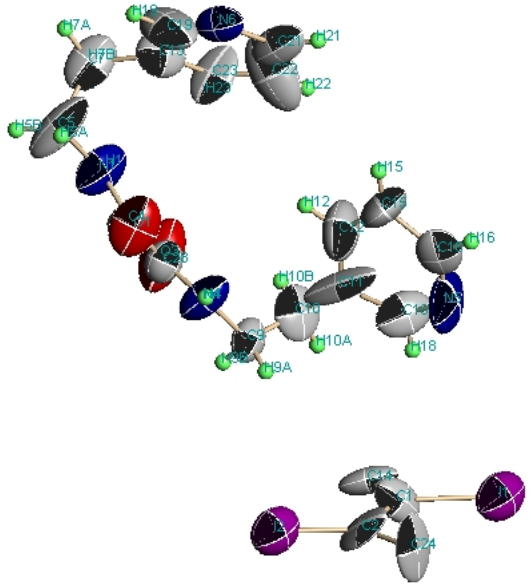

Table 1. Crystal data and structure refinement for cwnd111.

Identification code	cwnd111	
Empirical formula	C20 H18 I2 N4 O2	
Formula weight	600.18	
Temperature	273(2) K	
Wavelength	0.71073 Å	
Crystal system	Monoclinic	
Space group	P2(1)	
Unit cell dimensions	a = 4.9395(14) Å	α= 90°
	b = 27.966(9) Å	β= 95.382(8)°
	c = 7.868(2) Å	γ = 90°
Volume	1082.1(5) $Å^3$	
Z	2	
Density (calculated)	1.842 Mg/m^3	
Absorption coefficient	2.928 mm^{-1}	
F(000)	576	
Crystal size	0.2 x 0.1 x 0.1 mm^3	
Theta range for data collection	1.46 to 28.78°.	
Index ranges	-6<=h<=6, -37<=k<=37, -10<=l<=10	
Reflections collected	8092	
Independent reflections	4990 [R(int) = 0.1939]	
Completeness to theta = 28.78°	91.6 %	
Absorption correction	None	
Refinement method	Full-matrix least-squares on F^2	
Data / restraints / parameters	4990 / 1 / 253	

Goodness-of-fit on F^2	0.812
Final R indices [I>2sigma(I)]	R1 = 0.1300, wR2 = 0.3060
R indices (all data)	R1 = 0.2768, wR2 = 0.4034
Absolute structure parameter	0.35(16)
Largest diff. peak and hole	1.199 and -1.944 e.$Å^{-3}$

Table 2. Atomic coordinates (x 10^4) and equivalent isotropic displacement parameters ($Å^2$x 10^3) for cwnd111. U(eq) is defined as one third of the trace of the orthogonalized U^{ij} tensor.

	x	y	z	U(eq)
O(3)	12350(70)	3145(12)	4590(60)	141(16)
C(24)	-440(60)	1050(20)	5250(60)	121(19)
I(1)	3898(6)	592(1)	8129(4)	111(1)
I(2)	2804(5)	1526(1)	2553(4)	108(1)
C(2)	2380(100)	1157(10)	4530(60)	109(16)
C(1)	4470(60)	1006(15)	5790(50)	87(12)
C(7)	13000(90)	4810(15)	5990(70)	108(17)
C(4)	9290(50)	3835(11)	4320(50)	70(10)
N(1)	11690(60)	4113(12)	4520(50)	106(13)
O(1)	6810(50)	4008(11)	4260(40)	116(11)
C(5)	11470(80)	4639(14)	4250(90)	140(20)
C(11)	8020(120)	2478(14)	7940(90)	160(30)
C(14)	7270(70)	1019(11)	5540(60)	92(13)
C(13)	11490(80)	4673(18)	7630(60)	97(13)
C(9)	8250(70)	2511(12)	5070(50)	72(9)
C(10)	9430(70)	2358(19)	6600(60)	99(16)
C(12)	7520(110)	2922(19)	8790(60)	126(19)
N(6)	8320(70)	4909(11)	9320(50)	81(10)
N(5)	4630(110)	2176(18)	9940(60)	150(20)
C(18)	6240(70)	2142(17)	8870(70)	103(16)
C(19)	9650(180)	4994(18)	8150(80)	160(30)
C(16)	4370(70)	2598(19)	10560(60)	98(14)
C(21)	8650(90)	4443(13)	10300(60)	106(15)
C(15)	5830(130)	3042(16)	10050(80)	120(20)
C(22)	10480(130)	4100(30)	9810(80)	170(30)
C(23)	11750(80)	4247(12)	8510(70)	107(16)
N(4)	7990(70)	3049(11)	4740(50)	95(12)
C(28)	10260(80)	3285(13)	4460(50)	79(10)

Table 3. Bond lengths [Å] and angles [°] for cwnd111.

O(3)-C(28)	1.10(4)
C(24)-C(14)#1	1.18(4)
C(24)-C(2)	1.58(5)
I(1)-C(1)	2.21(4)
I(2)-C(2)	1.89(4)
C(2)-C(1)	1.43(5)

C(1)-C(14)	1.41(4)
C(7)-C(5)	1.58(7)
C(7)-C(13)	1.60(6)
C(4)-O(1)	1.31(3)
C(4)-N(1)	1.42(4)
C(4)-C(28)	1.61(5)
N(1)-C(5)	1.49(5)
C(11)-C(10)	1.36(8)
C(11)-C(12)	1.44(7)
C(11)-C(18)	1.52(7)
C(14)-C(24)#2	1.18(4)
C(13)-C(19)	1.37(7)
C(13)-C(23)	1.38(6)
C(9)-C(10)	1.35(5)
C(9)-N(4)	1.53(4)
C(12)-C(15)	1.39(7)
N(6)-C(19)	1.20(8)
N(6)-C(21)	1.52(5)
N(5)-C(18)	1.22(5)
N(5)-C(16)	1.29(6)
C(16)-C(15)	1.51(6)
C(21)-C(22)	1.40(7)
C(22)-C(23)	1.32(7)
N(4)-C(28)	1.34(5)
C(14)#1-C(24)-C(2)	168(4)
C(1)-C(2)-C(24)	107(3)
C(1)-C(2)-I(2)	127(3)
C(24)-C(2)-I(2)	125(3)
C(14)-C(1)-C(2)	123(4)
C(14)-C(1)-I(1)	109(3)
C(2)-C(1)-I(1)	126(2)
C(5)-C(7)-C(13)	114(4)
O(1)-C(4)-N(1)	125(3)
O(1)-C(4)-C(28)	129(3)
N(1)-C(4)-C(28)	106(3)
C(4)-N(1)-C(5)	119(3)
N(1)-C(5)-C(7)	99(4)
C(10)-C(11)-C(12)	134(5)
C(10)-C(11)-C(18)	125(4)
C(12)-C(11)-C(18)	100(6)
C(24)#2-C(14)-C(1)	176(5)
C(19)-C(13)-C(23)	117(4)
C(19)-C(13)-C(7)	117(5)
C(23)-C(13)-C(7)	126(4)
C(10)-C(9)-N(4)	119(4)
C(9)-C(10)-C(11)	114(3)
C(15)-C(12)-C(11)	133(5)
C(19)-N(6)-C(21)	121(5)
C(18)-N(5)-C(16)	115(5)
N(5)-C(18)-C(11)	137(5)

N(6)-C(19)-C(13)	122(5)
N(5)-C(16)-C(15)	126(4)
C(22)-C(21)-N(6)	120(5)
C(12)-C(15)-C(16)	109(5)
C(23)-C(22)-C(21)	111(6)
C(22)-C(23)-C(13)	129(4)
C(28)-N(4)-C(9)	117(3)
O(3)-C(28)-N(4)	127(4)
O(3)-C(28)-C(4)	128(4)
N(4)-C(28)-C(4)	103(3)

Symmetry transformations used to generate equivalent atoms:
#1 x-1,y,z #2 x+1,y,z

Table 4. Anisotropic displacement parameters ($Å^2 x\ 10^3$) for cwnd111. The anisotropic displacement factor exponent takes the form: $-2\pi^2[\ h^2\ a^{*2}U^{11} + ... + 2\ h\ k\ a^*\ b^*\ U^{12}\ ]$

	U^{11}	U^{22}	U^{33}	U^{23}	U^{13}	U^{12}
O(3)	90(20)	120(20)	220(40)	70(30)	80(20)	53(19)
C(24)	26(15)	230(50)	110(30)	80(30)	33(18)	-10(20)
I(1)	89(2)	109(2)	140(2)	-9(2)	45(2)	-5(2)
I(2)	82(2)	108(2)	138(2)	-7(2)	39(2)	-7(2)
C(2)	140(40)	19(16)	160(40)	35(19)	-20(30)	-17(18)
C(1)	42(15)	150(30)	70(20)	-20(20)	26(17)	2(18)
C(7)	70(30)	70(30)	180(50)	20(30)	30(30)	30(20)
C(4)	37(14)	57(19)	120(30)	-6(18)	6(17)	7(12)
N(1)	58(17)	100(30)	170(40)	-10(20)	60(20)	-7(16)
O(1)	45(13)	130(20)	180(30)	40(20)	16(16)	28(14)
C(5)	60(20)	60(30)	290(80)	70(40)	-20(40)	4(19)
C(11)	160(50)	30(20)	250(70)	30(30)	-160(50)	0(20)
C(14)	60(20)	51(19)	160(40)	-30(20)	-30(20)	-3(15)
C(13)	70(20)	110(40)	110(30)	-20(30)	30(20)	10(20)
C(9)	70(20)	65(19)	80(30)	9(17)	39(19)	11(16)
C(10)	48(18)	140(40)	110(40)	10(30)	50(20)	30(20)
C(12)	140(40)	120(40)	120(40)	30(30)	70(30)	10(30)
N(6)	80(20)	62(19)	90(30)	1(18)	-41(19)	10(15)
N(5)	210(50)	150(40)	130(40)	10(30)	130(40)	-30(30)
C(18)	47(19)	100(30)	170(50)	-30(30)	30(20)	11(19)
C(19)	300(100)	60(30)	110(50)	-20(30)	-20(50)	30(40)
C(16)	50(19)	150(40)	90(30)	10(30)	-19(19)	-20(20)
C(21)	90(30)	70(30)	140(40)	30(30)	-70(30)	-10(20)
C(15)	170(60)	60(20)	140(40)	0(20)	20(40)	-50(30)
C(22)	110(50)	300(90)	100(40)	40(50)	0(30)	90(50)
C(23)	90(30)	50(20)	180(50)	40(30)	30(30)	49(19)
N(4)	58(18)	61(18)	160(30)	22(19)	-20(20)	0(14)
C(28)	70(20)	80(30)	90(30)	10(20)	20(20)	-4(18)

Table 5. Hydrogen coordinates (x 10^4) and isotropic displacement parameters ($Å^2$x 10^{3}) for cwnd111.

	x	y	z	U(eq)
H(7A)	13205	5155	5955	130
H(7B)	14802	4671	6109	130
H(1)	13243	3981	4794	127
H(5A)	9596	4745	4110	168
H(5B)	12395	4742	3273	168
H(9A)	6443	2375	4915	86
H(9B)	9278	2376	4194	86
H(10A)	11244	2491	6783	119
H(10B)	9604	2012	6566	119
H(12)	8517	3179	8430	151
H(18)	6421	1827	8517	124
H(19)	9415	5285	7581	193
H(16)	3170	2633	11391	118
H(21)	7654	4387	11229	127
H(15)	5635	3346	10496	149
H(22)	10752	3801	10333	206
H(23)	13013	4034	8129	128
H(4)	6450	3193	4728	114

Host Molecule P2

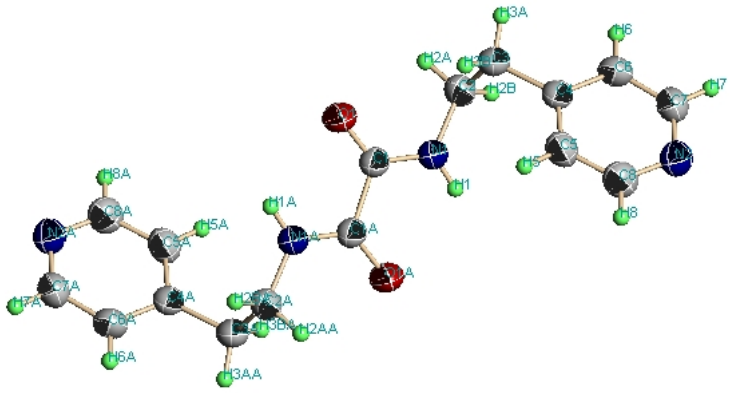

Table 1. Crystal data and structure refinement for cwcv111.

Identification code	cwcv111	
Empirical formula	C16 H18 N4 O2	
Formula weight	298.34	
Temperature	293(2) K	
Wavelength	0.71073 Å	
Crystal system	Monoclinic	
Space group	P2(1)/c	
Unit cell dimensions	a = 8.2229(13) Å	α= 90°
	b = 5.8390(9) Å	β= 101.242(3)°
	c = 15.797(3) Å	γ = 90°
Volume	743.9(2) Å^3	
Z	2	
Density (calculated)	1.332 Mg/m^3	
Absorption coefficient	0.091 mm^{-1}	
F(000)	316	
Crystal size	0.6 x 0.2 x 0.1 mm^3	
Theta range for data collection	2.53 to 28.48°.	
Index ranges	-10<=h<=9, -7<=k<=7, -21<=l<=19	
Reflections collected	4461	
Independent reflections	1703 [R(int) = 0.0841]	
Completeness to theta = 28.48°	90.5 %	
Absorption correction	None	
Refinement method	Full-matrix least-squares on F^2	
Data / restraints / parameters	1703 / 0 / 100	
Goodness-of-fit on F^2	1.093	
Final R indices [I>2sigma(I)]	R1 = 0.0623, wR2 = 0.1923	
R indices (all data)	R1 = 0.0850, wR2 = 0.2094	
Largest diff. peak and hole	0.191 and -0.261 e.Å^{-3}	

Table 2. Atomic coordinates (x 10^4) and equivalent isotropic displacement parameters ($Å^2$x 10^3) for cwcv111. U(eq) is defined as one third of the trace of the orthogonalized U^{ij} tensor.

	x	y	z	U(eq)
O(1)	-948(2)	10498(3)	3929(1)	63(1)
N(2)	6724(2)	4974(3)	4207(1)	58(1)
N(1)	673(2)	7538(3)	4496(1)	48(1)
C(1)	-103(2)	9512(4)	4544(1)	44(1)
C(6)	4140(3)	4415(4)	3235(2)	58(1)
C(4)	3492(3)	6443(4)	3484(1)	47(1)
C(3)	1724(3)	7135(4)	3131(1)	56(1)
C(7)	5728(3)	3775(4)	3609(2)	58(1)
C(5)	4538(3)	7710(4)	4090(2)	56(1)
C(2)	524(3)	6323(4)	3685(1)	54(1)
C(8)	6102(3)	6928(4)	4432(2)	61(1)

Table 3. Bond lengths [Å] and angles [°] for cwcv111.

O(1)-C(1)	1.223(2)
N(2)-C(7)	1.323(3)
N(2)-C(8)	1.327(3)
N(1)-C(1)	1.327(3)
N(1)-C(2)	1.449(3)
C(1)-C(1)#1	1.527(4)
C(6)-C(7)	1.376(3)
C(6)-C(4)	1.386(3)
C(4)-C(5)	1.372(3)
C(4)-C(3)	1.507(3)
C(3)-C(2)	1.517(3)
C(5)-C(8)	1.372(3)
C(7)-N(2)-C(8)	115.4(2)
C(1)-N(1)-C(2)	121.16(18)
O(1)-C(1)-N(1)	124.63(19)
O(1)-C(1)-C(1)#1	121.0(2)
N(1)-C(1)-C(1)#1	114.3(2)
C(7)-C(6)-C(4)	119.7(2)
C(5)-C(4)-C(6)	115.8(2)
C(5)-C(4)-C(3)	122.8(2)
C(6)-C(4)-C(3)	121.3(2)
C(4)-C(3)-C(2)	113.07(18)
N(2)-C(7)-C(6)	124.5(2)
C(8)-C(5)-C(4)	120.4(2)
N(1)-C(2)-C(3)	113.84(19)
N(2)-C(8)-C(5)	124.2(2)

Symmetry transformations used to generate equivalent atoms:
#1 -x,-y+2,-z+1

Table 4. Anisotropic displacement parameters ($Å^2 x\ 10^3$) for cwcv111. The anisotropic displacement factor exponent takes the form: $-2\pi^2[\ h^2\ a^{*2}U^{11} + ...\ + 2\ h\ k\ a^*\ b^*\ U^{12}\ ]$

	U^{11}	U^{22}	U^{33}	U^{23}	U^{13}	U^{12}
O(1)	73(1)	73(1)	39(1)	4(1)	3(1)	22(1)
N(2)	48(1)	70(1)	57(1)	1(1)	14(1)	5(1)
N(1)	45(1)	57(1)	40(1)	-2(1)	6(1)	7(1)
C(1)	42(1)	53(1)	38(1)	3(1)	9(1)	5(1)
C(6)	62(1)	64(1)	45(1)	-11(1)	5(1)	5(1)
C(4)	48(1)	57(1)	37(1)	1(1)	11(1)	5(1)
C(3)	56(1)	71(2)	38(1)	-4(1)	4(1)	13(1)
C(7)	59(1)	59(1)	57(1)	-5(1)	13(1)	10(1)
C(5)	54(1)	57(1)	60(2)	-9(1)	15(1)	3(1)
C(2)	48(1)	62(1)	49(1)	-12(1)	6(1)	5(1)
C(8)	47(1)	69(2)	66(2)	-12(1)	11(1)	-7(1)

Table 5. Hydrogen coordinates ($x\ 10^4$) and isotropic displacement parameters ($Å^2 x\ 10^{\ 3}$) for cwcv111.

	x	y	z	U(eq)
H(1)	1276	6971	4954	57
H(6)	3504	3492	2817	69
H(3A)	1387	6511	2555	67
H(3B)	1666	8791	3086	67
H(7)	6129	2405	3430	69
H(5)	4185	9110	4270	68
H(2A)	-599	6501	3361	64
H(2B)	708	4704	3804	64
H(8)	6767	7823	4848	73

Molecule M3

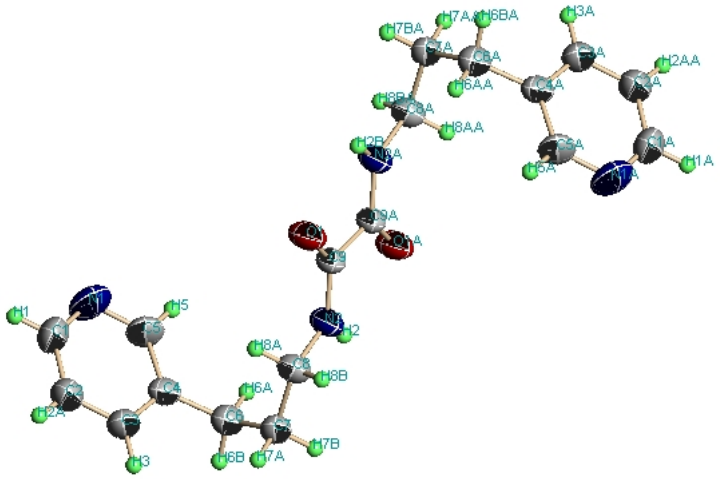

Table 1. Crystal data and structure refinement for cwde692.

Identification code	e:	
Empirical formula	C18 H22 N4 O2	
Formula weight	326.40	
Temperature	273(2) K	
Wavelength	0.71073 Å	
Crystal system	Monoclinic	
Space group	P2(1)/c	
Unit cell dimensions	a = 5.442(2) Å	α= 90°
	b = 31.709(12) Å	β= 109.562(8)°
	c = 5.185(2) Å	γ = 90°
Volume	843.1(6) Å^3	
Z	2	
Density (calculated)	1.286 Mg/m^3	
Absorption coefficient	0.086 mm^{-1}	
F(000)	348	
Crystal size	0.4 x 0.3 x 0.3 mm^3	
Theta range for data collection	1.28 to 28.54°.	
Index ranges	-7<=h<=7, -40<=k<=40, -6<=l<=4	
Reflections collected	5263	
Independent reflections	1938 [R(int) = 0.3432]	
Completeness to theta = 28.54°	90.4 %	
Absorption correction	None	
Refinement method	Full-matrix least-squares on F^2	
Data / restraints / parameters	1938 / 0 / 109	
Goodness-of-fit on F^2	0.715	
Final R indices [I>2sigma(I)]	R1 = 0.1149, wR2 = 0.2186	
R indices (all data)	R1 = 0.3020, wR2 = 0.2817	
Largest diff. peak and hole	0.522 and -0.358 e.Å^{-3}	

Table 2. Atomic coordinates (x 10^4) and equivalent isotropic displacement parameters ($Å^2$x 10^3) for cwde692. U(eq) is defined as one third of the trace of the orthogonalized U^{ij} tensor.

	x	y	z	U(eq)
O(1)	8458(7)	230(1)	7097(7)	60(1)
C(9)	8902(10)	157(1)	5012(11)	41(1)
N(2)	7666(9)	321(1)	2577(8)	51(1)
C(4)	7755(11)	1483(2)	1818(10)	51(2)
C(7)	4893(10)	862(1)	-443(10)	49(2)
C(6)	7068(11)	1163(2)	-460(10)	54(2)
C(8)	5454(11)	605(2)	2152(9)	52(2)
N(1)	10852(11)	1752(2)	5960(11)	86(2)
C(5)	10138(12)	1482(2)	3842(12)	68(2)
C(2)	6696(13)	2066(2)	4164(12)	73(2)
C(3)	6017(12)	1787(2)	1979(11)	65(2)
C(1)	9139(16)	2031(2)	6054(13)	77(2)

Table 3. Bond lengths [Å] and angles [°] for cwde692.

O(1)-C(9)	1.206(5)
C(9)-N(2)	1.322(6)
C(9)-C(9)#1	1.559(10)
N(2)-C(8)	1.459(6)
C(4)-C(5)	1.368(7)
C(4)-C(3)	1.374(7)
C(4)-C(6)	1.506(7)
C(7)-C(8)	1.514(6)
C(7)-C(6)	1.522(6)
N(1)-C(1)	1.298(8)
N(1)-C(5)	1.344(7)
C(2)-C(1)	1.367(8)
C(2)-C(3)	1.385(7)
O(1)-C(9)-N(2)	126.2(5)
O(1)-C(9)-C(9)#1	120.9(5)
N(2)-C(9)-C(9)#1	113.0(6)
C(9)-N(2)-C(8)	121.1(4)
C(5)-C(4)-C(3)	116.7(5)
C(5)-C(4)-C(6)	121.5(5)
C(3)-C(4)-C(6)	121.8(5)
C(8)-C(7)-C(6)	114.6(4)
C(4)-C(6)-C(7)	114.0(4)
N(2)-C(8)-C(7)	112.1(4)
C(1)-N(1)-C(5)	116.8(5)
N(1)-C(5)-C(4)	124.5(6)
C(1)-C(2)-C(3)	117.7(6)
C(4)-C(3)-C(2)	119.8(6)
N(1)-C(1)-C(2)	124.4(6)

Symmetry transformations used to generate equivalent atoms:
#1 -x+2,-y,-z+1

Table 4. Anisotropic displacement parameters ($Å^2 x\ 10^3$) for cwde692. The anisotropic displacement factor exponent takes the form: $-2\pi^2[\ h^2\ a^{*2}U^{11} + ...\ + 2\ h\ k\ a^*\ b^*\ U^{12}\ ]$

	U^{11}	U^{22}	U^{33}	U^{23}	U^{13}	U^{12}
O(1)	73(3)	59(3)	42(2)	10(2)	12(2)	24(2)
C(9)	50(3)	36(3)	30(3)	6(3)	5(3)	6(2)
N(2)	61(3)	44(3)	43(3)	7(2)	12(2)	16(2)
C(4)	47(4)	44(3)	50(3)	9(3)	-1(3)	-1(3)
C(7)	42(3)	41(3)	52(3)	1(3)	1(3)	5(3)
C(6)	55(4)	48(3)	52(3)	5(3)	6(3)	1(3)
C(8)	51(4)	46(3)	52(3)	8(3)	7(3)	10(3)
N(1)	54(4)	93(4)	80(4)	-19(4)	-18(3)	-2(4)
C(5)	39(4)	65(4)	76(4)	-3(4)	-14(3)	10(3)
C(2)	71(5)	47(4)	74(4)	-5(3)	-11(4)	10(3)
C(3)	54(4)	50(4)	66(4)	-1(3)	-12(3)	5(3)
C(1)	80(5)	50(4)	76(5)	-15(4)	-7(4)	-6(4)

Table 5. Hydrogen coordinates ($x\ 10^4$) and isotropic displacement parameters ($Å^2 x\ 10^{\ 3}$) for cwde692.

	x	y	z	U(eq)
H(2)	8175	260	1221	61
H(7A)	3315	1024	-714	58
H(7B)	4561	670	-1979	58
H(6A)	8613	999	-324	65
H(6B)	6546	1310	-2198	65
H(8A)	5816	795	3703	63
H(8B)	3922	441	2056	63
H(5)	11347	1280	3745	82
H(2A)	5529	2269	4339	87
H(3)	4389	1807	624	78
H(1)	9606	2221	7507	92

Co-crystal M3/1

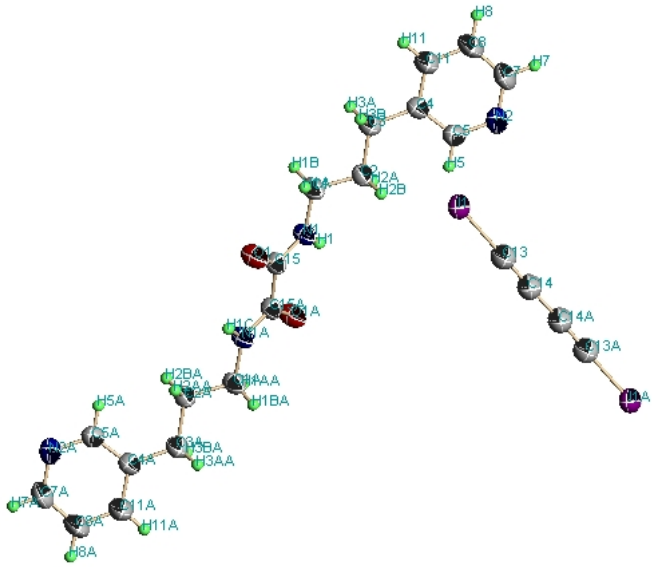

Table 1. Crystal data and structure refinement for cwdk111.

Identification code	cwdk111	
Empirical formula	C22 H22 I2 N4 O2	
Formula weight	628.24	
Temperature	293(2) K	
Wavelength	0.71073 Å	
Crystal system	Monoclinic	
Space group	P2(1)/n	
Unit cell dimensions	a = 5.1259(11) Å	α= 90°
	b = 14.607(3) Å	β= 90.000(4)°
	c = 15.828(4) Å	γ = 90°
Volume	1185.2(4) Å^3	
Z	2	
Density (calculated)	1.760 Mg/m^3	
Absorption coefficient	2.678 mm^{-1}	
F(000)	608	
Crystal size	0.6 x 0.3 x 0.2 mm^3	
Theta range for data collection	1.90 to 28.35°.	
Index ranges	-6<=h<=6, -19<=k<=19, -20<=l<=11	
Reflections collected	7007	
Independent reflections	2655 [R(int) = 0.0991]	
Completeness to theta = 28.35°	89.8 %	
Absorption correction	None	
Refinement method	Full-matrix least-squares on F^2	
Data / restraints / parameters	2655 / 0 / 136	
Goodness-of-fit on F^2	0.965	
Final R indices [I>2sigma(I)]	R1 = 0.0473, wR2 = 0.1248	

R indices (all data)	R1 = 0.0648, wR2 = 0.1339
Largest diff. peak and hole	1.399 and -1.224 e.Å^{-3}

Table 2. Atomic coordinates (x 10^4) and equivalent isotropic displacement parameters (Å^{2}x 10^3) for cwdk111. U(eq) is defined as one third of the trace of the orthogonalized U^{ij} tensor.

	x	y	z	U(eq)
C(15)	-349(8)	487(3)	127(3)	42(1)
I(1)	1489(1)	1993(1)	3829(1)	59(1)
C(5)	7020(11)	3035(3)	2445(3)	54(1)
O(1)	-2645(5)	739(2)	161(2)	57(1)
C(1)	1495(9)	1970(3)	520(4)	51(1)
N(1)	1676(6)	1007(2)	303(3)	45(1)
N(2)	8755(9)	3323(3)	3009(3)	63(1)
C(4)	5539(9)	3600(3)	1943(3)	48(1)
C(2)	3450(8)	2235(4)	1188(3)	47(1)
C(7)	9075(13)	4216(4)	3099(4)	77(2)
C(3)	3569(9)	3268(4)	1312(3)	53(1)
C(8)	7712(18)	4837(4)	2627(6)	104(3)
C(13)	3372(12)	957(4)	4422(4)	70(2)
C(14)	4406(13)	340(4)	4784(4)	71(2)
C(11)	5890(14)	4520(4)	2050(5)	85(2)

Table 3. Bond lengths [Å] and angles [°] for cwdk111.

C(15)-O(1)	1.234(5)
C(15)-N(1)	1.316(5)
C(15)-C(15)#1	1.522(9)
I(1)-C(13)	2.026(6)
C(5)-N(2)	1.329(7)
C(5)-C(4)	1.375(7)
C(1)-N(1)	1.450(5)
C(1)-C(2)	1.508(6)
N(2)-C(7)	1.323(7)
C(4)-C(11)	1.367(7)
C(4)-C(3)	1.501(6)
C(2)-C(3)	1.523(7)
C(7)-C(8)	1.367(9)
C(8)-C(11)	1.386(9)
C(13)-C(14)	1.192(8)
C(14)-C(14)#2	1.351(12)
O(1)-C(15)-N(1)	124.8(4)
O(1)-C(15)-C(15)#1	121.0(5)
N(1)-C(15)-C(15)#1	114.2(4)
N(2)-C(5)-C(4)	124.6(4)
N(1)-C(1)-C(2)	111.9(4)
C(15)-N(1)-C(1)	124.0(4)

C(7)-N(2)-C(5)	117.9(5)
C(11)-C(4)-C(5)	116.5(5)
C(11)-C(4)-C(3)	119.3(5)
C(5)-C(4)-C(3)	124.2(4)
C(1)-C(2)-C(3)	111.8(4)
N(2)-C(7)-C(8)	122.2(5)
C(4)-C(3)-C(2)	115.7(4)
C(7)-C(8)-C(11)	118.9(6)
C(14)-C(13)-I(1)	177.9(7)
C(13)-C(14)-C(14)#2	178.0(9)
C(4)-C(11)-C(8)	119.9(6)

Symmetry transformations used to generate equivalent atoms:
#1 -x,-y,-z #2 -x+1,-y,-z+1

Table 4. Anisotropic displacement parameters ($Å^2 x\ 10^3$) for cwdk111. The anisotropic displacement factor exponent takes the form: $-2\pi^2[\ h^2\ a^{*2}U^{11} + ...\ + 2\ h\ k\ a^*\ b^*\ U^{12}\ ]$

	U^{11}	U^{22}	U^{33}	U^{23}	U^{13}	U^{12}
C(15)	33(2)	46(2)	46(3)	-3(2)	-2(2)	0(2)
I(1)	72(1)	58(1)	49(1)	0(1)	-10(1)	-1(1)
C(5)	64(3)	46(3)	53(3)	2(2)	-5(2)	-8(2)
O(1)	30(2)	51(2)	89(3)	-14(2)	3(2)	2(1)
C(1)	40(2)	45(3)	67(3)	-9(2)	-8(2)	1(2)
N(1)	30(2)	42(2)	62(2)	-9(2)	-2(2)	1(1)
N(2)	75(3)	67(3)	47(3)	1(2)	-13(2)	-7(2)
C(4)	53(3)	43(2)	48(3)	-6(2)	-3(2)	-3(2)
C(2)	46(2)	44(2)	51(3)	-5(2)	-6(2)	1(2)
C(7)	100(5)	67(4)	64(4)	-14(3)	-31(3)	-10(3)
C(3)	58(3)	44(2)	57(3)	-6(2)	-8(2)	0(2)
C(8)	147(7)	46(3)	119(7)	-17(3)	-68(6)	-5(4)
C(13)	77(4)	58(3)	76(4)	-3(3)	-16(3)	1(3)
C(14)	80(4)	60(3)	72(4)	-1(3)	-21(3)	1(3)
C(11)	113(5)	48(3)	95(5)	-5(3)	-46(4)	0(3)

Table 5. Hydrogen coordinates (x 10^4) and isotropic displacement parameters ($Å^2$x 10^3) for cwdk111.

	x	y	z	U(eq)
H(5)	6792	2407	2385	65
H(1A)	-251	2101	724	61
H(1B)	1791	2335	18	61
H(1)	3200	762	288	54
H(2A)	5162	2012	1026	56
H(2B)	2980	1946	1718	56
H(7)	10267	4429	3496	92
H(3A)	3948	3550	771	64
H(3B)	1858	3479	1488	64
H(8)	8003	5462	2692	125
H(11)	4907	4934	1736	102

Solution-Sate NMR Data

Diiodobutadiyne Dissolved in Pyridine$_{d5}$

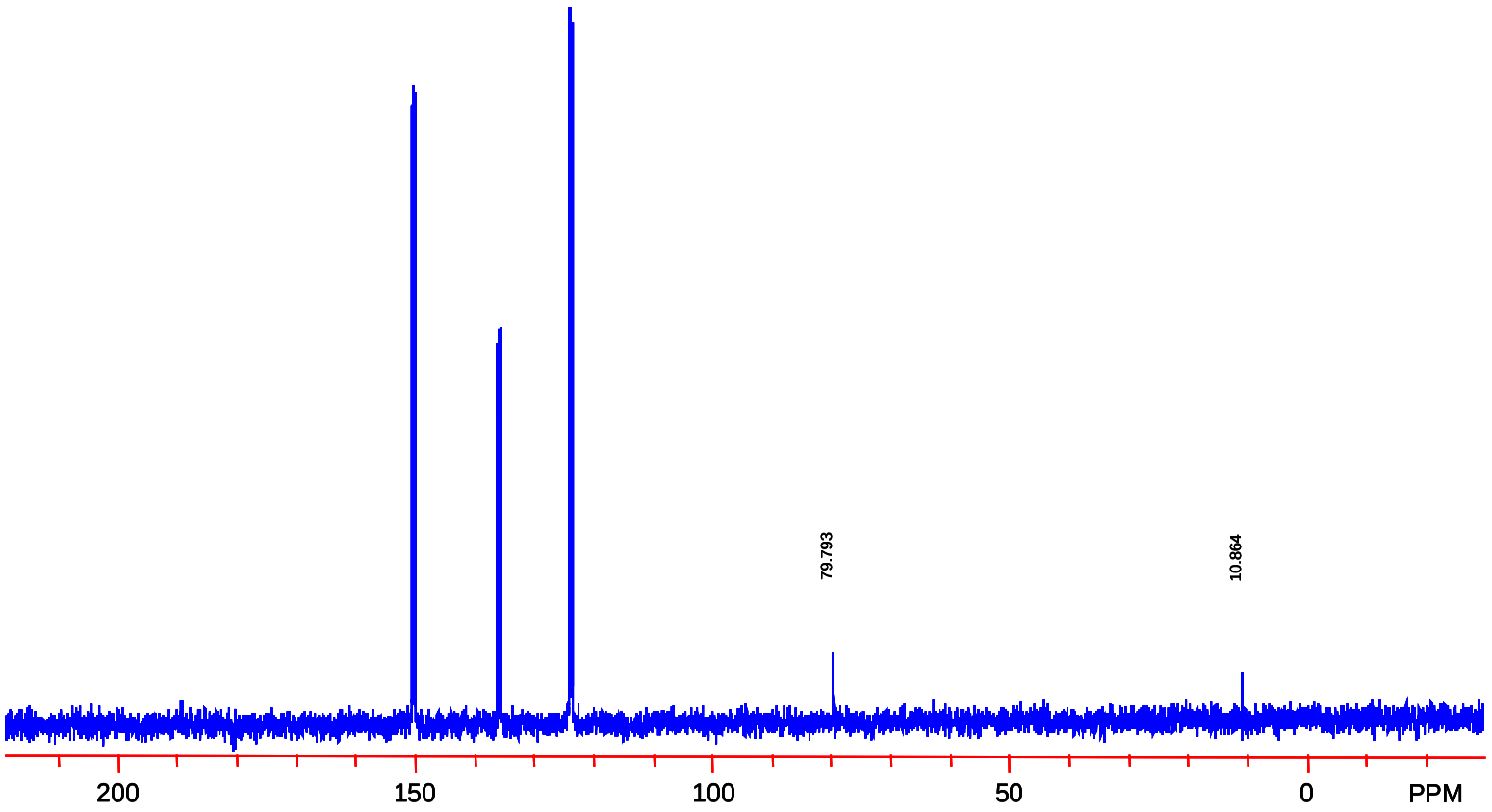

Diiodobutadiyne Dissolved in Hexanes$_{d14}$

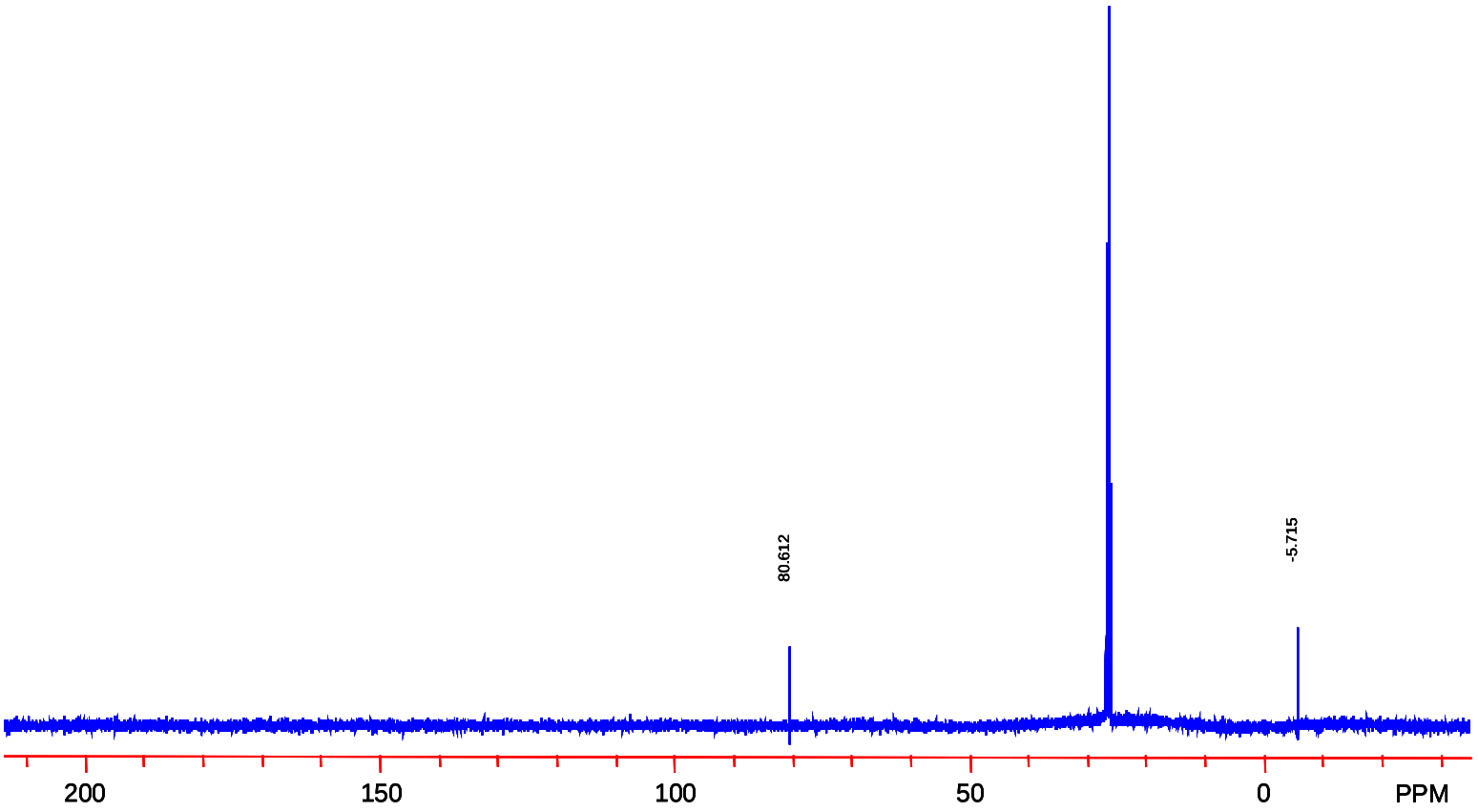

^{13}C NMR of 3-(2-aminoethyl)pyridine

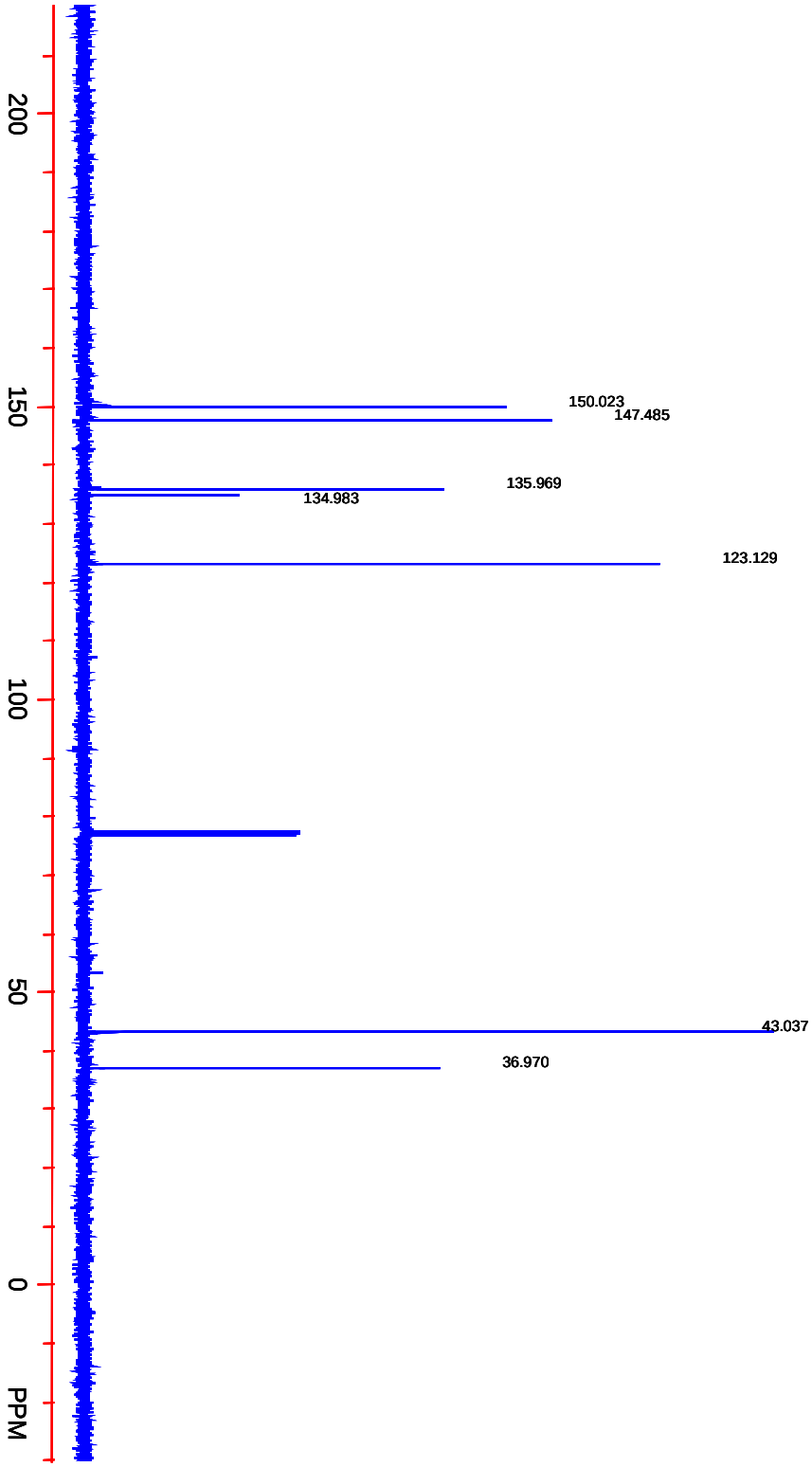

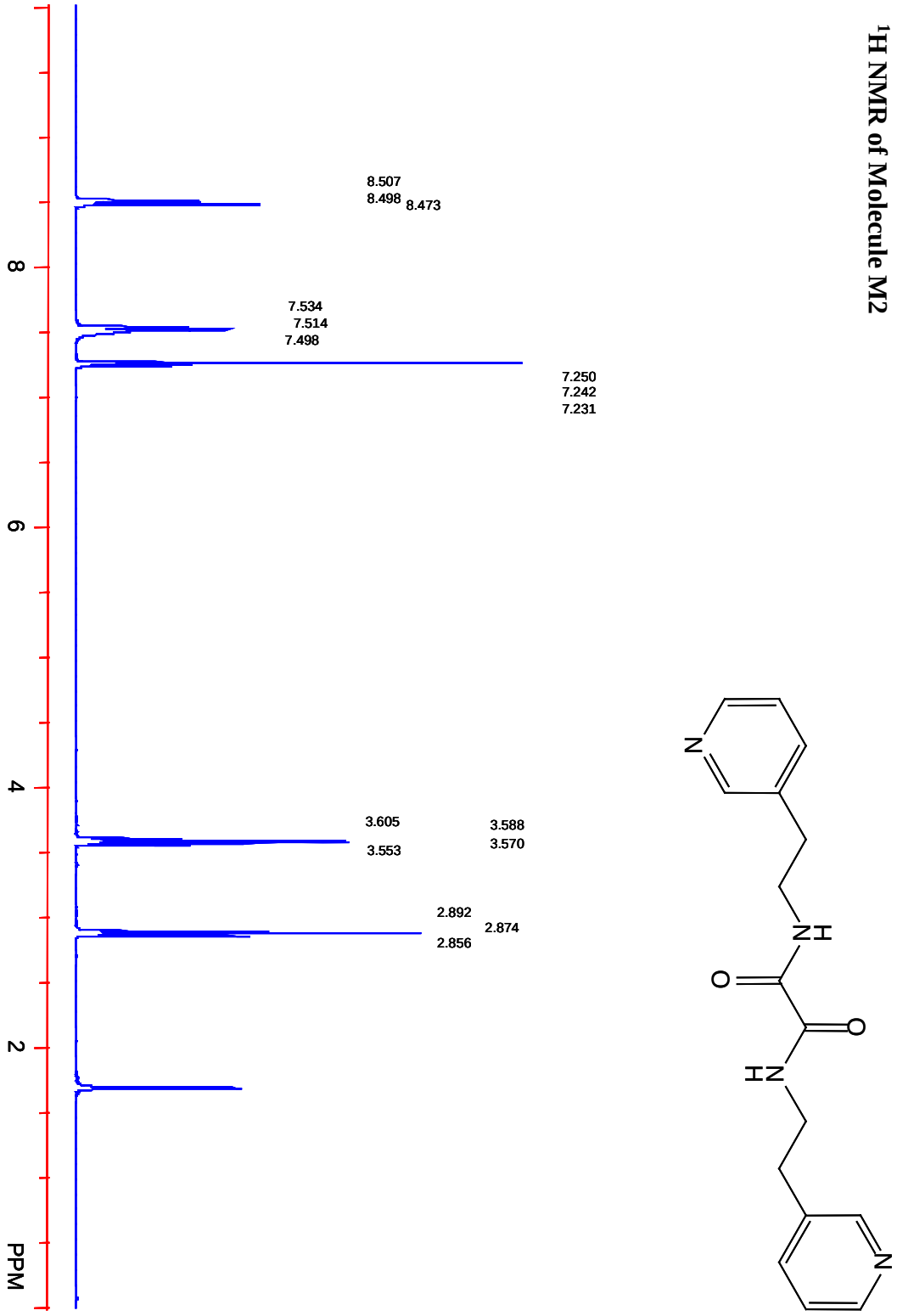

^{1}H NMR of Molecule M2

^{13}C NMR of Molecule M2

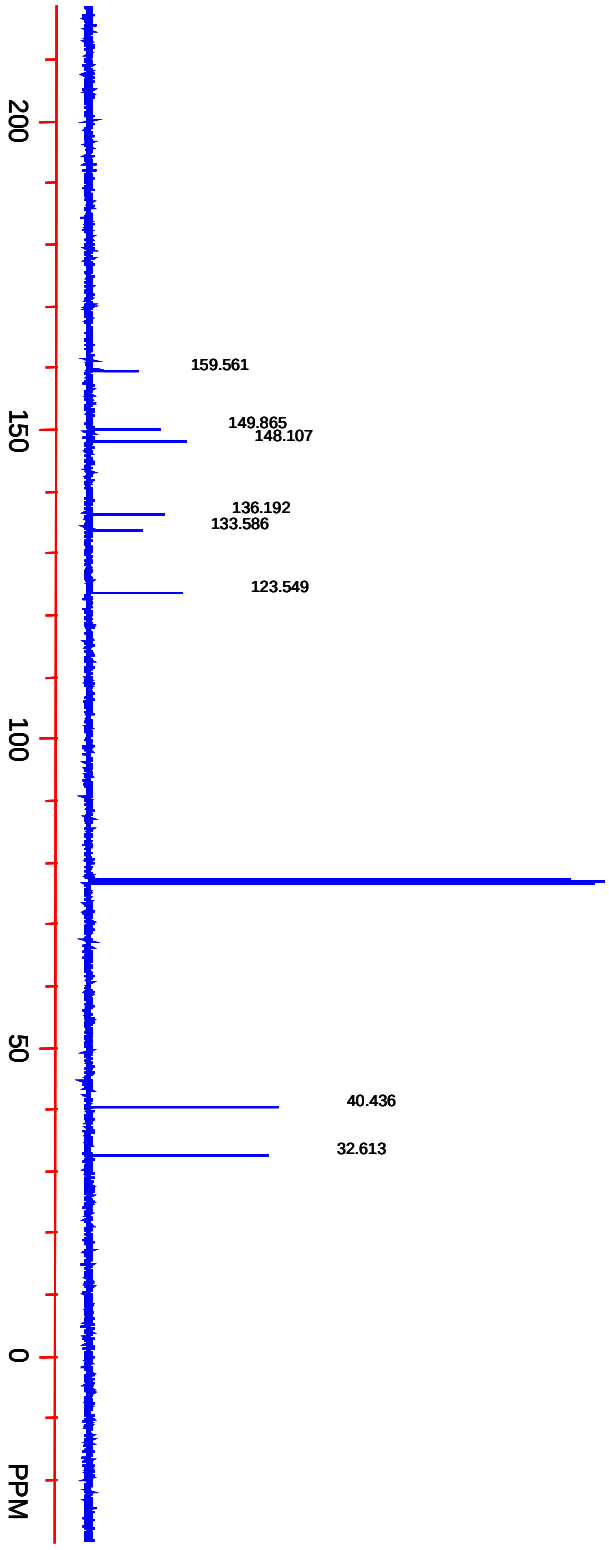

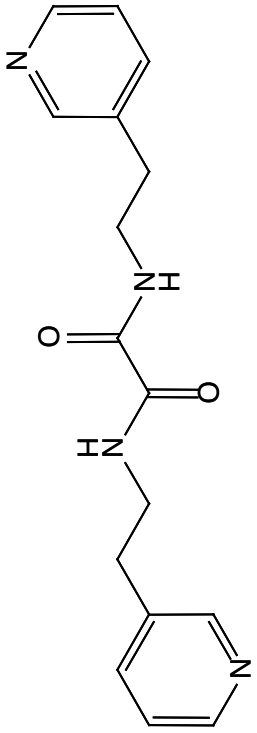

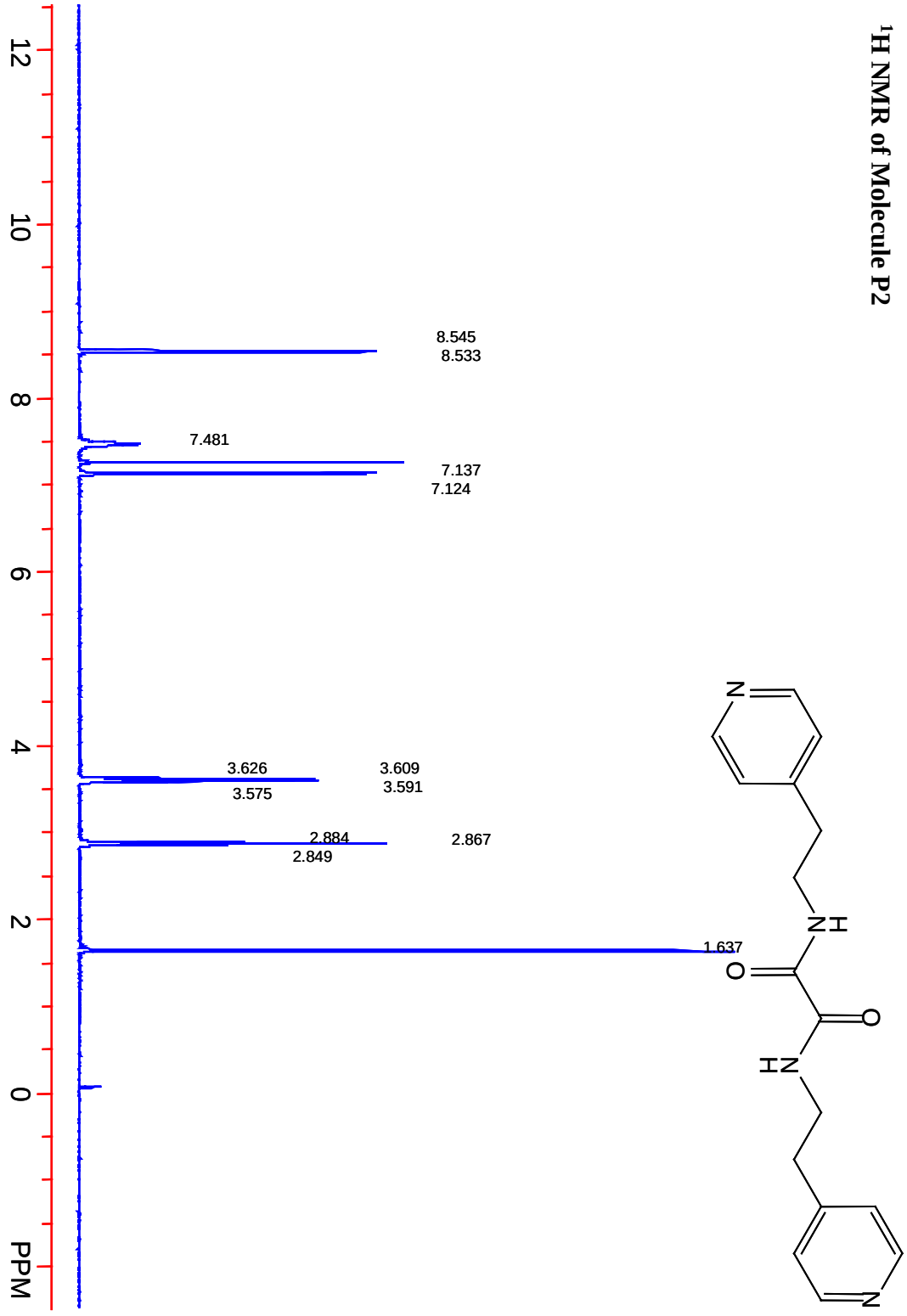

^{1}H NMR of Molecule P2

^{13}C NMR of Molecule P2

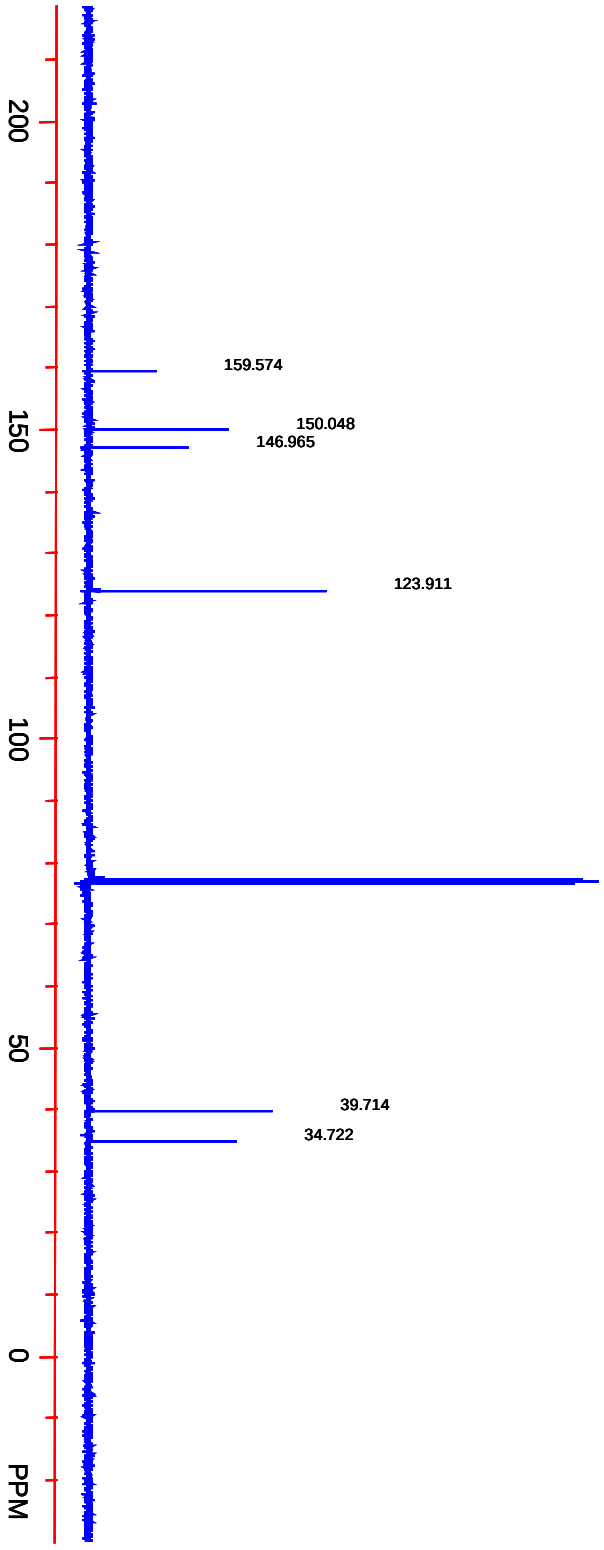

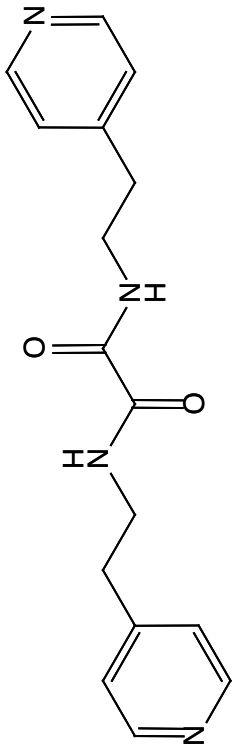

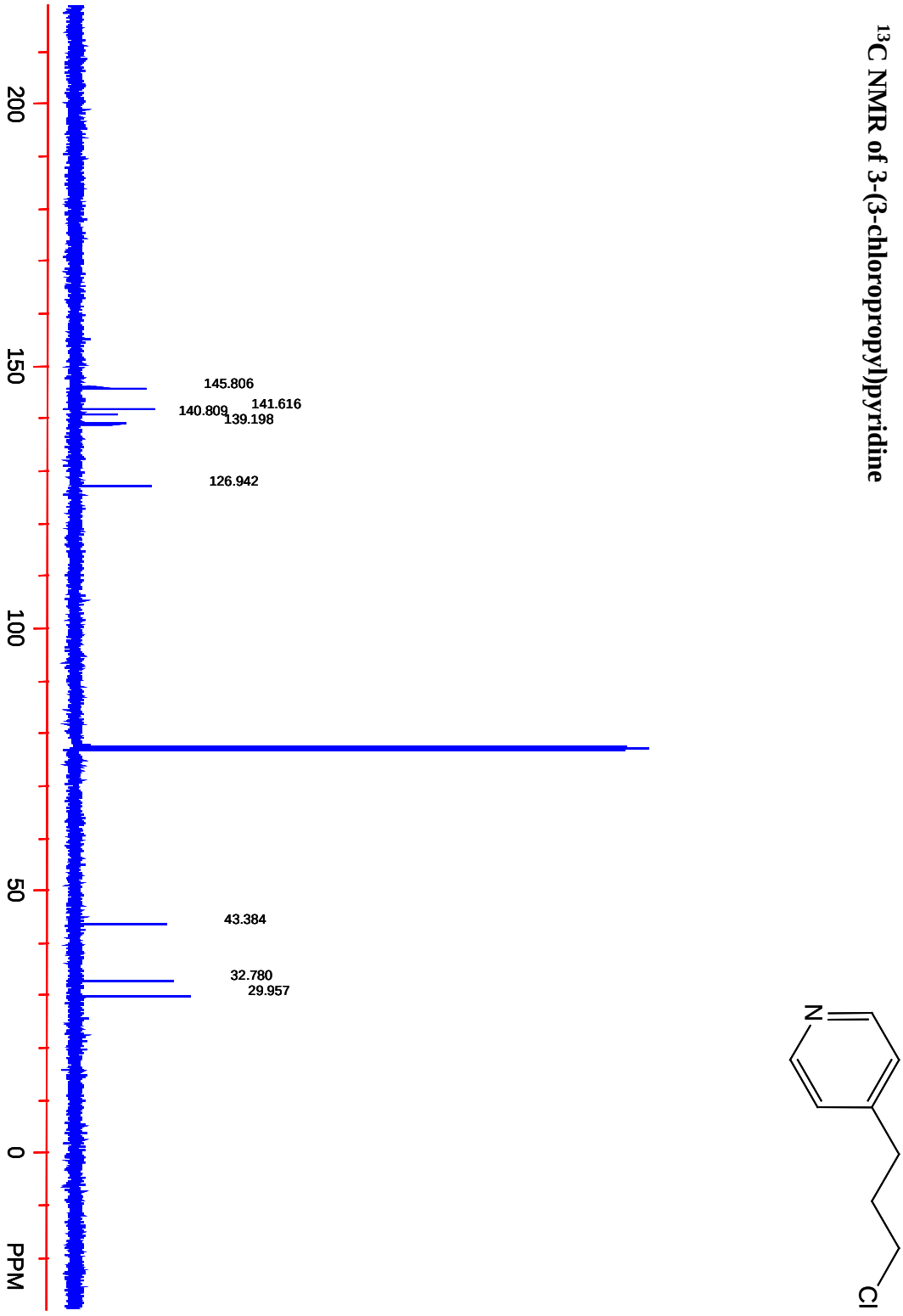

^{13}C NMR of 3-(3-chloropropyl)pyridine

^{13}C NMR of 4-pyridin-2-yl-butyronitrile

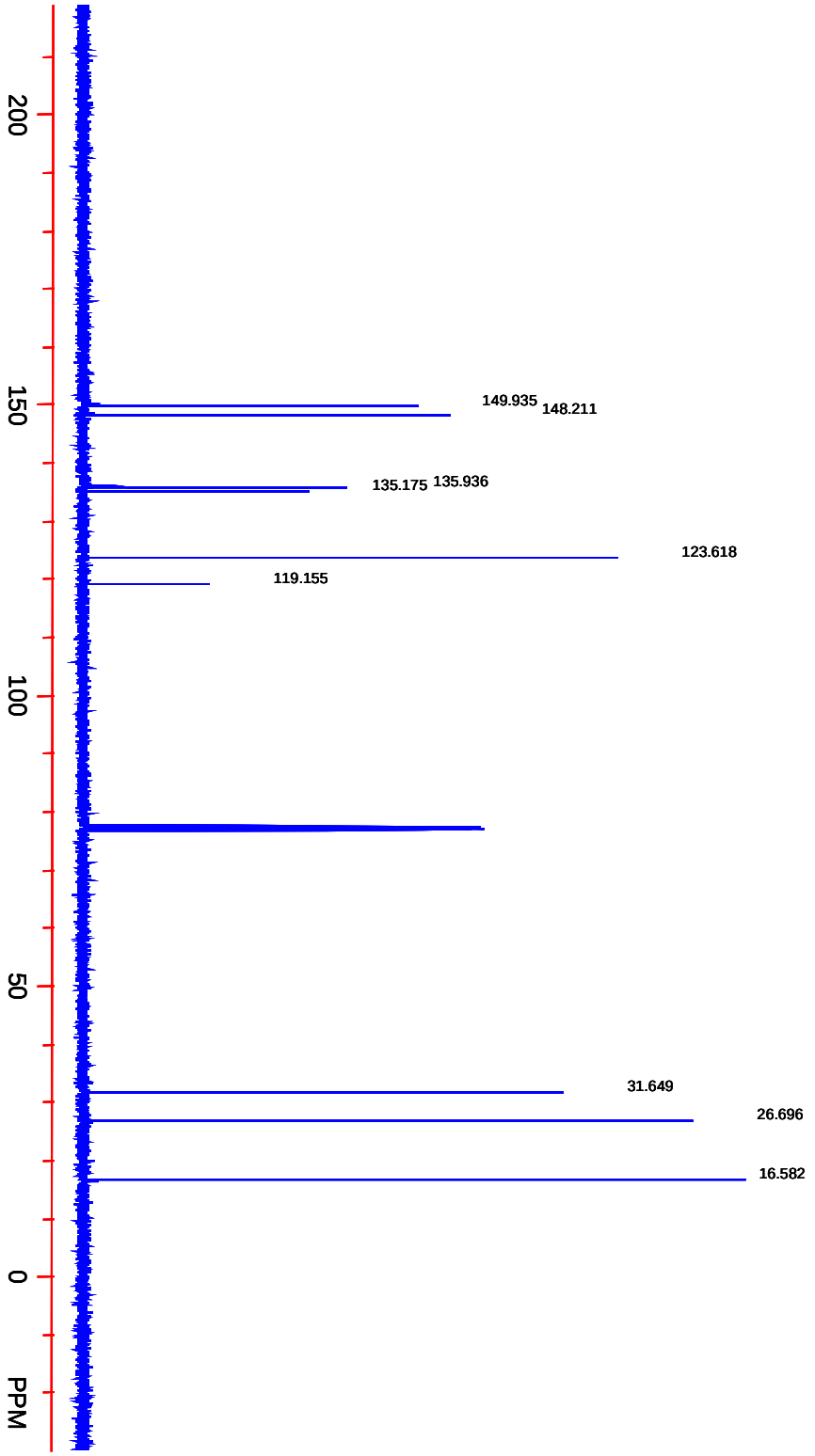

^{13}C NMR of 3-pyridinebutanamine

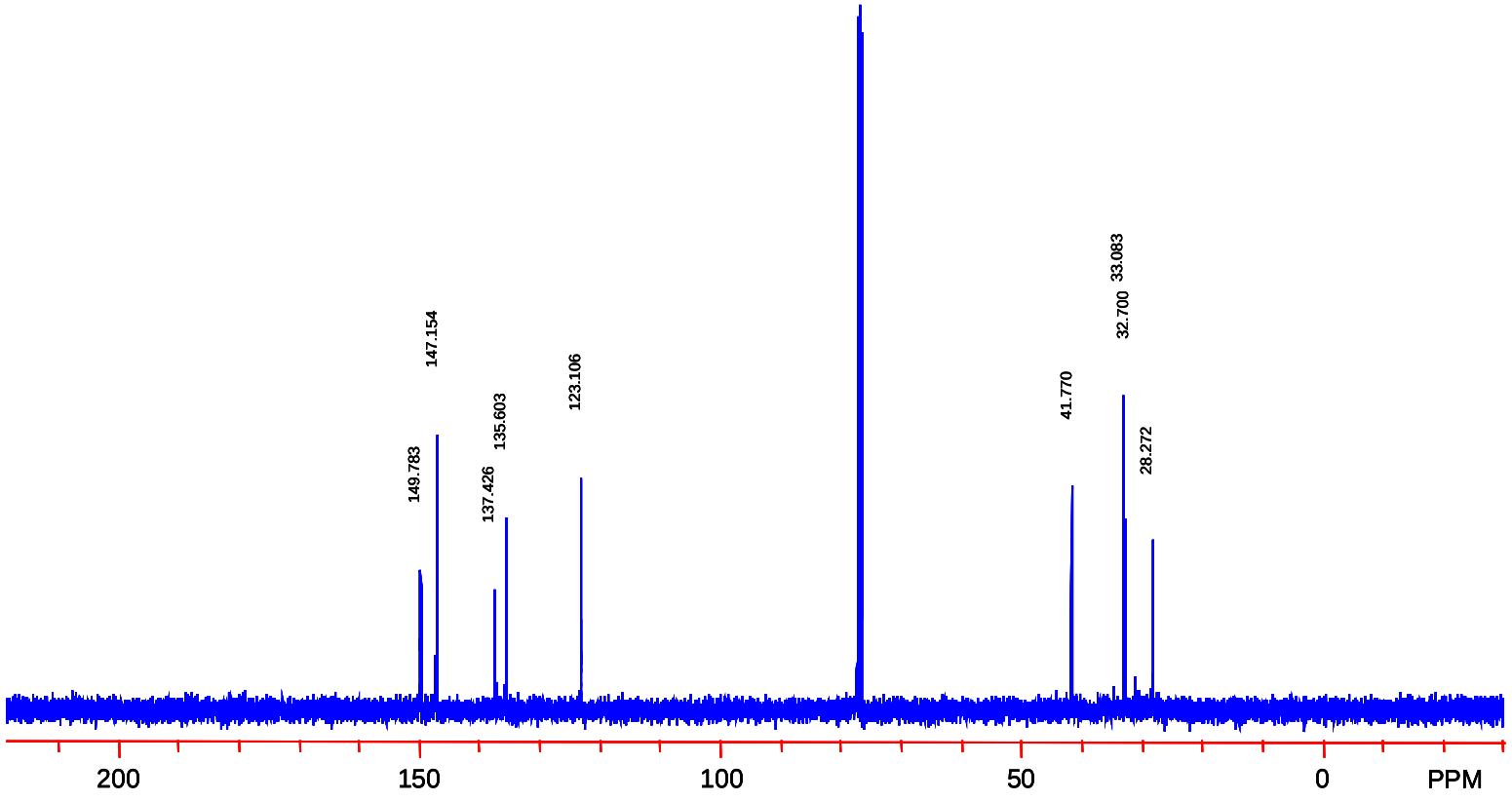

^{13}C NMR of Host Molecule M4